

LOW-COST SEISMIC BASE ISOLATION USING SCRAP TIRE PADS (STP)

A THESIS SUBMITTED TO  
THE GRADUATE SCHOOL OF NATURAL AND APPLIED SCIENCES  
OF  
MIDDLE EAST TECHNICAL UNIVERSITY

BY

BAYEZİD ÖZDEN

IN PARTIAL FULFILLMENT OF THE REQUIREMENTS  
FOR  
THE DEGREE OF MASTER OF SCIENCE  
IN  
CIVIL ENGINEERING

APRIL 2006

Approval of the Graduate School of Natural and Applied Sciences.

---

Prof. Dr. Canan ÖZGEN  
Director

I certify that this thesis satisfies all the requirements as a thesis for the degree of Master of Science.

---

Prof. Dr. Erdal ÇOKÇA  
Head of the Department

This is to certify that we have read this thesis and that in our opinion it is fully adequate, in scope and quality, as a thesis for the degree of Master of Science.

---

Assist. Prof. Dr. Ahmet TÜRER  
Supervisor

Prof. Dr. Çetin Yılmaz (METU, CE)

---

Assist. Prof. Dr. Ahmet TÜRER (METU, CE)

---

Assoc. Prof. Dr. Uğurhan AKYÜZ (METU, CE)

---

Assoc. Prof. Dr. Cem TOPKAYA (METU, CE)

---

Assist. Prof. Dr. H. Hüsnü KORKMAZ (Selçuk Univ., CE)

---

**I hereby declare that all information in this document has been obtained and presented in accordance with academic rules and ethical conduct. I also declare that, as required by these rules and conduct, I have fully cited and referenced all material and results that are not original to this work.**

Name, Last name: Bayezid Özden

Signature :

## **ABSTRACT**

### **LOW-COST SEISMIC BASE ISOLATION USING SCRAP TIRE PADS (STP)**

Özden, Bayezid

M. Sc., Department of Civil Engineering

Supervisor: Asst. Prof. Dr. Ahmet Türer

April 2006, 93 pages

This thesis focuses on the experimental studies conducted on the development of low-cost seismic base isolation pads using scrap automobile tires. Seismic base isolation is a well-defined building protection system against earthquakes, on which numerous studies have been conducted. The majority of the previous studies focus on the performance improvement of the base isolation systems. However, this study aims at cost and weight reduction of seismic base isolation pads by recycling otherwise useless material: scrap tires. Elastomer-based isolators have been heavily studied and used for the last 25 years. Steel or fiber reinforcement inside the elastomer isolators provides high vertical stiffness, whereas rubber segments between reinforcement layers provide low horizontal stiffness for the seismic base isolation. Since 1960's, automobile tires have been produced by means of vulcanizing rubber with steel mesh in different forms which have a similar effect as the steel plates or fibers inside the conventional elastomer-based isolators. Therefore, rectangular shaped layers cut from tread sections of used tires and then piled on top of each other can function as an elastomeric bearing. Since the tires are being designed for friction, load transfer between scrap tire layers would be large enough to keep all layers intact. A minimal slip generated between the piled layers at high strain rates may even help to dissipate some extra energy. Axial compression,

dynamic free vibration, static shear and shaking table tests have been conducted on Scrap Tire Pads (STP) prepared by using different tire brands for different number of layers and orientations. The results have shown that the average shear modulus of STPs change between 0.9MPa and 1.85MPa. At the end of the dynamic tests it has been noticed that the lateral stiffness of STPs can be simply adjusted by changing the number of tread layers placed on top of each other. The amount of wire mesh inside the tire tread layers is relatively low compared to the steel plates in regular elastomeric pads; consequently, axial load capacity of STPs has been found to be around 8.0MPa. Static large deformation shear experiments have been performed to obtain the horizontal stiffness and shear modulus values at high strains and the results are tabulated in the manuscript. Steel and rubber layers are produced separately and just put on top of each other without any adhesive to form the  $\frac{1}{4}$  scaled versions of STPs which were used to isolate a  $\frac{1}{4}$  scaled masonry house on the shaking table available in METU Structural Laboratory. The experiment showed that non-vulcanized rubber-steel layers put on top of each other can also be used to isolate structures. In conclusion, STPs may be used as a low-cost alternative to conventional elastomer-based pads for seismic isolation of massive structures (e.g. stone wall rural masonry) or for temperature induced deformation compensation of rural bridges. STP usage is demonstrated using three hypothetical design examples in the manuscript.

Keywords: Earthquake, seismic base isolation, elastomeric bearings, scrap tire

## ÖZ

### ARABA LASTİĞİ YASTIKLARI (ALY) KULLANARAK DÜŞÜK MALİYETLİ SİSMİK ZEMİN YALITIMI

Özden, Bayezid

Yüksek Lisans, İnşaat Mühendisliği Bölümü

Tez Yöneticisi: Yard. Doç. Dr. Ahmet Türer

Nisan 2006, 93 sayfa

Bu tez, otomobil lastiği kullanarak daha ucuz sismik izolatör üretmek amacıyla ODTÜ laboratuvarlarında yapılan deneysel çalışmaları içermektedir. Sismik yalıtım, üzerinde birçok çalışmanın yapıldığı, uluslararası literatürde geçerlilik kazanmış, depremden korunma yöntemlerinden biridir. Bu konuda yapılmakta olan çalışmaların çoğu sismik yalıtım sistemlerinin performans artırımı üzerinde odaklanmıştır. Bu çalışma, maliyet ve ağırlık azaltılması gibi kriterleri de göz önüne almayı amaçlamaktadır. Elastomer yastıklar, son çeyrek asırdır yoğun şekilde incelenmekte ve uygulanmaktadır. Elastomer yastıkların içerisindeki çelik veya fiber donatı yüksek düşey rijitlik sağlarken, donatı katmanlarının arasında bulunan kauçuk, yatay yönde gerekli esnekliği sağlayarak, sismik yalıtım açısından uygun bir yapı oluşturmaktadır. Otomobil lastikleri 1960'lardan beri içindeki çelik hasırın kauçuk ile çeşitli şekillerde pişirilmesi yoluyla üretilmektedir. Lastiklerin içerisindeki çelik hasır, elastomer-menşeli sismik yalıtıcılardaki donatıya benzer bir etkiye sahip olmaktadır. Bu nedenle, atık araba lastiklerinin yere temas eden kısımlarından (lastik tabanı) kesilmiş parçaların üst üste konması ile elde edilecek Atık Lastik Yastıkları (ALY) sismik yalıtıcı olarak kullanılabilirler. Araba lastikleri yol tutma kabiliyetleri esas alınarak tasarlandığından, üst üste konulmuş lastik katmanları arasındaki sürtünme kuvveti, katmanların devamlı temasını sağlayacak yeterlilikte olacak ve yüksek yatay deformasyonlarda katmanlar arasında gözlenen minimal kayma, daha

fazla enerji tüketimine olanak sağlayacaktır. Bu çalışmada ALY'ler üzerinde, çeşitli marka, katman sayısı ve konumda, eksenel basınç, serbest salınım, statik kesme ve sarsma tablası deneyleri gerçekleştirilmiştir. Deneylerin sonucunda ALY'lerin kesme modülleri 0.9MPa ile 1.85MPa arasında çıkmıştır. Dinamik deneyler sonucunda ALY'lerin yatay rijitlik değerlerinin üst üste konan lastik tabanı katman sayılarını değiştirerek istenilen değerlere ayarlanabildiği görülmüştür. Lastik tabanlarındaki çelik hasır oranı elastomer yastıkların içerisindeki çelik plakalara oranla daha azdır. Basınç deneyleri sonucunda ALY'lerin basınç kapasiteleri 8MPa civarında belirlenmiştir. Yüksek deformasyonlu statik kesme deneyleri sonucunda yatay rijitlik ve kesme modülü değerleri elde edilmiştir. Kauçuk ve çelik plakalar ayrı ayrı üretildikten sonra yapıştırıcı kullanılmadan sadece üst üste konarak oluşturulan ¼ ölçekli ALY örnekleri, ODTÜ Yapı Laboratuvarı'nda bulunan sarsma tablası üzerinde ¼ ölçekli bir yığma yapıyı izole etmek için kullanılmıştır. Sarsma tablası deneyleri, çelik ve kauçuk plakaların birbirlerine vulkanize edilmeden, sadece üst üste konulması ile elde edilen yastıkların yapıları izole edebileceklerini göstermiştir. Bu sonuçlar ışığında, ALY'lerin elastomer sismik yalıtıcılara nazaran daha ekonomik bir alternatif olarak kullanılabilmesi düşünülmektedir. ALY'lerin kullanım alanları düşük yoğunluklu trafik akımı taşıyacak kırsal alandaki köprü mesnetlerinin ve yığma yapıların sismik yalıtımı olarak öngörülmektedir.

Anahtar Kelimeler: Deprem, sismik zemin yalıtımı, elastomer yastık, atık lastik

*To my family and my love Gülem*

## ACKNOWLEDGEMENTS

I would like to express my deepest appreciation to my thesis supervisor, Assist. Prof. Dr. Ahmet TÜRER, for his invaluable support, guidance, encouragement, criticism, and insight throughout the research. It was a great pleasure for me to work with him.

This study was a part of “Seismic Performance Improvement of Masonry Houses” project, financed by World Bank DM-2003 and TÜBİTAK İÇTAG I599/01. I would like to thank my project friends Mustafa Gölalınış, Atilla Akaydın and Çağdaş Şimşek for their precious assistance and help throughout the experimental and analytical studies. The help of the project liaison, Mr. İbrahim Sirer, is also kindly acknowledged here.

I am also grateful to Bora Acun for his helps through the experiment measurements.

I could not be able to accomplish this research without supports of my friends and my colleagues Başar Özler, Koray Sığırtmaç, Cengiz Nergiz, Sezgin Küçükçoban, and Gökhan Özdemir.

Finally, I would like to thank my parents, Saliha and Ömer Özden and my dear brother Timur Özden, who encouraged me through my Master of Science Program. I am grateful to them since they were always with me whenever I need their help.

## TABLE OF CONTENTS

<b>PLAGIARISM .....</b>	<b>iii</b>
<b>ABSTRACT .....</b>	<b>iv</b>
<b>ÖZ.....</b>	<b>vi</b>
<b>ACKNOWLEDGEMENTS.....</b>	<b>ix</b>
<b>TABLE OF CONTENTS.....</b>	<b>x</b>
<b>LIST OF TABLES .....</b>	<b>xiii</b>
<b>LIST OF FIGURES .....</b>	<b>xiv</b>
<b>LIST OF SYMBOLS .....</b>	<b>xvii</b>
<b>CHAPTER 1 .....</b>	<b>1</b>
<b>INTRODUCTION.....</b>	<b>1</b>
<b>1.1 Philosophy of Seismic Base Isolation.....</b>	<b>1</b>
<b>1.2 Scope of the Study .....</b>	<b>4</b>
<b>CHAPTER 2 .....</b>	<b>6</b>
<b>LITERATURE REVIEW.....</b>	<b>6</b>
<b>2.1 Development of Seismic Base Isolation Systems .....</b>	<b>6</b>
<b>2.2 History of Rubber and Tire Technology.....</b>	<b>10</b>
<b>2.3 Construction of Tire and Tire Terminology.....</b>	<b>11</b>
<b>CHAPTER 3 .....</b>	<b>15</b>
<b>ELASTOMERIC ISOLATORS .....</b>	<b>15</b>
<b>3.1 Introduction .....</b>	<b>15</b>
<b>3.2 Mechanical Characteristics of Elastomeric Isolators .....</b>	<b>16</b>
<b>3.3 Stability of Elastomeric Bearings .....</b>	<b>18</b>
<b>3.4 Code Provisions for Isolated Structures and Base Isolation Systems .....</b>	<b>19</b>
<b>3.4.1 Equivalent-Lateral Force Procedure .....</b>	<b>21</b>
<b>3.4.1 Required Tests for Seismic Base Isolation Systems .....</b>	<b>25</b>
<b>CHAPTER 4 .....</b>	<b>28</b>
<b>EXPERIMENTS .....</b>	<b>28</b>
<b>4.1 Introduction .....</b>	<b>28</b>

<b>4.2 Preparation of STP Specimens .....</b>	<b>28</b>
<b>4.3 Axial Compression Experiment .....</b>	<b>30</b>
<b>4.3.1 Test Specimens and Experiment Setup .....</b>	<b>30</b>
<b>4.3.2 Measurements.....</b>	<b>31</b>
<b>4.3.3 Discussion of Results .....</b>	<b>35</b>
<b>4.4 Static Shear Experiments: Inclined Compression Test .....</b>	<b>37</b>
<b>4.4.1 Test Specimens and Experiment Setup .....</b>	<b>37</b>
<b>4.4.2 Measurements.....</b>	<b>38</b>
<b>4.4.3 Discussion of Inclined Compression Test Results .....</b>	<b>43</b>
<b>4.5 Static Shear Experiments: Reverse Cyclic Load Test .....</b>	<b>45</b>
<b>4.5.1 Test Specimens and Experiment Set up .....</b>	<b>45</b>
<b>4.5.2 Measurements.....</b>	<b>46</b>
<b>4.5.2 Discussion of Reverse Cyclic Test Results .....</b>	<b>50</b>
<b>4.6 Dynamic Experiments.....</b>	<b>53</b>
<b>4.6.1 Preliminary Free Vibration Tests using Lumped Beam Masses .....</b>	<b>53</b>
<b>4.6.1.1 Test Specimens and Experiment Setup .....</b>	<b>54</b>
<b>4.6.1.2 Half Power Bandwidth Method .....</b>	<b>55</b>
<b>4.6.1.3 Measurements.....</b>	<b>55</b>
<b>4.6.1.4 Discussion of Results .....</b>	<b>59</b>
<b>4.6.2 Free Vibration Experiment on Known Brand STPs.....</b>	<b>60</b>
<b>4.6.2.1 Measurements.....</b>	<b>60</b>
<b>4.6.2.2 Discussion of Results .....</b>	<b>61</b>
<b>4.6.3 Free Vibration Experiment using Slab Mass .....</b>	<b>62</b>
<b>4.6.3.1 Test Specimens and Experiment Setup .....</b>	<b>62</b>
<b>4.6.3.2 Measurements.....</b>	<b>65</b>
<b>4.6.3.3 Discussion of Results .....</b>	<b>67</b>
<b>4.7 Shaking Table Experiment.....</b>	<b>71</b>
<b>4.7.1 Test Specimens .....</b>	<b>73</b>
<b>4.7.2 Experiment Setup.....</b>	<b>77</b>
<b>4.7.3 Measurements.....</b>	<b>77</b>
<b>4.7.4 Discussion of Results .....</b>	<b>80</b>
<b>4.8 Hypothetical Studies .....</b>	<b>85</b>

<b>CHAPTER 5</b> .....	<b>88</b>
<b>CONCLUSIONS</b> .....	<b>88</b>
<b>REFERENCES</b> .....	<b>91</b>

## LIST OF TABLES

<b>Table 1: Damping Coefficients, <math>B_D</math> or <math>B_M</math> [1]</b> .....	<b>22</b>
<b>Table 2: Compression experiment results</b> .....	<b>35</b>
<b>Table 3: Inclined compression test results</b> .....	<b>44</b>
<b>Table 4: Reverse cyclic test results</b> .....	<b>52</b>
<b>Table 5: Experiment results, <math>f</math>, <math>\zeta</math> and <math>C</math> values</b> .....	<b>58</b>
<b>Table 6: Dynamic experiment -2 results</b> .....	<b>61</b>
<b>Table 7: Dynamic experiment-3 measurements</b> .....	<b>66</b>
<b>Table 8: Principal direction stiffness differences (N/mm)</b> .....	<b>69</b>
<b>Table 9: Maximum accelerations in g (<math>9.81\text{m/s}^2</math>)</b> .....	<b>80</b>
<b>Table 10: Isolation Ratios (max table acc / max building acc)</b> .....	<b>80</b>
<b>Table 11: Effect of soil type on S(T) for STP base isolation</b> .....	<b>86</b>

## LIST OF FIGURES

Figure 1: Force-deformation relationship of an ordinary structure.....	2
Figure 2: Period shift effect by seismic base isolation [4].....	3
Figure 3: Rigid body response [3].....	3
Figure 4: Steel reinforced elastomer isolator, SREI.....	7
Figure 5: Lead-plug rubber bearing.....	7
Figure 6: Friction Pendulum System, FP.....	8
Figure 7: TASS System.....	9
Figure 8: Tire construction line [19].....	12
Figure 9: Details of a car tire [18].....	13
Figure 10: Sections and components of a standard car tire [18].....	13
Figure 11: Tire marking [20].....	14
Figure 12: Design response spectrum.....	21
Figure 13: Seismic Base Isolation System Design Flowchart.....	23
Figure 14: Plan dimensions of a building for calculation of $D_{TD}$ and $D_{TM}$ [5]....	24
Figure 15: Preparation of scrap tire pad (STP).....	29
Figure 16: Compression experiment setup.....	30
Figure 17: $\sigma \sim \varepsilon$ Curve of SREI.....	32
Figure 18: $\sigma \sim \varepsilon$ Curve of G-STP composed of 4 and 6 layers.....	32
Figure 19: $\sigma \sim \varepsilon$ Curve of M-STP.....	33
Figure 20: $\sigma \sim \varepsilon$ Curve of P-STP.....	33
Figure 21: $\sigma \sim \varepsilon$ Curve of L-STP.....	34
Figure 22: Comparison of $\sigma \sim \varepsilon$ Curves for STP and SREI specimens.....	34
Figure 23: Inclined compression test setup [27].....	37
Figure 24: Elastomer isolator under shear force.....	38
Figure 25: H vs. $\Delta_s$ curve for SREI.....	39
Figure 26: H vs. $\Delta_s$ curve for G-STP in longitudinal direction.....	39

<b>Figure 27: H vs. <math>\Delta_s</math> curve for G-STP in transverse direction</b> .....	<b>40</b>
<b>Figure 28: H vs. <math>\Delta_s</math> curve for M-STP in longitudinal direction</b> .....	<b>40</b>
<b>Figure 29: H vs. <math>\Delta_s</math> curve for M-STP in transverse direction</b> .....	<b>41</b>
<b>Figure 30: H vs. <math>\Delta_s</math> curve for P-STP in longitudinal direction</b> .....	<b>41</b>
<b>Figure 31: H vs. <math>\Delta_s</math> curve for P-STP in transverse direction</b> .....	<b>42</b>
<b>Figure 32: H vs. <math>\Delta_s</math> curve for L-STP in longitudinal direction</b> .....	<b>42</b>
<b>Figure 33: H vs. <math>\Delta_s</math> curve for L-STP in transverse direction</b> .....	<b>43</b>
<b>Figure 34: Reverse cyclic test set up</b> .....	<b>46</b>
<b>Figure 35: H vs. <math>\Delta</math> curve for G-STP (N = 150kN, <math>\sigma</math> = 4.16MPa)</b> .....	<b>46</b>
<b>Figure 36: H vs. <math>\Delta</math> curve for G-STP (N = 150kN, <math>\sigma</math> = 4.16MPa)</b> .....	<b>47</b>
<b>Figure 37: H vs. <math>\Delta</math> curve for M-STP (N = 150kN, <math>\sigma</math> = 4.16MPa)</b> .....	<b>47</b>
<b>Figure 38: H vs. <math>\Delta</math> curve for M-STP (N = 150kN, <math>\sigma</math> = 4.16MPa)</b> .....	<b>48</b>
<b>Figure 39: H vs. <math>\Delta</math> curve for P-STP (N = 200kN, <math>\sigma</math> = 5.55MPa)</b> .....	<b>48</b>
<b>Figure 40: H vs. <math>\Delta</math> curve for P-STP (N = 200kN, <math>\sigma</math> = 5.55MPa)</b> .....	<b>49</b>
<b>Figure 41: H vs. <math>\Delta</math> curve for B-STP (N = 300kN, <math>\sigma</math> = 8.33MPa)</b> .....	<b>49</b>
<b>Figure 42: H vs. <math>\Delta</math> curve for B-STP (N = 300kN, <math>\sigma</math> = 8.33MPa)</b> .....	<b>50</b>
<b>Figure 43: Dynamic experiment-1 setup</b> .....	<b>54</b>
<b>Figure 44: Half Power Bandwidth Method</b> .....	<b>55</b>
<b>Figure 45: Test-1 and Test-2 measurements</b> .....	<b>56</b>
<b>Figure 46: Test-3 and Test-4 measurements</b> .....	<b>56</b>
<b>Figure 47: Test-5 and Test-6 measurements</b> .....	<b>57</b>
<b>Figure 48: Test-7 and Test-8 measurements</b> .....	<b>57</b>
<b>Figure 49: Dynamic experiment -1 measurements</b> .....	<b>58</b>
<b>Figure 50: Dynamic experiment-3 setup</b> .....	<b>64</b>
<b>Figure 51: Dynamic experiment-3 results</b> .....	<b>67</b>
<b>Figure 52: Horizontal stiffness differences, predicted versus calculated</b> .....	<b>70</b>
<b>Figure 53: STP models</b> .....	<b>72</b>
<b>Figure 54: Young's modulus vs. shore hardness degree</b> .....	<b>75</b>
<b>Figure 55: Test specimen dimensions</b> .....	<b>76</b>
<b>Figure 56: Test specimens used in shaking table test</b> .....	<b>76</b>
<b>Figure 57: Shaking table experiment setup</b> .....	<b>77</b>

<b>Figure 58: 1999 Bolu Earthquake, 20%.....</b>	<b>78</b>
<b>Figure 59: 1995 Erzincan Earthquake, 20% .....</b>	<b>78</b>
<b>Figure 60: 1995 Kobe Earthquake, 20% .....</b>	<b>79</b>
<b>Figure 61: 1992 Northridge Earthquake, 40%.....</b>	<b>79</b>
<b>Figure 62: Comparison of accelerations during 10% of events.....</b>	<b>82</b>
<b>Figure 63: Comparison of accelerations during 20% of events.....</b>	<b>82</b>
<b>Figure 64: Bolu Earthquake Response Spectrum.....</b>	<b>83</b>
<b>Figure 65: Erzincan Earthquake Response Spectrum .....</b>	<b>83</b>
<b>Figure 66: Kobe Earthquake Response Spectrum.....</b>	<b>84</b>
<b>Figure 67: Northridge Earthquake Response Spectrum.....</b>	<b>84</b>

## LIST OF SYMBOLS

A:	Area
$B_D$ :	Effective damping coefficient
$D_D$ :	Design displacement
$D_M$ :	Maximum displacement
$E_0$ :	Young's modulus
$E_{c,ins}$ :	Instantaneous compression modulus
$E_c$ :	Compression modulus
$E_d$ :	Dissipated energy
$E_{so}$ :	Absorbed energy
G:	Shear modulus
H:	Horizontal load
$K_{angular}$ :	Angular stiffness
$K_{eff}$ :	Effective horizontal stiffness
$K_H$ :	Horizontal stiffness
$K_{H0}$ :	Horizontal stiffness at zero axial load
$K_V$ :	Vertical stiffness
$K_\theta$ :	Rotational stiffness
LVDT:	Displacement transducer
M:	Mass
P:	Vertical load on an elastomer isolator
$P_{crit}$ :	Vertical buckling load of an elastomer isolator
R:	Radius of surface of friction pendulum isolator
S:	Shape factor
$S_1$ :	Spectral acceleration for period (T=1 sec)
$S_{D1}$ :	Design considered 5% damped spectral acceleration
$S_{M1}$ :	Maximum considered 5% damped spectral acceleration

SREI:	Steel reinforced elastomeric isolator
STP:	Scrap tire pad
T:	Period
$T_D$ :	Effective design period
V:	Shear load, horizontal load
W:	Vertical compression load
a:	Side dimension of square elastomer isolator
g:	Gravitational acceleration
$h_p$ :	Pad total thickness
s:	Surface slope of the aluminum plates
t:	Thickness of rubber layer
$t_r$ :	Total thickness of the rubber
$\beta_{eq}$ :	Equivalent damping coefficient
$\gamma$ :	Shear strain
$\Delta, \Delta_s$ :	Horizontal displacement
$\varepsilon$ :	Axial strain
$\zeta$ :	Damping ratio
$\sigma$ :	Compression stress
$\ddot{u}_g$ :	Ground motion acceleration
$\Phi$ :	Diameter of circular elastomer isolator

## CHAPTER 1

### INTRODUCTION

#### 1.1 Philosophy of Seismic Base Isolation

All of the engineered structures should satisfy the basic equation below. The capacity of the structures should always be greater than the demand on the structures [1].

$$\text{CAPACITY} > \text{DEMAND} \quad (1)$$

In conventional earthquake resistant design method, the engineer can obtain the solution of Equation 1 either by:

- ✓ increasing the capacity of the structure, or
- ✓ limiting the demand by considering the ductility of the structure.

The first solution above requires enlargement of the structural member sizes to increase the capacity of the structure, which is not an economical way to solve the problem. Thus, the conventional design codes prefer latter option, which is a more economical solution.

The lateral force vs. lateral displacement curve of a building is similar to the curve shown in Figure 1. The conventional design codes assume that, in cases of small and medium ground motions, the structure stays in elastic range. However, in case of a strong ground motion, it is accepted that the structure passes beyond the elastic limit. If the structural members have enough ductility, the structure shows high level of

displacements and does not collapse and survives a severe earthquake [2]. Hence, the conventional codes give ductility requirements for the designer to obey. The high levels of displacements cause considerable damage on both structural and non-structural members of a building. Plastic hinges occur at the connections of columns and girders. The building may not be functional after a strong earthquake because of the damage observed on structural members. Furthermore, large inter-story drifts may create significant damage on non-structural members such as infill walls and windows.

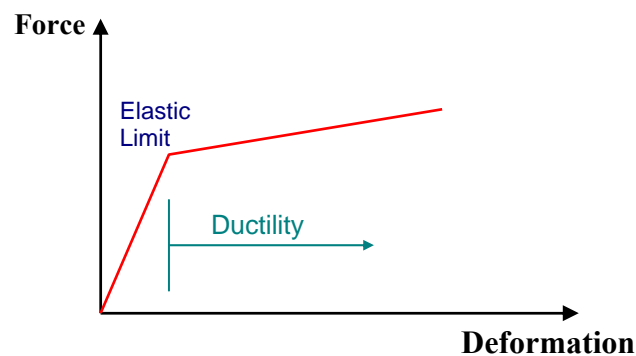


**Figure 1:** Force-deformation relationship of an ordinary structure

Seismic base isolation takes a different approach to the earthquake resistant design problem. Instead of increasing the capacity of the structure or detailing for the ductility of the structural system, it rather attempts to reduce the seismic demand by modifying the dynamic response of the structure. Seismic base isolation is simply composed of laterally flexible system located under the isolated superstructure. As shown in Figure 2, the base isolation system shifts natural period of the structural system from about 0.1-0.9 seconds to 2.0-3.0 seconds and reduces the spectral accelerations that structure responds. Inter-story drifts are considerably decreased and the superstructure on the isolation system behaves like a rigid body as shown in Figure 3 [3]. Hence, the structural members of the isolated building do not suffer any damage during a strong ground motion. After the event, even nonstructural elements of the isolated buildings continue to perform their functions without any corruption.

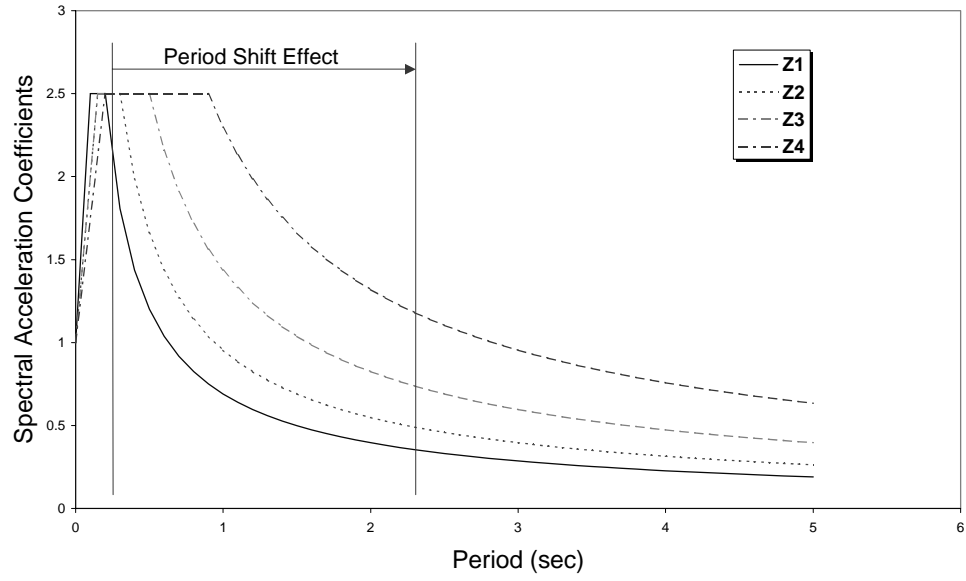


**Figure 2:** Period shift effect by seismic base isolation [4]

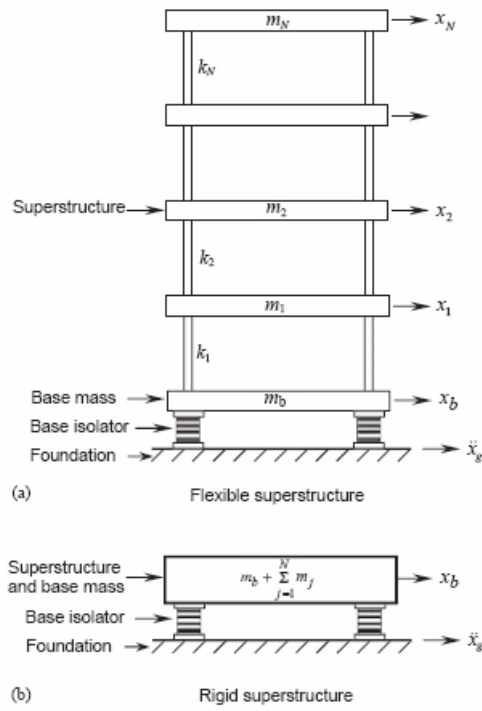


**Figure 3:** Rigid body response [3]

## **1.2 Scope of the Study**

This thesis focuses on the experimental studies conducted on the development of low-cost seismic base isolation bearings using scrap automobile tires. Numerous studies have been conducted on seismic base isolation systems for almost a quarter decade. Although majority of the studies focus on the performance improvement of the base isolation systems, this study aims at cost and weight reduction in seismic base isolation pads by recycling otherwise useless material: scrap tires.

In elastomer isolators, steel or fiber reinforcement vulcanized with rubber provides high vertical stiffness, whereas rubber segments between reinforcement layers provide low horizontal stiffness for the seismic base isolation.

Since 1960's, automobile tires have been produced by means of vulcanizing rubber with steel mesh in different forms which has a similar effect as the steel plates or fibers inside the conventional elastomer-based isolators. Therefore, rectangular shaped layers cut from tread sections of used tires and then piled on top of each other to form Scrap Tire Pad (STP) can function as an elastomeric pad.

In order to search for the mechanical properties of STPs an experiment program was planned. A commercially available Steel Reinforced Elastomeric Isolator (SREI) was also tested and the results of SREI were compared with STP results.

Throughout the experiment program, an axial compression experiment, large deformation-static shear experiments, small deformation-free vibration experiments and a shaking table experiment were conducted. The specimens were tested for different numbers of tire layers, tire brands, dimensions and directions.

The axial compression test was performed to determine and compare the compressive behavior of STP and SREI specimens. Static shear experiments were conducted to obtain the horizontal behavior of the specimens under large shear strains. Dynamic free vibration tests were conducted to obtain the damping ratio and

small-strain-horizontal-stiffness values of STP specimens. As a final stage of the experiment schedule, a shaking table test was performed. A set of four scaled STP models, which are composed of non-vulcanized steel and rubber sheet piles, were used to isolate a  $\frac{1}{4}$  scaled masonry building under four different earthquake motions.

Literature survey performed on seismic base isolation, history of rubber, and tire technology are presented in Chapter 2. Since, scrap tire pad (STP) concept is thought to be related mainly with steel reinforced elastomeric isolators (SREI), mechanical properties, design procedures and code provisions of SREI are examined in Chapter 3. The experimental program is presented in Chapter 4. Chapter 5 includes conclusions of the thesis study.

## CHAPTER 2

### LITERATURE REVIEW

#### 2.1 Development of Seismic Base Isolation Systems

A medical doctor named J.A. Calanterients, in 1909, proposed the first seismic base isolation method. His isolation system was totally based on sliding. Mr. Calanterients claimed that if a structure is built on a fine material such as sand, mica, or talc, this fine soil would let the superstructure to slide during an earthquake. Hence, the horizontal force transmitted to the building would be reduced and the structure would survive the event. Although the isolation system that Mr. Calanterients proposed was a primitive earthquake resistant design, the basic idea behind his method is same with the philosophy of seismic base isolation today [5].

Early examples of seismic base isolation methods were composed of sliding basement, balls, sliding rollers etc. John Milne, who was a Professor of Mining Engineering in University of Tokyo, performed his first seismic base isolation experiments with sliding balls. He began his tests with rollers that are 10 inches in diameter. However, in order to improve the wind resistance of his seismic isolation system he reduced the diameter of his sliders to  $\frac{1}{4}$  inches at the end of his studies [6].

Till the ends of 70's, a few seismically isolated buildings were constructed in Japan. It was the development of laminated elastomer isolators that made seismic base isolation a practical method of earthquake resistant design [5]. First, rubber was used under building basements to isolate the structures. Steel plates were then vulcanized with rubber in order to increase the vertical stiffness of the isolators (Figure 4).

Today steel reinforced elastomeric isolators (SREI) are being used for seismic base isolation of several types of structures; such as residential buildings, governmental buildings, bridges, industrial structures, LPG tanks, etc.

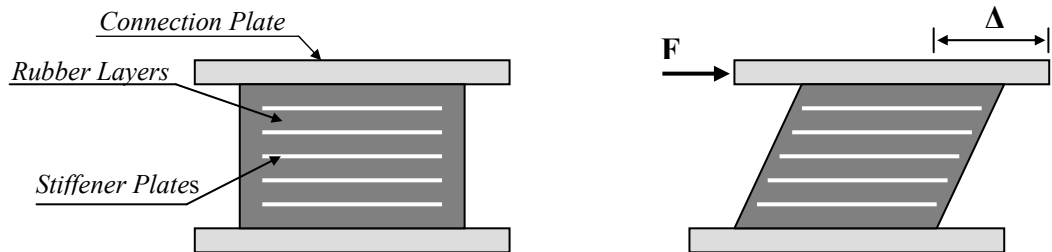


**Figure 4:** Steel reinforced elastomer isolator, SREI

Lead-plug rubber bearings are steel reinforced elastomeric isolators with one or more circular holes as shown in Figure 5 [5]. The lead-plug is inserted in these holes in order to increase the damping of the isolator. However, addition of damping may increase the contribution of secondary modes on the structure response. This may decrease the efficiency of the isolation system. Hence, lead-plug rubber isolators are used with enough number of SREIs to achieve the required superstructure response.

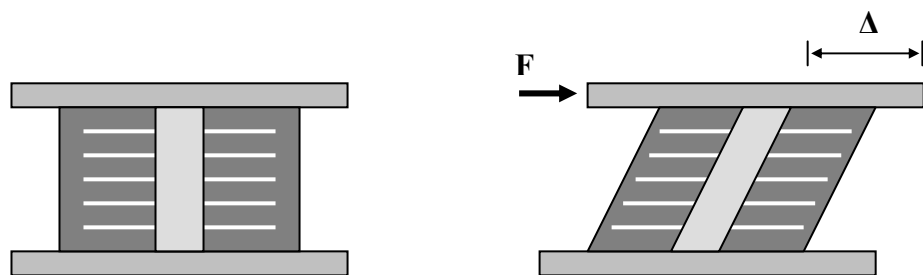


**Figure 5:** Lead-plug rubber bearing

SREI samples used under buildings are too heavy because of steel plates inside the isolators. This heaviness makes both production and construction of elastomeric isolators difficult. This causes significant increase in the cost of the system. In order to achieve this problem, Kelly et al. tried to use lightweight fiber reinforcement inside the elastomeric isolators [7].

Fiber-reinforced elastomeric isolators are a newly introduced concept in the field of seismic base isolation. Kang et al. searched for hole and lead plug effect on fiber reinforced elastomeric isolators [8]. The elasticity of the fiber material is a factor affecting the compression modulus of fiber reinforced elastomeric isolators. Tsai, Kelly and Takhirov conducted admirable experimental and analytical studies on compression behavior of fiber reinforced elastomeric isolators [9, 10, 11, 12].

Early proposed sliding-based seismic isolation methods were deficient to re-center the building to its original location. Zayas et al. studied friction pendulum system in order to handle re-centering deficiency of sliding rollers [13]. The system is composed of two concave Teflon spherical surfaces with an articulated slider in-between these concave surfaces. FP is capable of re-centering the superstructure to its original position with the help the horizontal component of the weight of the structure resting on the isolation system. The energy dissipation is ensured through the friction between the surface of the concave plates and the articulated slider that are presented in Figure 6.

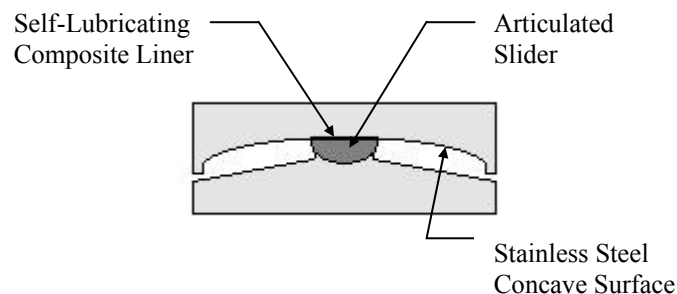


**Figure 6:** Friction Pendulum System, FP

As indicated in Equation 2 below, the period of the structure resting on friction pendulum system depends on the radius of the concave surface of FP system but not the mass of the superstructure. This property of FP system enabled seismic base isolation of lightweight structures also.

$$T = 2 \cdot \pi \cdot \sqrt{\frac{R}{g}} \quad (2)$$

The TASS system, the Resilient-Friction Base Isolator System, Sliding Disc Bearing and Helical Spring system are the other common restoring systems used to isolate the structures [14, 15]. In TASS system, parallel rubber blocks provide the re-centering capability. Resilient-Friction Base Isolator system is composed of Teflon-coated steel plates with a rubber core to enable re-centering of the isolation system. A building isolated with Sliding Disc Bearing and Helical Spring system slides on Teflon bearings and re-center to its original location with the help of helical springs.

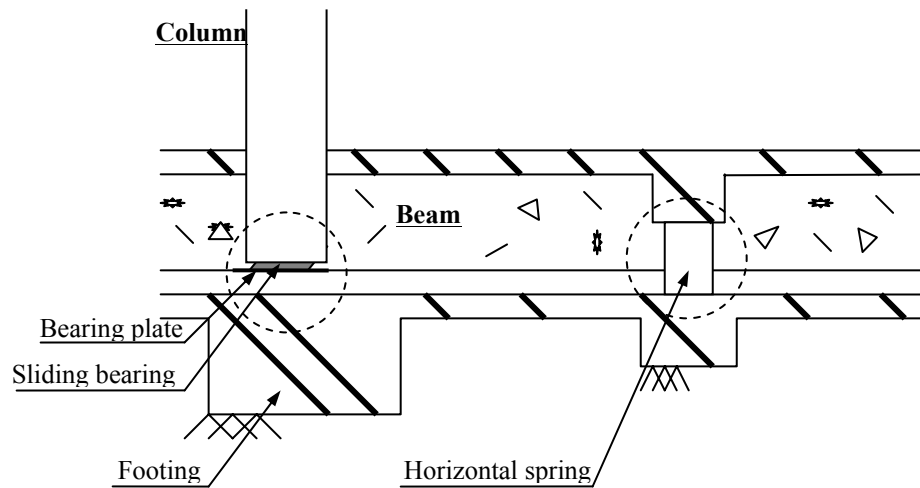


**Figure 7: TASS System**

## 2.2 History of Rubber and Tire Technology

Tires that we use in our cars today are being produced from *synthetic rubber* that is an end product of petroleum. The development of tire production process is inspired by the interest in improving the performance of *natural rubber*.

Natural rubber is one of the most important products to come out of rainforests. It is obtained from *Hevea Brasiliensis*, a tree indigenous to South America, where it grows wild to a height above 30 meters. Natural rubber is extracted in the form of *latex* from Hevea tree. Once it is collected in this form, it can be coagulated using acids and then rolled into sheets where the many different manipulations can then be done [16].

In industrial age, natural rubber was first used for making waterproof fabrics and a wide range of other consumer and industrial goods. However, natural rubber products are best appreciated at room temperature only. In cold weather rubber products froze stiff and cracked. In the high heat of summer, rubber products melted down to useless, glue-like dough.

In 1839, Charles Goodyear tried mixing rubber with various dry powders, seeking a way to absorb the stickiness of native rubber and to make it not just waterproof, but also weatherproof. In that year, he accidentally dropped a piece of rubber and sulfur on a hot stovetop, causing it to a char like leather yet remains plastic and elastic. In the following years, Goodyear experimented with ways to perfect this process. He got the best results by applying steam heat, under pressure, for four to six hours at 270 degrees Fahrenheit [17].

Vulcanization, a refined version of this process, transformed the white sap from the bark of the Hevea tree into an essential product for the industrial age. The development of the inflatable rubber tire not only provided rubber with its biggest market; it made the automotive industry possible also. Today, automobile tires are

being produced by means of vulcanizing steel cords within rubber in different forms and sizes.

### **2.3 Construction of Tire and Tire Terminology**

Since this study searches using scrap automobile tires as seismic base isolators, brief information about tire production and terminology should be presented here in the manuscript.

Automobile tires are produced via processing rubber, textile and steel cords together in a production line shown in Figure 8. First, raw materials rubber and chemicals are treated together in a special mixer and prepared for tire construction process. In the mean time in another workbench, fabric and steel cords are manufactured from textiles and steel respectively.

In following steps, tire components bead, tread and sidewalls are produced. Then, as a final step, all the components are merged and the tire is constructed. The rest of the steps are composed of curing and some inspections for improving the performance of the end product “tire”.

Tire producers use a terminology in order to define the components of tire. Figure 9 and Figure 10 are presented below for defining these components of a standard car tire.

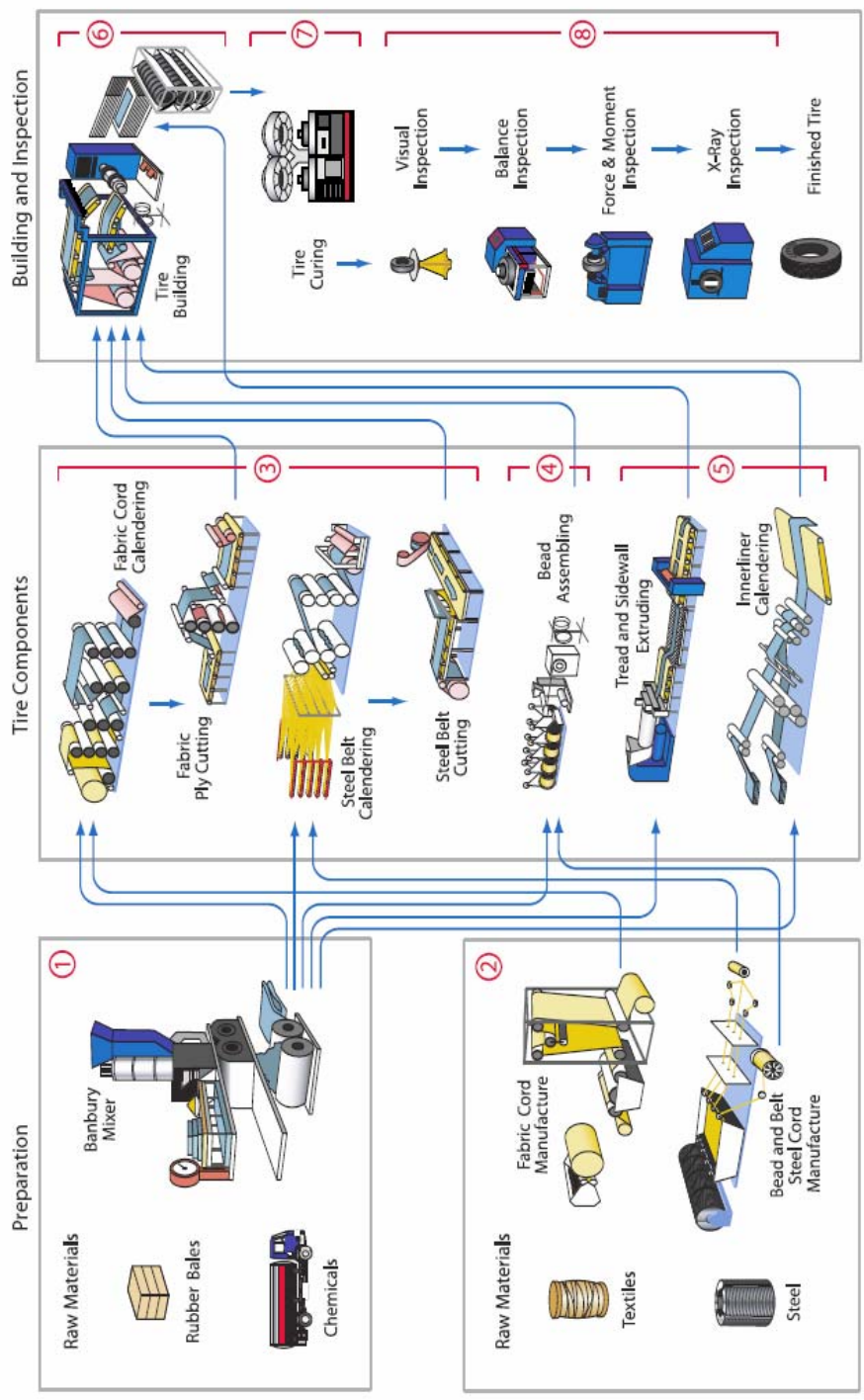


**Figure 8:** Tire construction line [19]

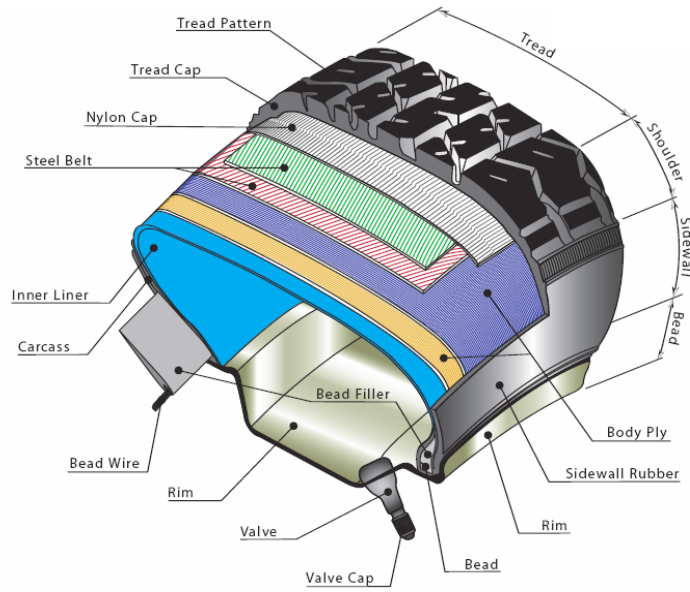


**Figure 9:** Details of a car tire [18]

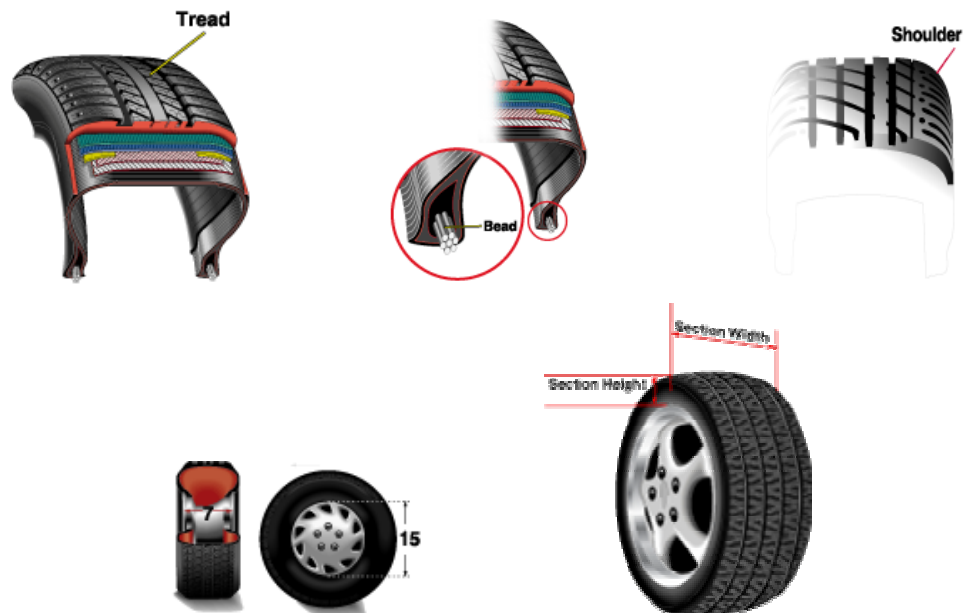


**Figure 10:** Sections and components of a standard car tire [18]

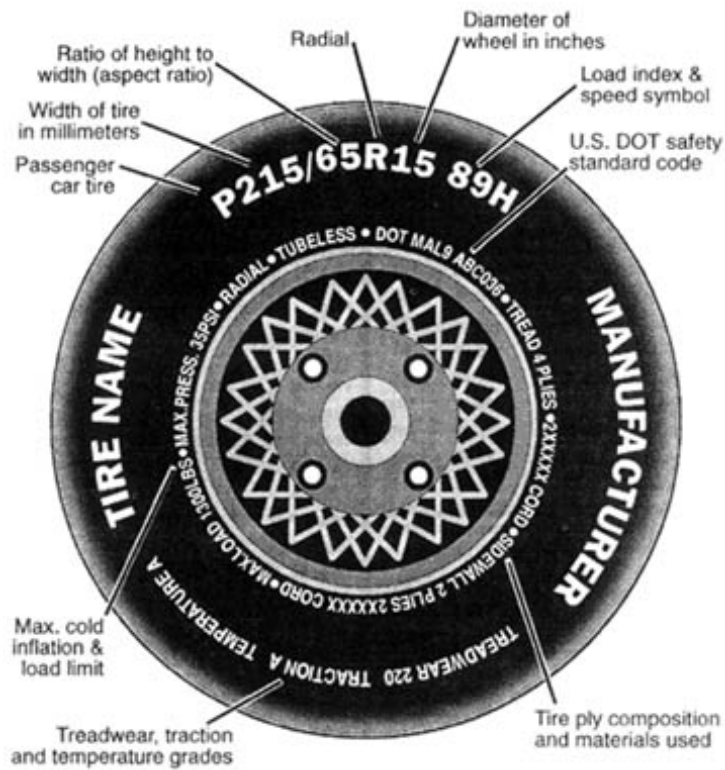


**Figure 11:** Tire marking [20]

Automobile tires are marked with a special designation of numbers that is defined by international tire producer organizations such as T&RA and ETRTO. These numbers are written on tire sidewalls and represent tread, sidewall and rim dimensions. For instance the first number in the designation “215 / 65R15” in Figure 11 denotes that tread section is 215mm wide. Second number “65” shows the percentage of the section height to the section width. The last number “15” designates the diameter of the rim in inches. The rest gives some special information about the load and the velocity that the tire should be applied through its lifetime.

## CHAPTER 3

### ELASTOMERIC ISOLATORS

#### 3.1 Introduction

The design of seismic base isolation systems is an iterative procedure similar to the other common design methods. Hence, the speed of the seismic base isolation system design is mainly based on the designer's experience on the issue. The steps of the design procedure can be conducted easily by either using spreadsheets or developing own design software programs.

The design of seismic base isolation systems begin with a preliminary design step on which the structural mass and vertical loads on the isolators are calculated. After the target period of the isolated structure is assumed, the required horizontal stiffness is determined. Then, the maximum horizontal displacement that the isolator should satisfy is computed. Finally, a seismic base isolation system is designed in accordance with the parameters of vertical load capacity, target period, required horizontal stiffness, horizontal displacement limit and stability of the isolation system.

The mechanical characteristics and code provisions of elastomeric isolators are presented in the following sections of the manuscript. The information given here are mainly based on several chapters from Naeim and Kelly [5] book and IBC 2000 [21].

### 3.2 Mechanical Characteristics of Elastomeric Isolators

The vertical stiffness of a structure is high enough to withstand vertical components of ground motion. However, it is the horizontal component of the event which engenders seismic damage on buildings. Hence, the most important property of elastomeric isolators is the horizontal stiffness calculated by Equation 3 below.

$$K_H = \frac{G \cdot A}{t_r} \quad (3)$$

In the above equation,  $G$  stands for shear modulus of the elastomer,  $A$  is the cross-sectional area of the isolator and  $t_r$  is the total thickness of rubber.

The vertical frequency of an isolated structure is dominated by vertical stiffness of the isolation system and should be excessively larger than the horizontal frequency of the isolated structure in order to prevent rocking motion of the superstructure. The vertical stiffness of an elastomeric isolator is computed using Equation 4.

$$K_V = \frac{E_C \cdot A}{t_r} \quad (4)$$

$E_C$  stands for the instantaneous compression modulus of a single layer of rubber corresponding to the level of vertical load acting on the isolator. As shown in Equation 5, Tsai showed that the total compression modulus of a laminated rubber isolator is equal to the compression modulus of a single layer of that isolator [10]. The rubber layers can be assumed as springs in series.

$$(E_C)_{rigid} = \frac{n}{\sum_{i=1}^n \frac{1}{E_C^{(i)}}} = \frac{\#}{\frac{\#}{E_C^i}} = E_C^i \quad (5)$$

Lindley defines compression modulus ( $E_C$ ) as a vertical behavior parameter for rubber which is dependent on Young's modulus ( $E$ ) and shape factor ( $S$ ) of the

rubber segment [22]. Since rubber is accepted as an incompressible material with almost  $\nu \approx 0.5$ , modulus of elasticity of rubber is equal to three times the shear modulus of rubber ( $E = 3G$ ). Then;

$$E_C = 3 \cdot G \cdot (1 + 2 \cdot S^2) \quad (6)$$

$$S = \frac{\text{Loaded area}}{\text{Force free area}} \quad (7)$$

Shape factor ( $S$ ) is a dimensionless factor of aspect ratio of the single layer of rubber. The loaded area in Equation 7 refers to the area of contact surface, and force free area refers to the side surface area of a single layer of rubber. For instance, for a square elastomer isolator having side dimension “ $a$ ” and thickness “ $t$ ”,  $S$  is calculated to be:

$$S = \frac{a}{4 \cdot t} \quad (8)$$

For a circular isolator having diameter of  $\Phi$ ,  $S$  similarly yields to be:

$$S = \frac{\Phi}{4 \cdot t} \quad (9)$$

Kelly [5] defines compression modulus ( $E_C$ ) for circular isolator as shown in Equation 10.  $E_C$  for square bearings is also given in Equation 11.

$$E_C = 6 \cdot G \cdot S^2 \quad (10)$$

$$E_C = 6.73 \cdot G \cdot S^2 \quad (11)$$

### 3.3 Stability of Elastomeric Bearings

The stability of elastomeric isolators depends on the ratio of vertical load on the isolator to the critical buckling load. The critical buckling load for a *circular* steel reinforced elastomer bearing is obtained by Equation 12.

$$P = \left( G \cdot A \cdot \frac{h}{t_r} \right)^{\frac{1}{2}} \cdot \left( \frac{\pi^2}{h^2} \cdot \frac{1}{3} \cdot 6 \cdot G \cdot S^2 \cdot A \cdot r^2 \cdot \frac{h}{t_r} \right)^{\frac{1}{2}} \quad (12)$$

The radius of gyration is denoted by  $r = \sqrt{I/A} = \Phi/4$  for a circular bearing with diameter  $\Phi$ . The critical buckling load given above can also be calculated by using the simplified Equation 13 below for circular steel reinforced elastomer isolators.

$$P_{crit} = \frac{\sqrt{2} \cdot \pi \cdot G \cdot A \cdot S \cdot r}{t_r} \quad (13)$$

The horizontal stiffness dependence on axial load is approximated by Buckle and Kelly as shown in Equation 14 [23, 24].  $P$  in Equation 14 stands for the axial load on the isolator.  $K_{H0}$  is stiffness at zero axial load level and  $K_{eff}$  is the corresponding modified stiffness at that axial load level. The vertical load on a seismic isolator has a minimizing effect on horizontal stiffness of the isolator.

$$K_{eff} = K_{H0} \cdot \left[ 1 - \left( \frac{P}{P_{crit}} \right)^2 \right] \quad (14)$$

### 3.4 Code Provisions for Isolated Structures and Base Isolation Systems

The design procedure of seismically isolated structures and seismic base isolation systems should be based on national or international codes or standards. There is no any referable code for seismic base isolation in Turkey yet. Uniform Building Code 1997 (UBC-1997) and International Building Code 2000 (IBC 2000) are the two of the well-known design codes, which have chapters for design of seismic base isolation. In IBC 2000, provisions for the seismic base isolation system are also available.

The provisions in IBC 2000 for seismically isolated structures and seismic base isolation systems are summarized below.

In the code, the selection of the design procedure depends on some specific requirements which are peculiar to the selected method. On the condition that the requirements are satisfied, the designer decides to use one of the three procedures which are equivalent-lateral force procedure, response-spectrum analysis procedure and time-history analysis procedure. The structural engineer needs to perform equivalent-lateral-force procedure in all of his base isolation designs. Thus, he would be able to state a minimum level for design displacements and forces. The equivalent-lateral-force procedure is also practical for the preliminary design of the seismic base isolation system [5].

The equivalent-lateral-response procedure is permitted in IBC 2000 provided that the structure satisfies the following requirements:

- The structure is located at a site with  $S_I$  (spectral acceleration for  $T=1$ sec) less than or equal to  $0.60g$ ;
- The structure is located on a Class A, B, C, or D site;
- The structure above the isolation interface is less than or equal to four stories or  $19.8$  m ( $65$  ft) in height;

- The effective period of the isolated structure at maximum displacement,  $T_M$ , is less than or equal to 3.0 sec;
- The effective period of the isolated structure at the design displacement,  $T_D$ , is greater than three times the elastic, fixed-base period of the structure above the isolation system;
- The structure above the isolation system is of regular configuration; and
- The isolation system meets the following criteria:
  - The effective stiffness of the isolation system at the design displacement is greater than one third of the effective stiffness at 20% of the design displacement,
  - The isolation system is capable of producing restoring forces,
  - The isolation system has force-deflection properties that are independent of the rate of loading,
  - The isolation system has force-deflection properties that are independent of vertical load and bilateral load, and
  - The isolation system does not limit maximum considered earthquake displacement to less than  $S_{M1}/S_{D1}$  times the total design displacement.

In accordance with section 1623.1.3.5 of IBC 2000, the isolated structures which do not satisfy the requirements presented above should be designed using dynamic analysis. Response-spectrum analysis can be used in cases that:

- The structure is located on a Class A, B, C, or D Site; and
- The isolation system meets the last item that is required for equivalent-lateral-force procedure application.

Otherwise, time-history analysis should be conducted for the design of all seismically isolated structures that do not satisfy the requirements above.

### 3.4.1 Equivalent-Lateral Force Procedure

According to the code, the isolation system needs to be designed to resist minimum displacements and forces specified with this static analysis method.

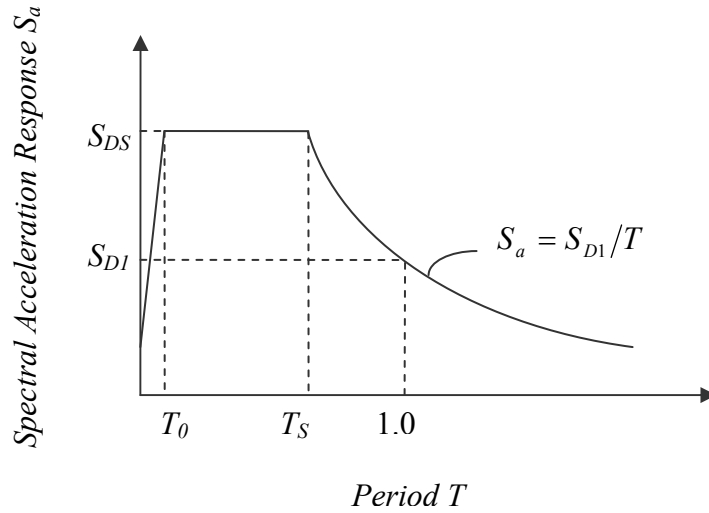


**Figure 12:** Design response spectrum

The design displacement ( $D_D$ ) that the seismic base isolation system should withstand is obtained by Equation 15.  $g$  stands for the acceleration of gravity.  $S_{D1}$  is the design 5% damped spectral acceleration at 1 second period [21].

$$D_D = \frac{g \cdot S_{D1} \cdot T_D}{4 \cdot \pi^2 \cdot B_D} \quad (15)$$

$T_D$  is the effective period of the isolated structure in seconds, and  $B_D$  is a numerical coefficient related to the effective damping of the isolation system at the design displacement and can be taken from Table 1.

**Table 1:** Damping Coefficients,  $B_D$  or  $B_M$  [1]

<b>Pad Effective Damping, <math>\beta_D</math> or <math>\beta_M</math> (Percentage of Critical)</b>	<b><math>B_D</math> or <math>B_M</math> Factor</b>
$\leq 2\%$	0.8
5%	1.0
10%	1.2
20%	1.5
30%	1.7
40%	1.9
$\geq 50\%$	2.0

The effective period of the isolated structure at the design displacement ( $T_D$ ) is found by using Equation 16.  $W$  is the total weight above the isolation system. The value of  $W$  is calculated in kN (kips) according to IBC 2000. Variable  $k_{Dmin}$  stands for the minimum effective stiffness in kN/m (kips/in.) of the isolation system at the design displacement in the horizontal direction under consideration.

$$T_D = 2\pi \cdot \sqrt{\frac{W}{k_{Dmin} \cdot g}} \quad (16)$$

The isolation system should not only withstand the design displacement but also the maximum lateral displacement in the most critical direction, which is calculated using Equation 17.

$$D_M = \frac{g \cdot S_{M1} \cdot T_M}{4 \cdot \pi^2 \cdot B_M} \quad (17)$$

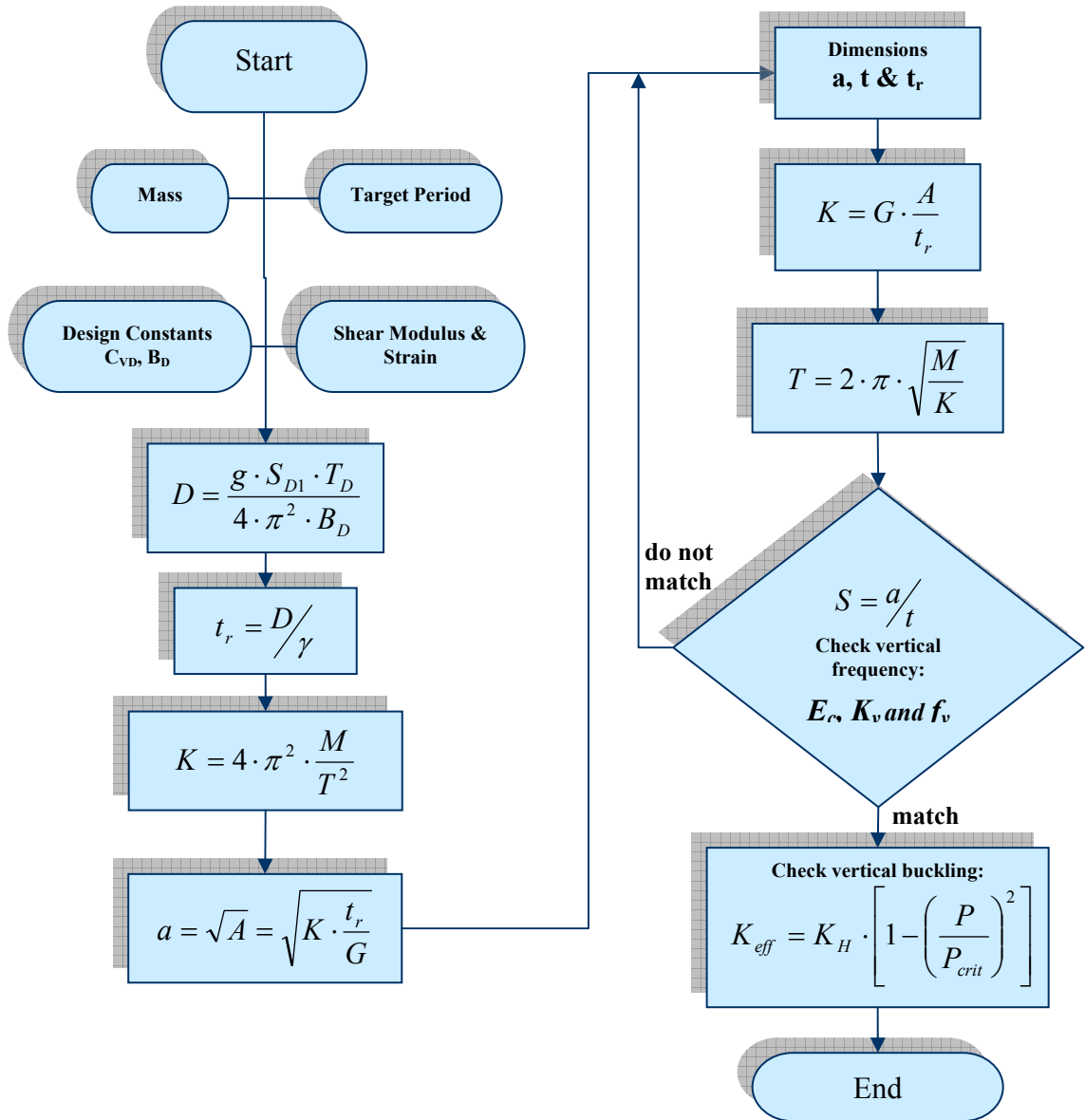


**Figure 13:** Seismic Base Isolation System Design Flowchart

$S_{MI}$  is the maximum considered 5% damped spectral acceleration at 1.0 second period.  $B_M$  is taken from Table 1623.2.2.1 of the code, which is also given in Table 1. The effective period ( $T_M$ ) of seismically isolated structure at the maximum displacement is calculated in accordance with Equation 18. Variable  $k_{Mmin}$  is the minimum effective stiffness of the isolation system at the maximum displacement in the horizontal direction under consideration.

$$T_M = 2\pi \cdot \sqrt{\frac{W}{k_{M \min} \cdot g}} \quad (18)$$

In conventional seismic design procedures, the buildings are first examined in the principle directions of the plan of the building. Then, the final design includes the accidental torsion and mass eccentricity of the building. Similarly, the design of seismic base isolation systems should also include the additional displacements due to actual and accidental torsion calculated from the spatial distribution of the lateral stiffness of the isolation system and the eccentricity of the location of the mass center. Thus, the total design displacement ( $D_{TD}$ ) and the total maximum displacement ( $D_{TM}$ ) are calculated according to the Equation 19 and Equation 20, respectively. The variables  $y$ ,  $e$ ,  $b$ , and  $d$  are shown in Figure 14 below.

$$D_{TD} = D_D \left[ 1 + y \frac{12e}{b^2 + d^2} \right] \quad (19)$$

$$D_{TM} = D_M \left[ 1 + y \frac{12e}{b^2 + d^2} \right] \quad (20)$$

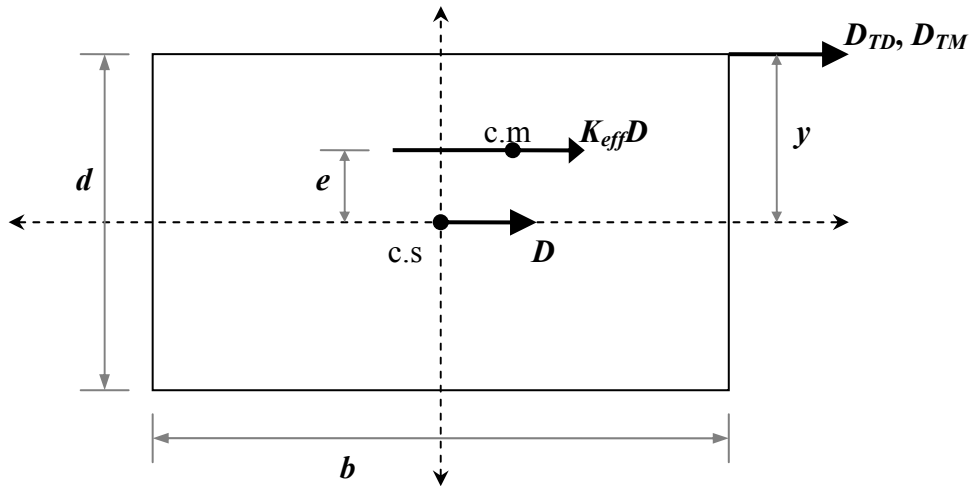


**Figure 14:** Plan dimensions of a building for calculation of  $D_{TD}$  and  $D_{TM}$  [5]

The foundation, all structural elements below the isolation system and the isolation system itself should withstand the lateral seismic force ( $V_b$ ), which is calculated using the Equation 21. Parameter  $k_{D_{max}}$  is the maximum effective stiffness in kN/m (kips/in.) of the isolation system at the design displacement. Structural elements above the isolation system should be designed to withstand the shear force ( $V_s$ ) above the isolation system which is calculated by the Equation 22. The  $R_I$  factor is a seismic load reduction (ductility) factor related with the type of the lateral-force-resisting system of the building above the isolation system.

$$V_b = k_{D_{max}} D_D \quad (21)$$

$$V_s = \frac{k_{D_{max}} D_D}{R_I} \quad (22)$$

The value of  $R_I$  will be taken as the 3/8 of the  $R$  values presented in the Table 9.5.2.2 of IBC 2000. The lower bound of RI value is 1.0 whereas the upper bound is 2.0 ( $1.0 \leq R_I = 3/8 R \leq 2.0$ ).

### 3.4.1 Required Tests for Seismic Base Isolation Systems

Seismic base isolations system deformation characteristics and damping values should be based on tests performed on the selected samples. In IBC 2000 section 1623.8, these prototype tests are summarized.

In accordance with the code, the tests should be conducted for two full-size specimens and these specimens should not be used in the construction after test is performed. The force-deflection behavior of the specimen should be recorded for each cycle of the experiment.

The code also gives the sequence and the requirements of the cycles that will be carried on the specimens. The tests should be performed at a vertical load of the sum of the dead load effect and the half of the live load effect on the common type of the isolators.

1. Twenty fully reversed cycles of loading at a lateral force corresponding to the wind load
2. Three fully reversed cycles of loading at each of the increments of the total displacement;  $0.25 D_D$ ,  $0.5 D_D$ ,  $1.0 D_D$ , and  $1.0 D_M$ .
3. Three fully reversed cycles of loading at the total maximum displacement,  $1.0 D_{TM}$ .
4.  $15 S_{D1} B_D / S_{DS}$ , but not less than 10, fully reversed cycles of loading at one total design displacement,  $1.0 D_{TD}$ .

If an isolator is also vertical-load carrying unit, then item 2 presented should be performed also for the two additional following load combinations:  $1.2D + 0.5L + |E|$  and  $0.8D - |E|$ .

The force-deflection characteristics of the isolation system are based on the cyclic load tests of the isolator prototypes. The effective lateral stiffness of the isolator is calculated by the following equation where  $F^+$  and  $F^-$  are the positive and the negative forces at  $\Delta^+$  and  $\Delta^-$  displacements.

$$k_{eff} = \frac{|F^+| + |F^-|}{|\Delta^+| + |\Delta^-|} \quad (23)$$

The effective damping of the isolator shall be calculated for each cycle of loading by Equation 24 below considering the energy dissipated by each cycle, the effective stiffness of the isolator and the peak displacements.

$$\beta_{eff} = \frac{2}{\pi} \cdot \left[ \frac{E_{loop}}{k_{eff} \cdot |\Delta^+| + k_{eff} \cdot |\Delta^-|} \right] \quad (24)$$

Maximum and minimum effective stiffness values of the isolated system at design displacement values,  $k_{Dmax}$  and  $k_{Dmin}$  shall be based on the cyclic tests and Equations 25 and 26 will be used to calculate these values.

$$k_{D\max} = \frac{\sum |F_D^+|_{\max} + \sum |F_D^-|_{\max}}{2 \cdot D_D} \quad (25)$$

$$k_{D\min} = \frac{\sum |F_D^+|_{\min} + \sum |F_D^-|_{\min}}{2 \cdot D_D} \quad (26)$$

Maximum and minimum effective stiffness values of the isolated system at maximum displacement values,  $k_{M\max}$  and  $k_{M\min}$  shall be based on the cyclic tests and Equations 27 and 28 will be used to calculate these values. These values will be obtained from the results of the item 2 provided above.

$$k_{M\max} = \frac{\sum |F_M^+|_{\max} + \sum |F_M^-|_{\max}}{2 \cdot D_M} \quad (27)$$

$$k_{M\min} = \frac{\sum |F_M^+|_{\min} + \sum |F_M^-|_{\min}}{2 \cdot D_M} \quad (28)$$

The effective damping values will be based on the results of item 2 again and calculated by Equation 29 below for the design displacement.

$$\beta_D = \frac{1}{2\pi} \cdot \left[ \frac{\sum E_D}{k_{D\max} \cdot D_D^2} \right] \quad (29)$$

At maximum displacement, the effective damping will be calculated by Equation 30 below.

$$\beta_M = \frac{1}{2\pi} \cdot \left[ \frac{\sum E_M}{k_{M\max} \cdot D_M^2} \right] \quad (30)$$

## CHAPTER 4

### EXPERIMENTS

#### 4.1 Introduction

This chapter focuses on the experimental studies performed for the development of scrap tire pads (STP). In order to obtain the basic design parameters and investigate the behavior of STPs under compression and shear forces, several tests have been conducted on specimens prepared from various tire brands.

Axial compression tests have been performed to obtain the compression behavior of STP specimens. Two types of static shear experiments have been performed to obtain the large deformation-horizontal behavior of STPs. Three dynamic free vibration experiments were conducted to obtain damping ratios of STP specimens. Finally, a ¼ scaled masonry house was isolated using artificially manufactured scrap tire models and tested on the shaking table available in the METU Structural Mechanics Laboratory. The results and conclusions of the experiments are summarized in the following chapter.

#### 4.2 Preparation of STP Specimens

*Scrap tires* are old used car tires (Figure 15a). The existence of scrap tires on rubbish areas is an earnest threat for the health of both community and environment. *Tire ring* is the part that touches ground (tread) after the sidewalls of the tire is removed by cutting off (Figure 15b). *Tire band* is the same part after cutting the ring in transverse direction (Figure 15c). *Tire layers* are 20 cm long pieces of scrap tire band (Figure 15d). *Scrap tire pad (STP)* is formed when a set of scrap tire layers are placed on each other (Figure 15e). Tire layers composing STP may be fixed together

with using glue or any adhesive. However, they may just be put on each other since the frictional force between tire layers would be high enough to maintain the stability of STP layers.



(a)



(b)



(c)



(d)



(e)

**Figure 15:** Preparation of scrap tire pad (STP)

### 4.3 Axial Compression Experiment

The objective of this experiment was to obtain the behavior of STP and available SREI specimens under compression. The specimens were tested in compression machine under cycling loading. Vertical load applied and corresponding vertical displacement was recorded simultaneously. The results are presented as graphical data in the following pages. The results of STP specimens were compared with the results of the SREI specimen.

#### 4.3.1 Test Specimens and Experiment Setup

STP specimens experimented in compression machine were produced from four well-known tire brands, which will be referred by letters G, M, P, and L here. The trademarks of the specimens will not be mentioned in the manuscript. The SREI specimen was a standard 150mm x 150mm x 40mm elastomeric bridge bearing with a single layer of 3mm steel reinforcement.

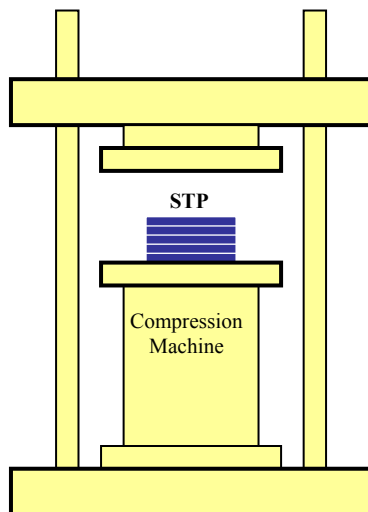


**Figure 16:** Compression experiment setup

The experiment setup given above is composed of a compression machine with 300 tons vertical load capacity, four displacement transducers and a calibrated pressure gage (load cell) for measurement of axial load, which are connected to a 16 channel data acquisition system. The data was simultaneously collected at 0.125 second intervals at a speed of 8 Hz. STP specimens were tested under compression as four tire layers which were placed on top of each other. G-STP was also tested with 6 layers in addition to 4 layers to search for the effect of tire layer number on the vertical stiffness of STP specimens.

#### **4.3.2 Measurements**

The specimens were tested under cyclic axial load with gradual increments. The measured responses are shown in Figure 17 to Figure 21. Strength and instantaneous compression modulus of specimens are given in Table 2. Since STPs failed between strains of 0.20 and 0.25, the compression modulus values are calculated at strain levels of  $\varepsilon = 0.1$  and  $\varepsilon = 0.15$ .

The STPs failure is initiated by series of snapping sounds at about 8MPa axial stress level. The bridge bearing tested here has a vertical strength of 40MPa. The sounds heard from STPs came from failing mesh wire strands inside the tires. The compression modulus and axial load capacity of G-STPs are remained constant for 4 and 6 tire layers. Each identical tire layer of STP samples has its own steel mesh causing the total behavior of STP remains similar regardless of the tire layer numbers: the STP behaves as a spring in series.

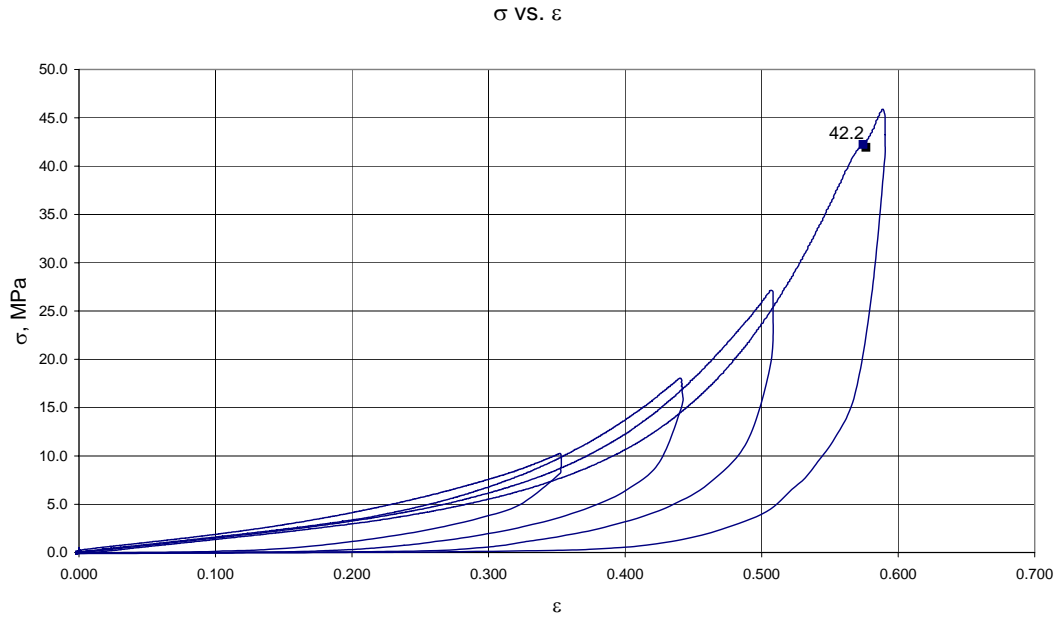


**Figure 17:**  $\sigma \sim \epsilon$  Curve of SREI

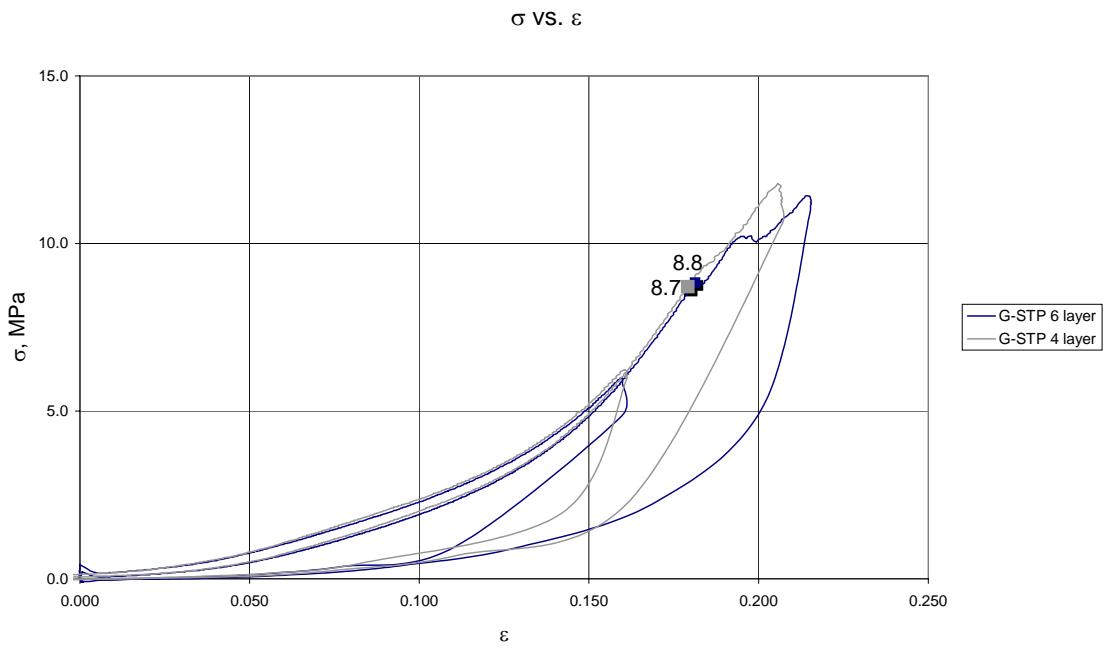


**Figure 18:**  $\sigma \sim \epsilon$  Curve of G-STP composed of 4 and 6 layers

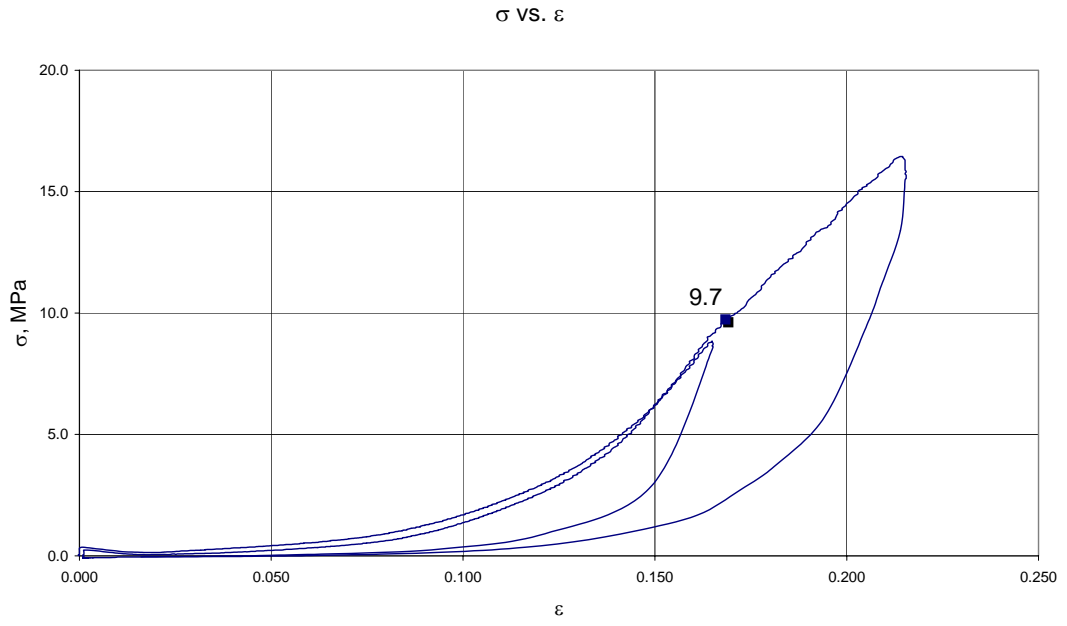


**Figure 19:**  $\sigma \sim \varepsilon$  Curve of M-STP

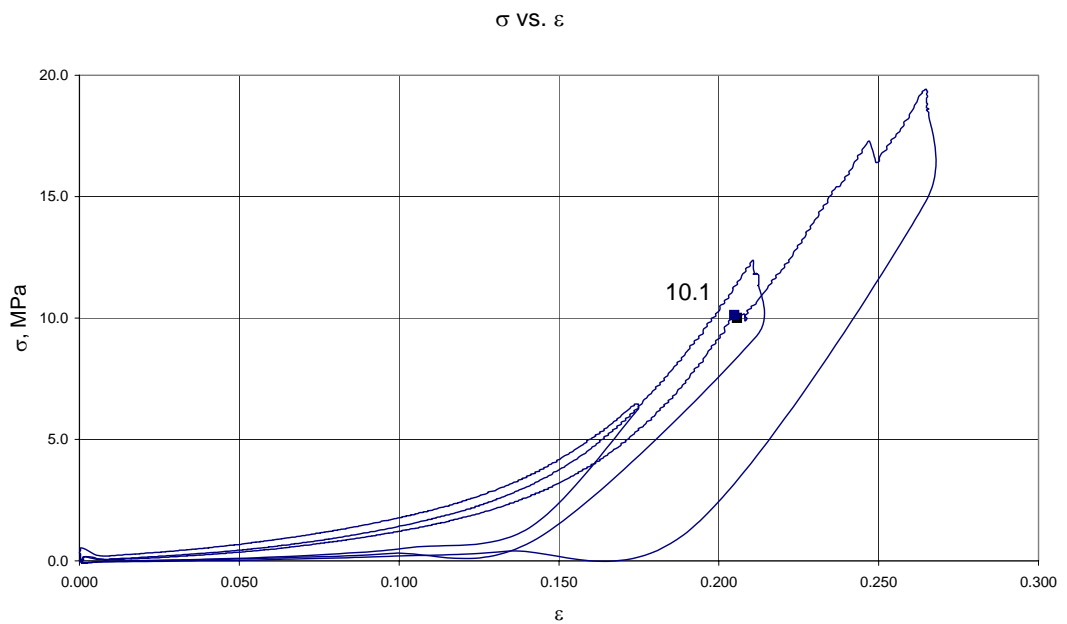


**Figure 20:**  $\sigma \sim \varepsilon$  Curve of P-STP

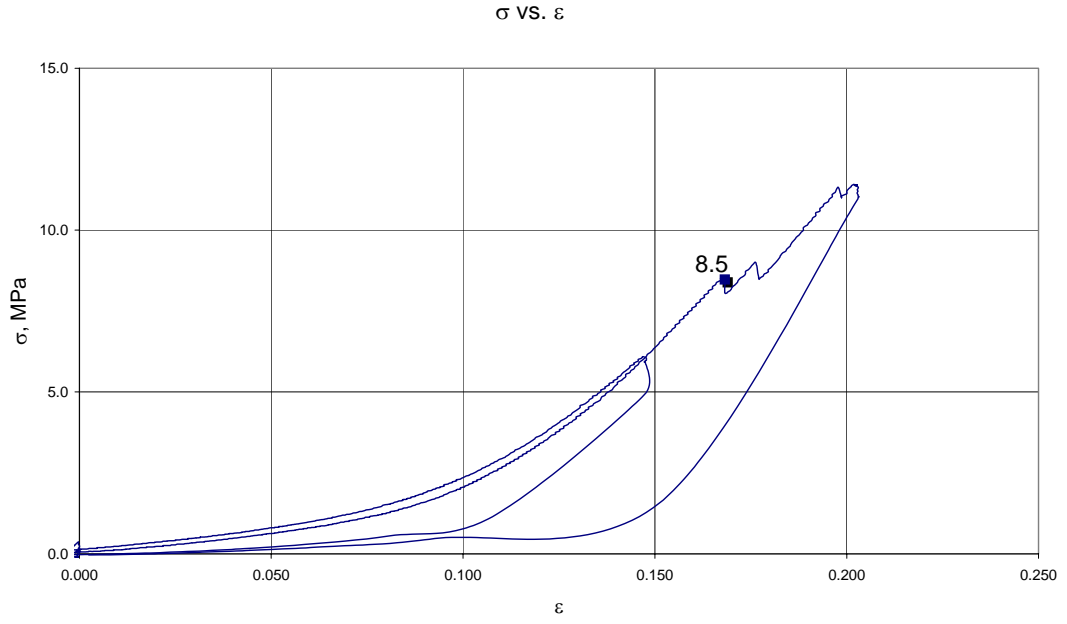


**Figure 21:**  $\sigma \sim \epsilon$  Curve of L-STP

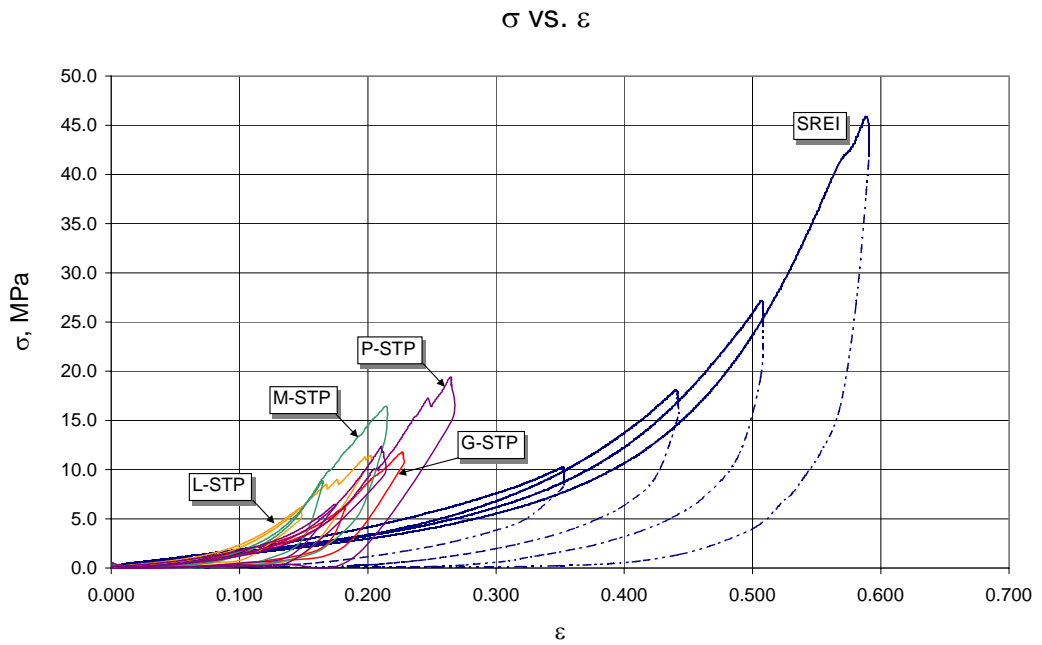


**Figure 22:** Comparison of  $\sigma \sim \epsilon$  Curves for STP and SREI specimens

**Table 2:** Compression experiment results

Specimen Types	Dimensions (mm)	Number of Layers	Strength (MPa)	Compression	Compression
				Modulus (MPa) ( $\epsilon=0.10$ )	Modulus (MPa) ( $\epsilon=0.15$ )
SREI	150 x 150 x 40	-	42.2	25	25
G-STP	200 x 180 x 46	4	8.7	33	95
G-STP	200 x 180 x 69	6	8.8	34	94
M-STP	200 x 190 x 46	4	9.7	50	181
P-STP	200 x 175 x 40	4	10.1	30	74
L-STP	200 x 180 x 50	4	8.5	55	124

### 4.3.3 Discussion of Results

The Hookean formula can be accepted as a good approximation for the compressive behavior of rubber when the deformations are small.

$$\sigma = E_0 \cdot \varepsilon \quad (31)$$

$\sigma$  = stress,  $E_0$  = Young's modulus,  $\varepsilon$  = strain. However, Lindley uses compression modulus  $E_c$  instead of using Young's modulus  $E_0$  [25].

$$E_c = E_0 \cdot (1 + 2S^2) \quad (32)$$

The empirical formulas given above can be used to estimate the deformations of rubber under a given stress. For simple applications, these formulas can be preferred.

The loading data shown in Figure 22 displays the similarity between nonlinear behaviors of STP and SREI specimens. The slopes of the curves increase with increasing vertical strain. The vertical stress design level of common elastomer bearings are around 3.0MPa. In order to compare the instantaneous compression

modulus values ( $E_{c,ins}$ ), the slopes of the curves at the same strain levels are compared using Equation 33.

$$E_{c,ins} = \frac{\partial \sigma}{\partial \varepsilon} \quad (33)$$

The slopes at vertical strain levels of  $\varepsilon = 0.10$  and  $\varepsilon = 0.15$  are presented in the last two columns of Table 2. These results show that at same strain levels, the instantaneous compression modulus values of STP specimens are higher than that of the SREI values. The slope changes of STP specimens start earlier and fail at much lower strains compared to SREI specimen. The SREI specimen has a single steel layer whereas STP samples have 4 to 6 layers of wire mesh which makes the SREI softer. The high vertical stiffness of STP layers combined with relatively low amount of steel content makes STP layers stiffer and lower strength compared to SREI.

#### 4.4 Static Shear Experiments: Inclined Compression Test

The objective of this experiment was to obtain large strain (up to 70%) shear modulus values of STP and SREI specimens using inclined compression test method recommended by Topkaya and Yura [27, 28]. Same specimens used in compression tests are used for shear tests, prior to being tested to failure under compression. The six layer G-STP is left out of the shear test program due to the physical limitations of the inclined plate setup.

##### 4.4.1 Test Specimens and Experiment Setup

Experiment set up is composed of a compression machine and inclined high strength aluminum plates, which have 10% surface slopes. STP bearings are tested between three inclined aluminum plates under compressive forces (Figure 23).

Lateral displacement of the middle plate is measured by means of an LVDT. The compressive force applied on the top and bottom plates are also measured and recorded simultaneously with the lateral displacement. The lateral component of applied axial force causes the middle plate to shift sideways.

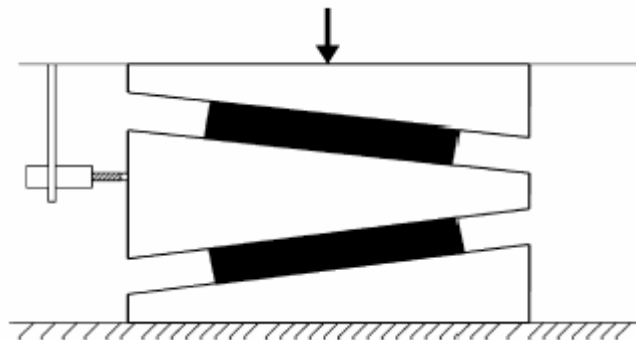


**Figure 23:** Inclined compression test setup [27]

#### 4.4.2 Measurements

Horizontal shear force acting on the plates is calculated by multiplying surface slope of aluminum plate with the vertical load measured simultaneously.

$$V = s \times W \quad (34)$$

In Equation 34,  $s$  is the surface slope of aluminum plates,  $W$  is the vertical load applied on specimens and  $V$  stands for the shear force that is the lateral component of the vertical load  $W$ . The shear strain  $\gamma$  is equal to the ratio between lateral displacement  $\Delta_s$  and total rubber thickness  $t_r$ , which can be substituted into the general shear formula Equation 36. The shear modulus can be obtained as shear stress is further replaced by Equation 37 to yield Equation 38.

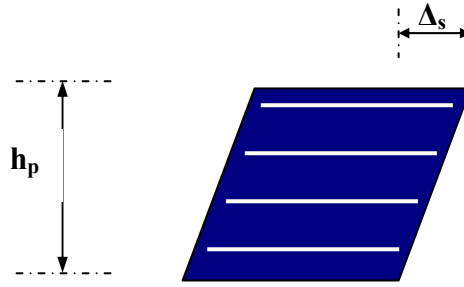


**Figure 24:** Elastomer isolator under shear force

$$\gamma = \frac{\Delta_s}{t_r} \quad (35)$$

$$\tau = G \times \gamma \quad (36)$$

$$\tau = \frac{V}{A} \quad (37)$$

$$G = \frac{V \cdot t_r}{A \cdot \Delta_s} \quad (38)$$

At the end of the measurements, horizontal load vs. horizontal displacement curves of the specimens were obtained and presented in Figure 25 to Figure 33. Large strain shear modulus values of STP and SREI specimens are obtained using Equation 31 and presented in Table 3.

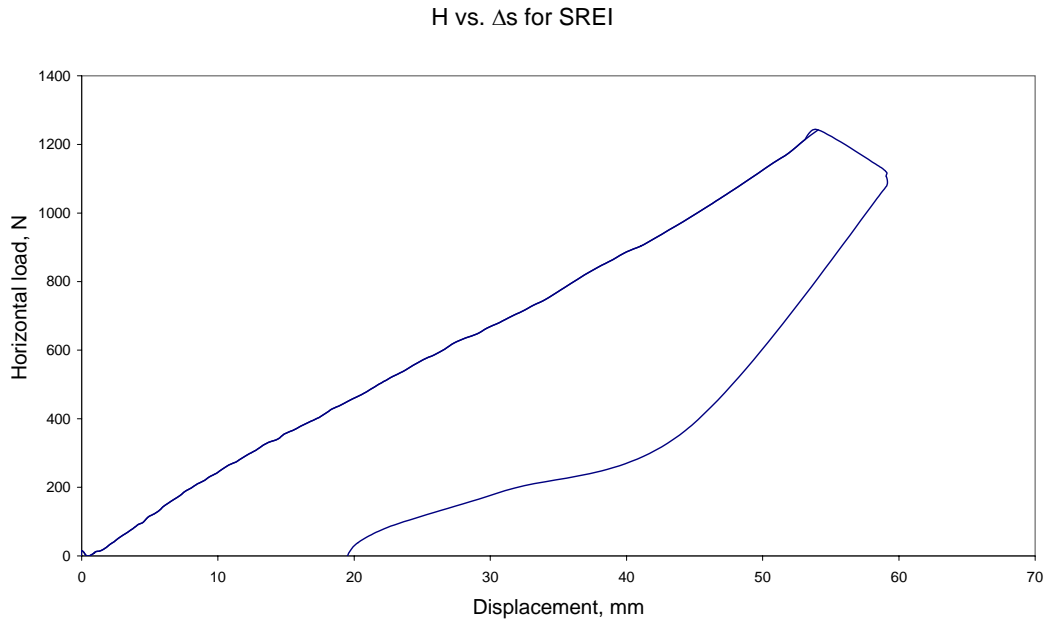


**Figure 25:** H vs.  $\Delta_s$  curve for SREI

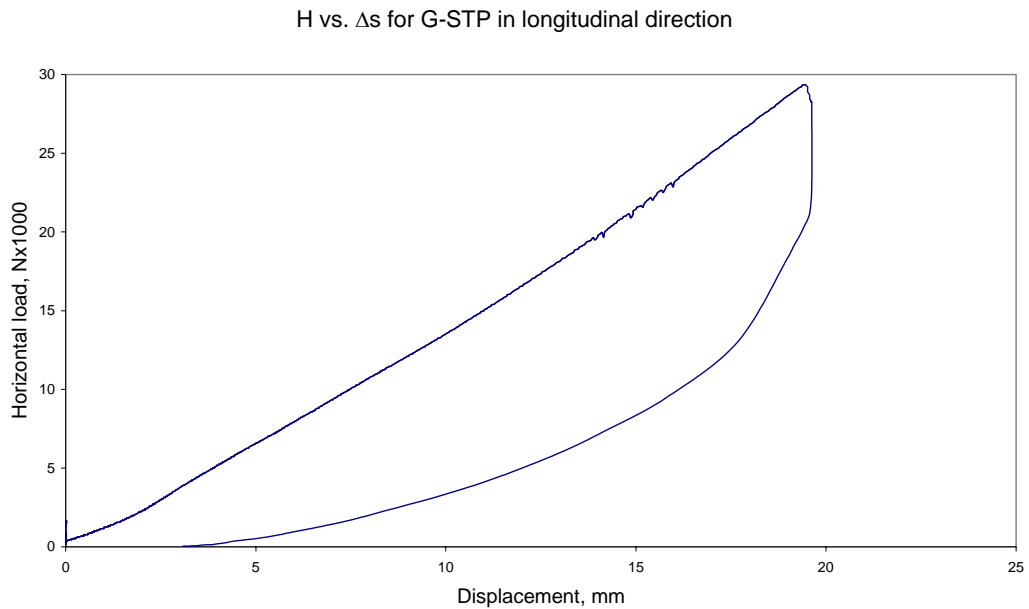


**Figure 26:** H vs.  $\Delta_s$  curve for G-STP in longitudinal direction

H vs.  $\Delta_s$  for G-STP in transverse direction

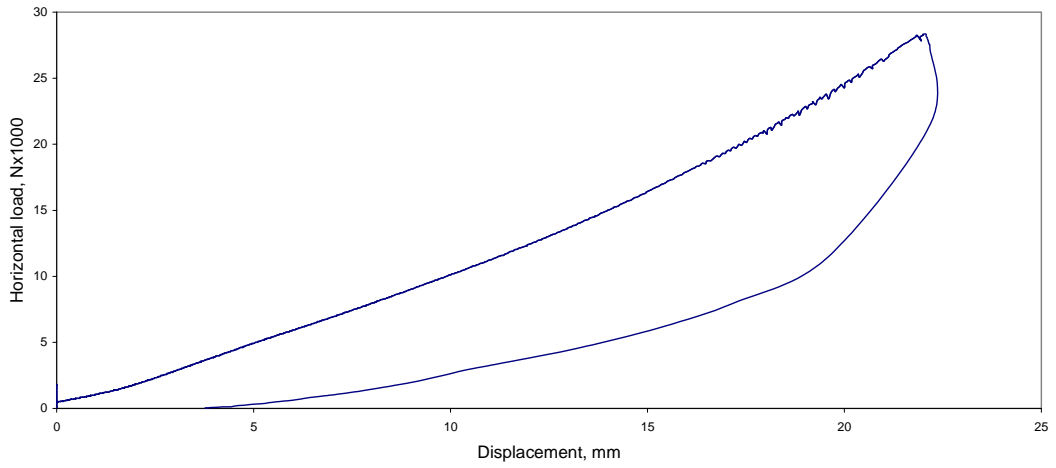


**Figure 27:** H vs.  $\Delta_s$  curve for G-STP in transverse direction

H vs.  $\Delta_s$  for M-STP in longitudinal direction

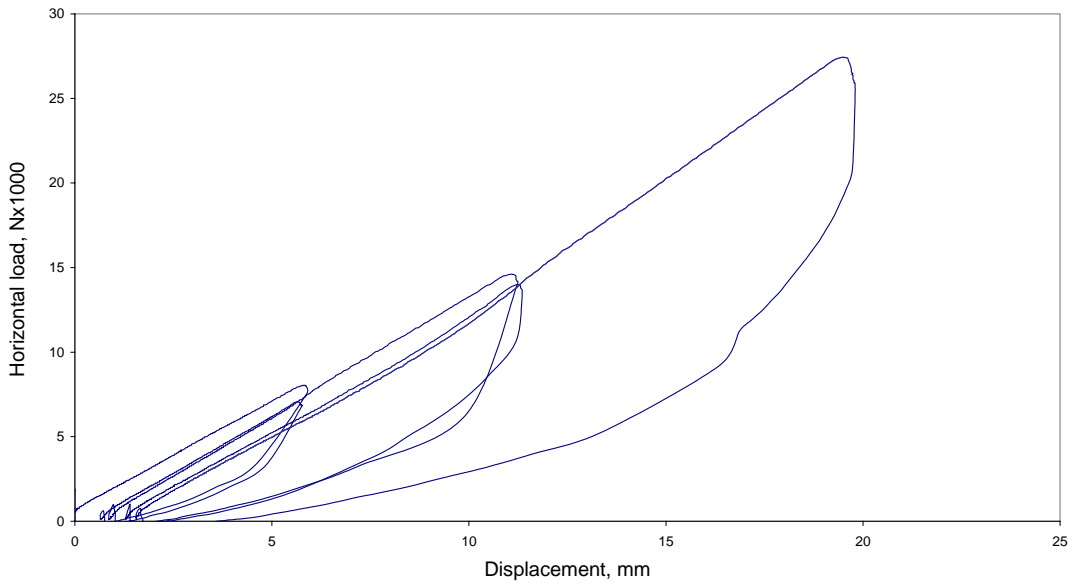


**Figure 28:** H vs.  $\Delta_s$  curve for M-STP in longitudinal direction

H vs.  $\Delta_s$  for M-STP in transverse direction

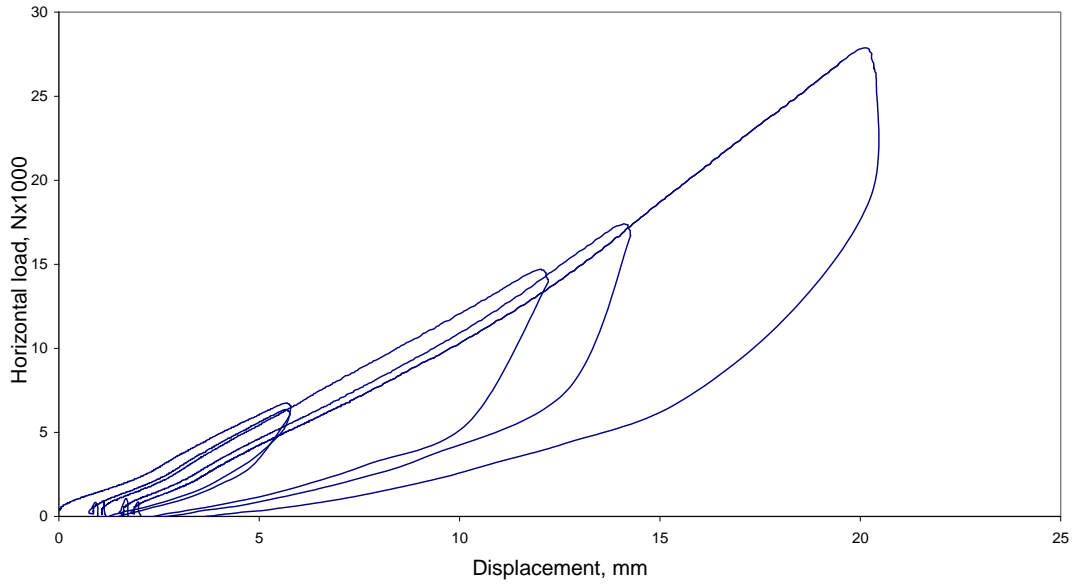


**Figure 29:** H vs.  $\Delta_s$  curve for M-STP in transverse direction

H vs.  $\Delta_s$  for P-STP in longitudinal direction

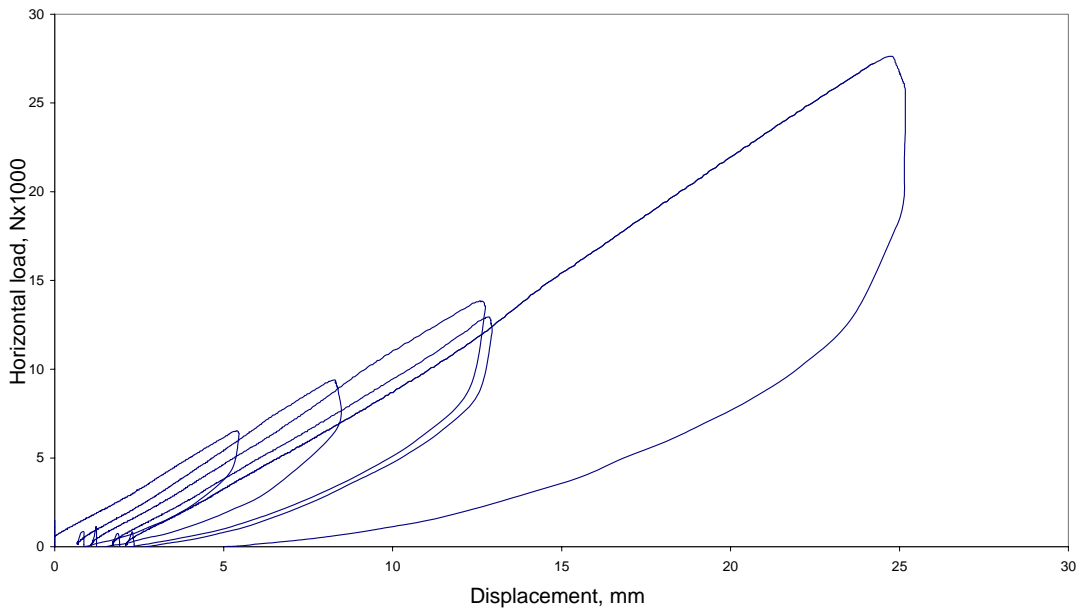


**Figure 30:** H vs.  $\Delta_s$  curve for P-STP in longitudinal direction

H vs.  $\Delta_s$  for P-STP in transverse direction

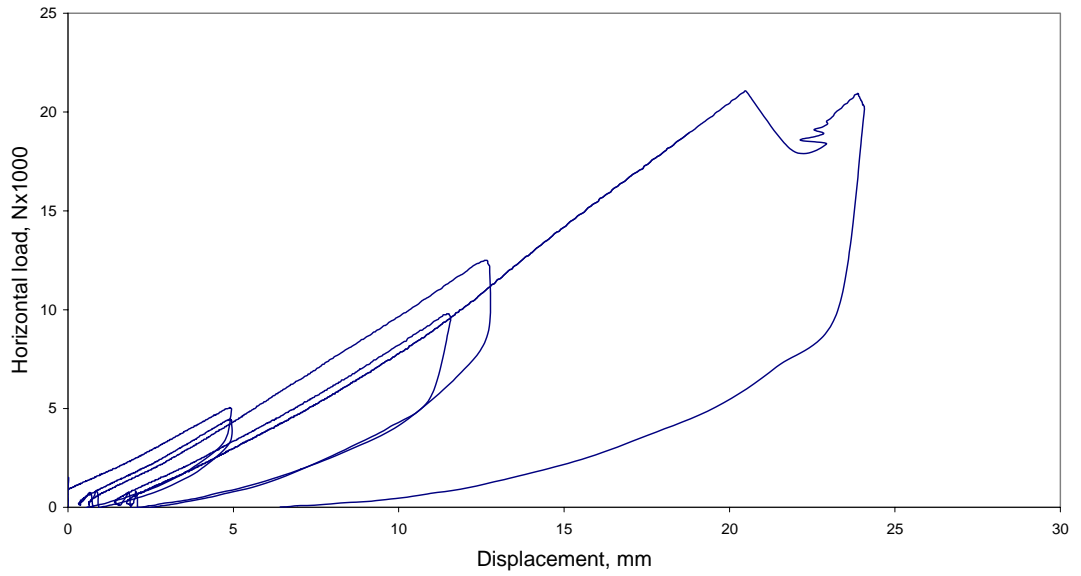


**Figure 31:** H vs.  $\Delta_s$  curve for P-STP in transverse direction

H vs.  $\Delta_s$  for L-STP in longitudinal direction

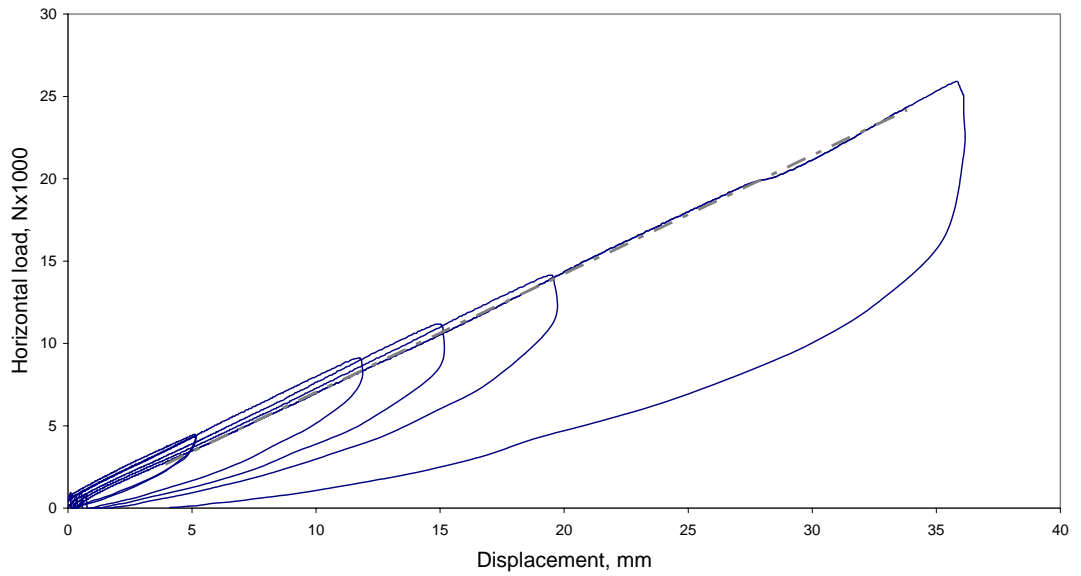


**Figure 32:** H vs.  $\Delta_s$  curve for L-STP in longitudinal direction

H vs.  $\Delta_s$  for L-STP in transverse direction

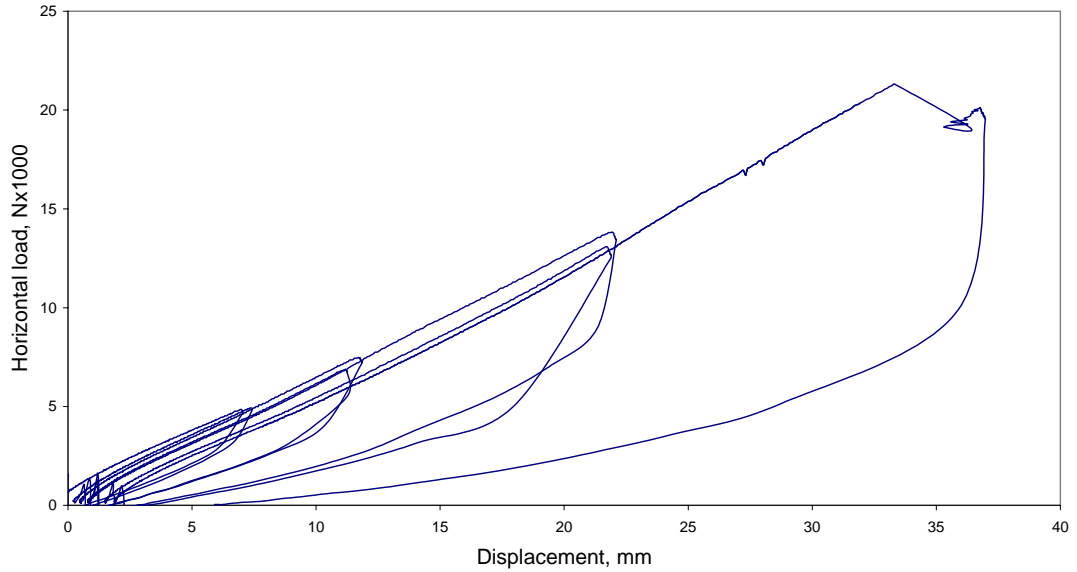


**Figure 33:** H vs.  $\Delta_s$  curve for L-STP in transverse direction

#### 4.4.3 Discussion of Inclined Compression Test Results

Large strain shear modulus values that are obtained from inclined compression tests show variations according to tire brand and loading direction (Table 3). Shear modulus of same specimen is expected to be equal in both directions since it is a material property and independent from loading direction. However, it is seen that longitudinal direction is stiffer than transverse direction causing shear modulus difference between two orthogonal directions. This difference shows the shape effect on lateral stiffness of rectangular elastomer isolators. The difference between longitudinal and transverse directions is also seen in the results obtained by Kelly and Takhirov [29]. The difference in STP experiments would potentially come from the asymmetric rectangular shape of the specimens. The stability of the STP layers may be one of the reasons for this difference.

The shear modulus values given in Table 3 can be accepted as approximate values which give an idea about the range of the STP rubber's shear modulus.

**Table 3:** Inclined compression test results

<b>Specimen Types</b>	<b>Dimensions (mm)</b>	<b>Direction</b>	<b>Height (mm)</b>	<b>Horizontal Stiffness</b>	<b>Shear Modulus</b>
SREI	150 x 150	-	37	225 kN/m	0.37 MPa
G-STP	200 x 180	Longitudinal	46	1448 kN/m	1.85 MPa
G-STP	200 x 180	Transverse	46	1166 kN/m	1.49 MPa
M-STP	200 x 190	Longitudinal	46	1512 kN/m	1.83 MPa
M-STP	200 x 190	Transverse	46	1470 kN/m	1.78 MPa
P-STP	200 x 175	Longitudinal	40	1234 kN/m	1.41 MPa
P-STP	200 x 175	Transverse	40	1243 kN/m	1.42 MPa
L-STP	200 x 180	Longitudinal	50	720 kN/m	1.00 MPa
L-STP	200 x 180	Transverse	50	684 kN/m	0.95 MPa

The shear modulus values of the STP specimens reveal that the rubber used in tires are harder when compared with natural rubber. The rubber used in tires is expected to be harder since tires should be durable under arduous nature conditions. The high shear modulus values of STPs would allow the isolation of large amount of masses only.

#### **4.5 Static Shear Experiments: Reverse Cyclic Load Test**

Inclined compression test is an alternative to reverse cyclic load experiments. In the previous inclined shear experiment, the loading of the specimens was not identical to an isolation case since the axial load on the specimens change through the lateral motion.

Hence, in order to satisfy the constant axial load requirement, a reverse cyclic load test was also performed to obtain the high-strain shear behavior of STP specimens under constant axial force.

##### **4.5.1 Test Specimens and Experiment Set up**

Since dynamic, inclined, and compression tests were prior to this (large deformation reverse cyclic static shear) test and specimens were damaged during the compression experiment before, the specimens are prepared again from same tire brands again except for the L-STP specimen. Instead, another pad B-STP is prepared for this test and experimented together with the other STP specimens.

The vertical load capacity of the testing machine used in the experiment is 3000 kN. The maximum horizontal load that can be applied on the specimens is 300 kN. The mechanism of the experiment set up enables to apply vertical and horizontal loads simultaneously.

Two displacement transducers were used to record horizontal displacements of the specimens.

Vertical load applied on specimens was measured using a pressure gage attached to the vertical piston. Horizontal shear force acting on the plates between specimens was measured using a +300/-600kN load cell.



**Figure 34:** Reverse cyclic test set up

#### 4.5.2 Measurements

After the vertical load was kept constant around 150-300kN (4-8MPa) reverse cyclic displacement was applied on the steel plate between the two STP specimens using the horizontal piston of the testing machine. The measurements are presented in Figure 35 to Figure 42. The horizontal stiffness and corresponding shear modulus values are calculated and presented in Table 4.

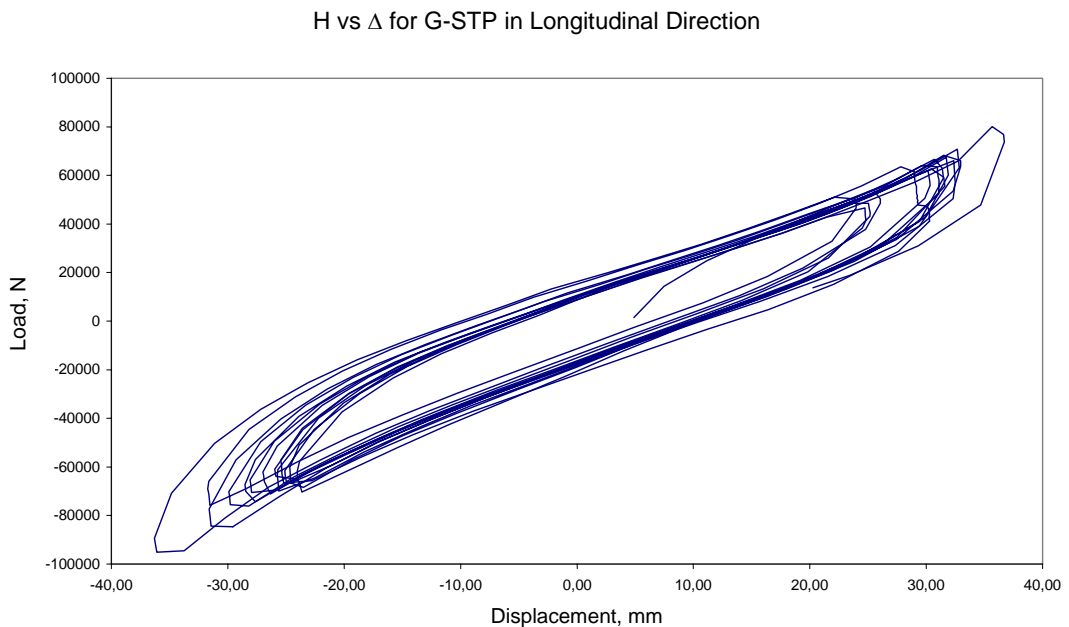


**Figure 35:** H vs.  $\Delta$  curve for G-STP ( $N = 150\text{kN}$ ,  $\sigma = 4.16\text{MPa}$ )

H vs  $\Delta$  for G-STP in Transverse Direction

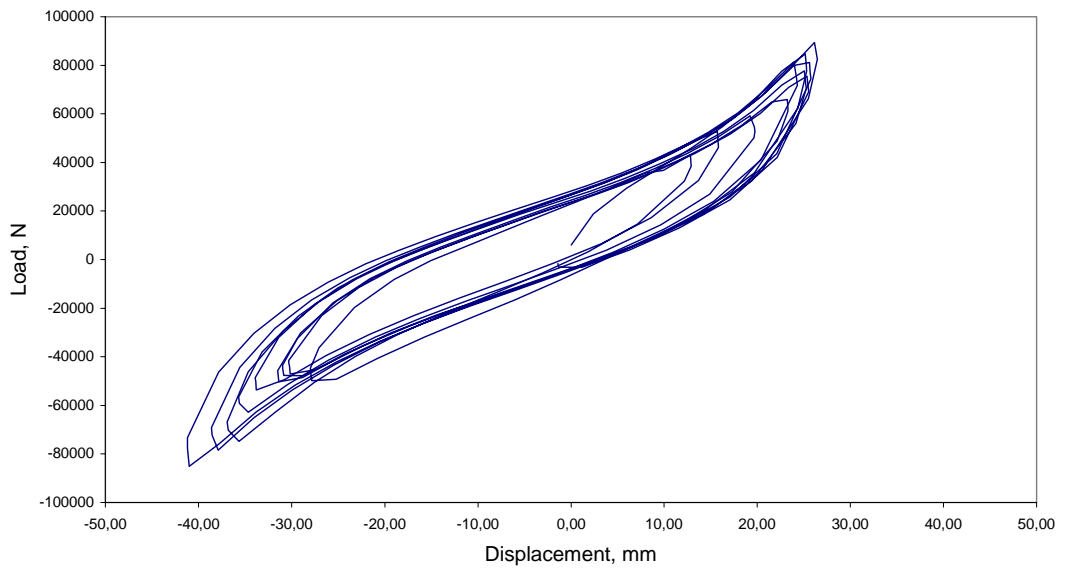


**Figure 36:** H vs.  $\Delta$  curve for G-STP ( $N = 150\text{kN}$ ,  $\sigma = 4.16\text{MPa}$ )

H vs  $\Delta$  for M-STP in Longitudinal Direction

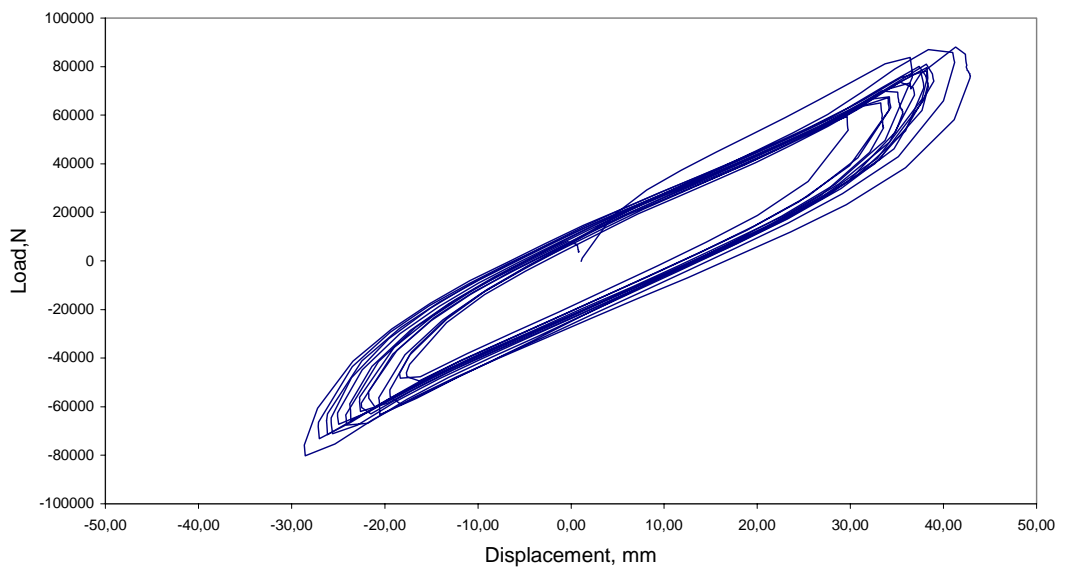


**Figure 37:** H vs.  $\Delta$  curve for M-STP ( $N = 150\text{kN}$ ,  $\sigma = 4.16\text{MPa}$ )

H vs  $\Delta$  for M-STP in Transverse Direction

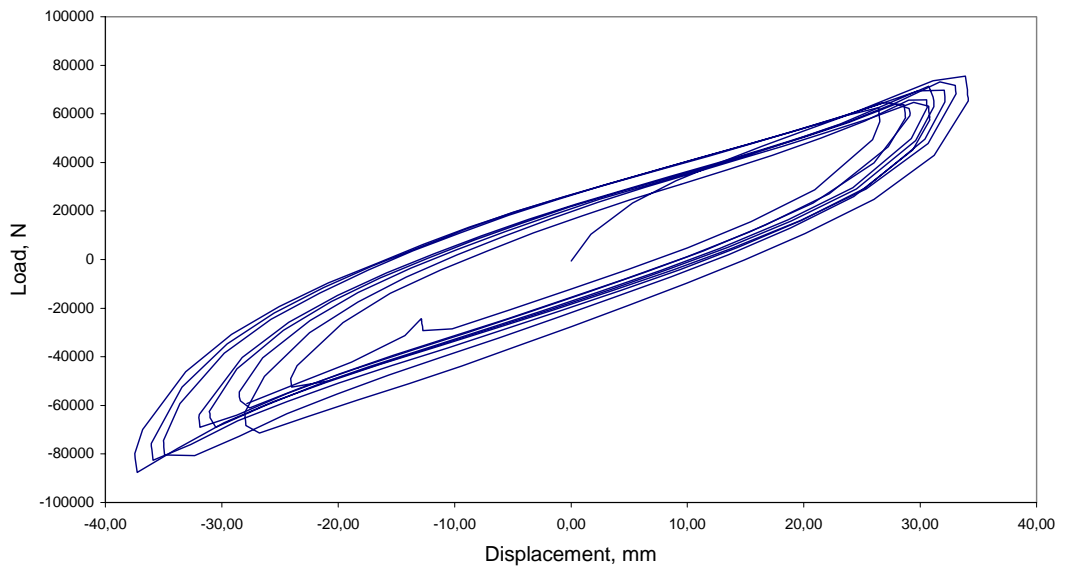


**Figure 38:** H vs.  $\Delta$  curve for M-STP ( $N = 150\text{kN}$ ,  $\sigma = 4.16\text{MPa}$ )

H vs  $\Delta$  for P-STP in Longitudinal Direction

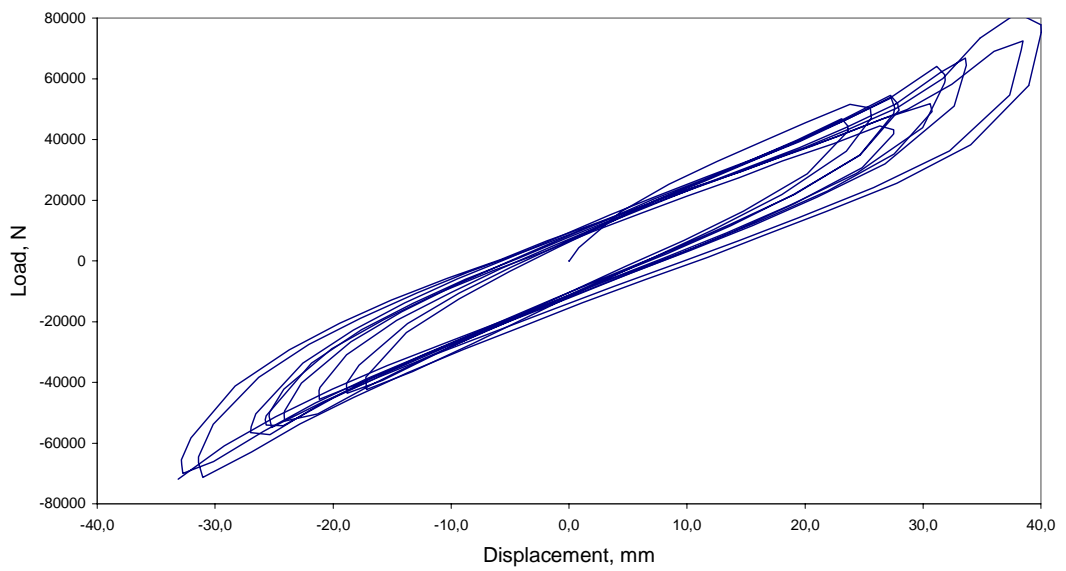


**Figure 39:** H vs.  $\Delta$  curve for P-STP ( $N = 200\text{kN}$ ,  $\sigma = 5.55\text{MPa}$ )

H vs  $\Delta$  for P-STP in Transverse Direction

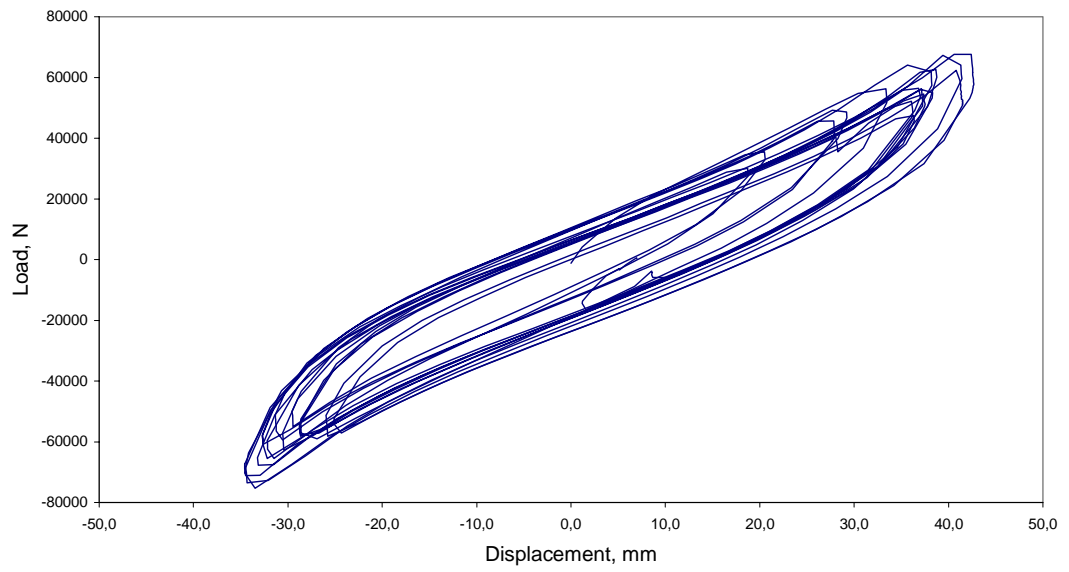


**Figure 40:** H vs.  $\Delta$  curve for P-STP ( $N = 200\text{kN}$ ,  $\sigma = 5.55\text{MPa}$ )

H vs  $\Delta$  for B-STP in Longitudinal Direction

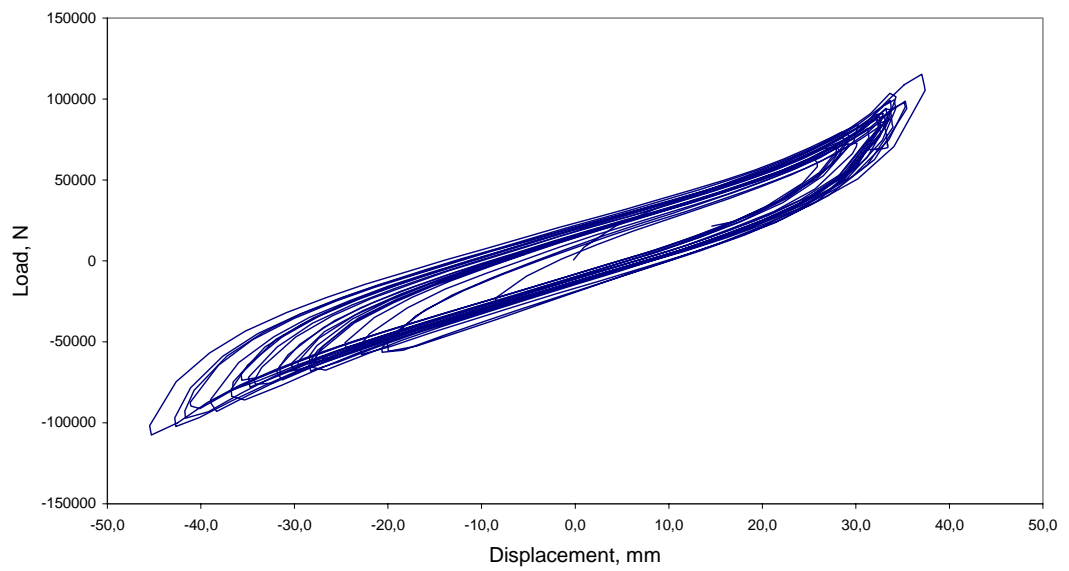


**Figure 41:** H vs.  $\Delta$  curve for B-STP ( $N = 300\text{kN}$ ,  $\sigma = 8.33\text{MPa}$ )

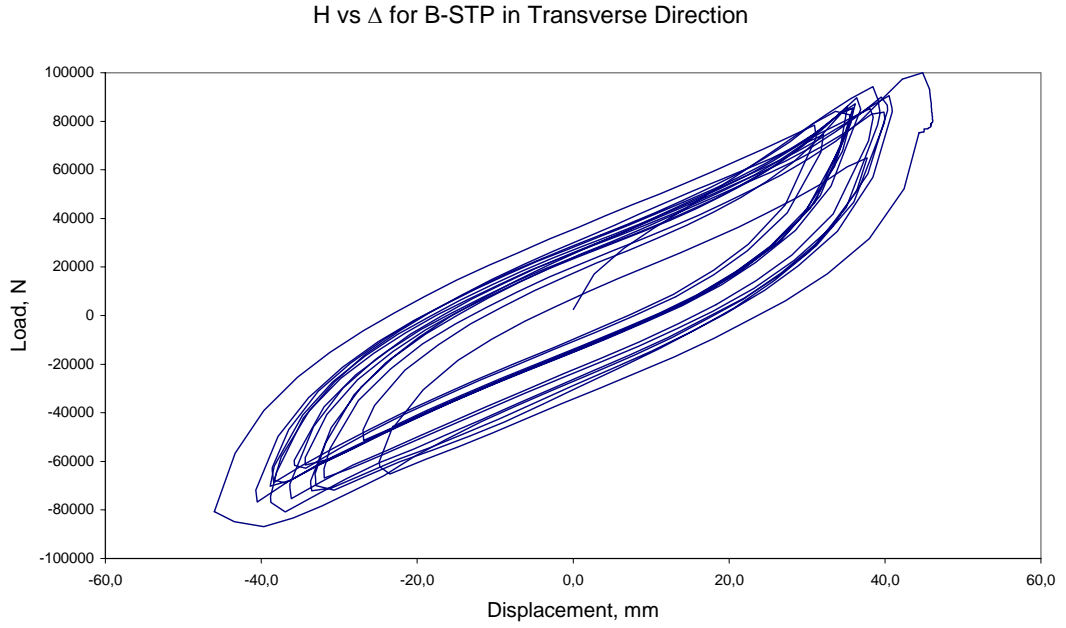


**Figure 42:** H vs.  $\Delta$  curve for B-STP ( $N = 300\text{kN}$ ,  $\sigma = 8.33\text{MPa}$ )

#### 4.5.2 Discussion of Reverse Cyclic Test Results

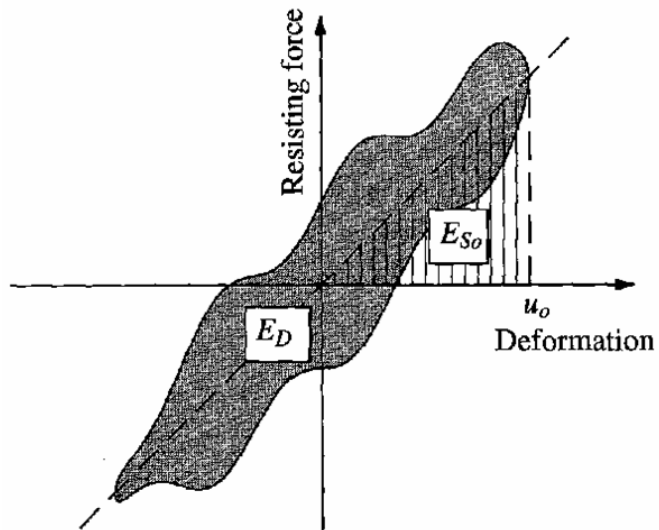
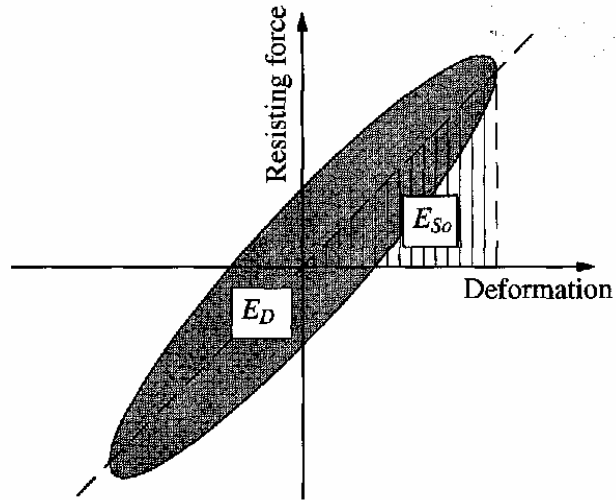
The effective horizontal stiffness values of the specimens are calculated from the secant line of the hysteretic loops using Equation 39. Two sets of specimens were tested at the same time. The curves presented in Figure 35 to Figure 42 belong to two sets of STPs together. The stiffness values are then divided into two in order to obtain the stiffness of one STP specimen and presented in Table 4.

$$K_{eff} = \frac{F_{max} - F_{min}}{\Delta_{max} - \Delta_{min}} \quad (39)$$

Shear modulus values are derived by back substitution of effective stiffness values in Equation 40 and shown in Table 4.

$$K = G \cdot \frac{A}{t_r} \quad (40)$$

The equivalent viscous damping ratios are obtained by considering the energy dissipated ( $E_d$  - the enclosed area of the hysteresis loop) and energy absorbed ( $E_{so}$ ) in each cycle. The equivalent viscous damping is calculated using Equation 41 [31].



$$\beta_{eq} = \frac{E_d}{4\pi \cdot E_{so}} = \frac{E_d}{2\pi \cdot K \cdot \Delta_{max}^2} \quad (41)$$

The results presented in Table 4 show a scattered behavior with respect to the tire specimen brand. The stiffness values change between 906kN/m and 1210kN/m. The corresponding shear modulus values are between 1.01 and 1.50 MPa. The damping values of the specimens change between 13 – 22 %.

**Table 4:** Reverse cyclic test results

<b>Specimen Types</b>	<b>Dimensions (mm)</b>	<b>Direction</b>	<b>Horizontal Stiffness</b>	<b>Shear Modulus</b>	<b>Equivalent viscous damping ratio (<math>\zeta</math> %)</b>
G-STP	200x180x46	Longitudinal	1140 kN/m	1.46	17
G-STP	200x180x46	Transverse	1170 kN/m	1.50	13
M-STP	200x190x46	Longitudinal	1138 kN/m	1.38	19
M-STP	200x190x46	Transverse	1096 kN/m	1.32	22
P-STP	200x180x40	Longitudinal	1084 kN/m	1.21	20
P-STP	200x180x40	Transverse	906 kN/m	1.01	18
B-STP	200x190x47	Longitudinal	1210 kN/m	1.50	16
B-STP	200x190x47	Transverse	1027 kN/m	1.27	22

## **4.6 Dynamic Experiments**

STPs were also dynamically tested to learn more about the damping of the specimens. Moreover, the small strain stiffness values were tried to be extracted using vibration frequency and fundamental dynamic equations. The same SREI sample tested before was also dynamically tested and the results of both tests were compared.

Three dynamic experiments were performed. Dynamic experiment-1 was one of the initial experiments of the thesis study. The tests were conducted without recording the tire brands since these were preliminary tests. The damping values of an arbitrarily selected STP were tried to be extracted using an RC beam mass placed on two sets of STP samples, impact hammer, and spectrum analyzer.

Second dynamic test was performed on the specimens tested in the previous direct and inclined compression tests. The small strain dynamic stiffness values of the specimens and damping values were obtained. The results are compared with the large strain shear stiffness values of the shear experiments presented before.

Dynamic experiment-3 was the last stage of the dynamic experiments, which was performed to investigate the stability of STP. The specimens were tested under a heavier mass of 4.5 tons. At every trial, the number of tire layers was increased from 4 layers up to 12 layers, and the corresponding frequencies were recorded. The frequency change depending on the height of STP specimens was determined.

### **4.6.1 Preliminary Free Vibration Tests using Lumped Beam Masses**

The objective of this experiment is to obtain free vibration frequencies and damping ratios of SREI and STP specimens using beam masses. SREI specimen used in this experiment is the same as the specimen used in the compression experiment. However, STP samples are prepared from arbitrarily selected scrap tires.

#### 4.6.1.1 Test Specimens and Experiment Setup

A four meter long reinforced concrete beam having rectangular cross-section of 30cm x 40cm is used as a lumped mass (1100 kg) of the experiment set up. The vertical stress level on STPs yields to be around 0.15MPa per beam lump mass. A piezoelectric accelerometer and an HP 3582A Spectrum Analyzer is used to obtain the Fast-Fourier Transforms of the measured acceleration data from free vibration of the R/C beam supported on elastomeric pads. An impact hammer is used to excite the beam. Test setup is shown in Figure 43 below.

The STP specimens are tested both in longitudinal and transverse directions. The beam weight is also changed by using two beams on top of each other. The dynamic tests are repeated for two and three supporting pads under the beam(s).

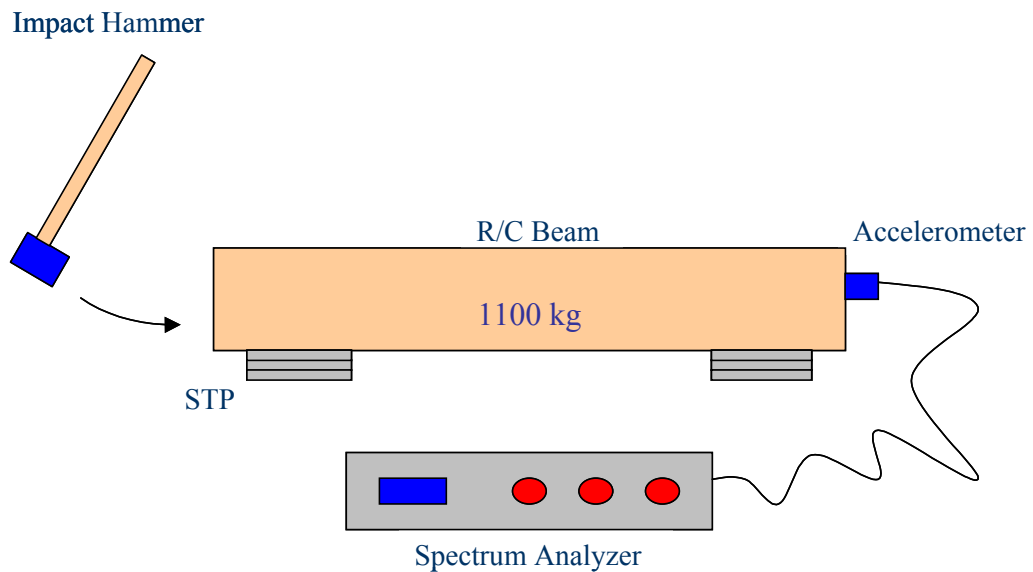


**Figure 43:** Dynamic experiment-1 setup

#### 4.6.1.2 Half Power Bandwidth Method

The data recorded is processed using Half Power Bandwidth method in order to obtain damping coefficients of every trial. This method is given in detail through Chopra [31] (Figure 44). The damping coefficient of the oscillation can be easily calculated using Equation 42.

$$\zeta = \frac{f_2 - f_1}{2 \cdot a} \quad (42)$$

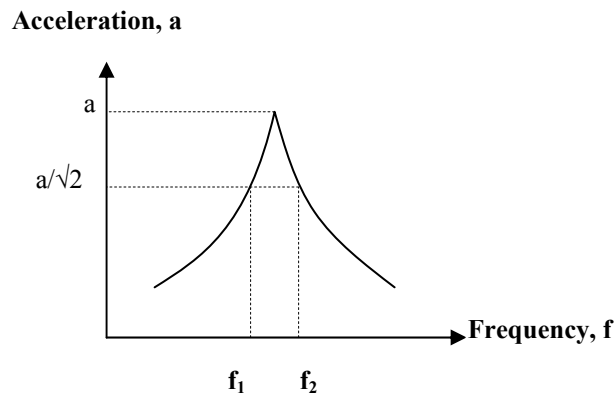


**Figure 44:** Half Power Bandwidth Method

#### 4.6.1.3 Measurements

The acceleration data is measured with the help of spectrum analyzer that automatically gives out the Fast Fourier Transform of the acceleration data. The output data of spectrum analyzer are presented in the following graphs and Table 5.

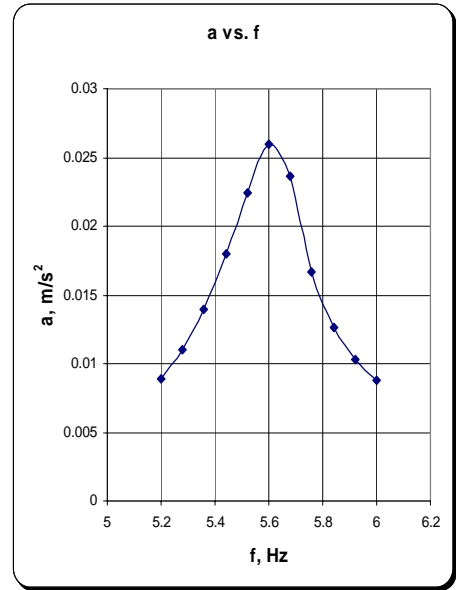
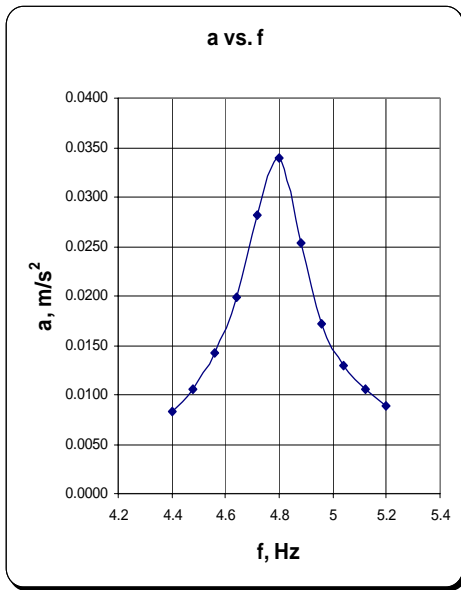


**Figure 45:** Test-1 and Test-2 measurements

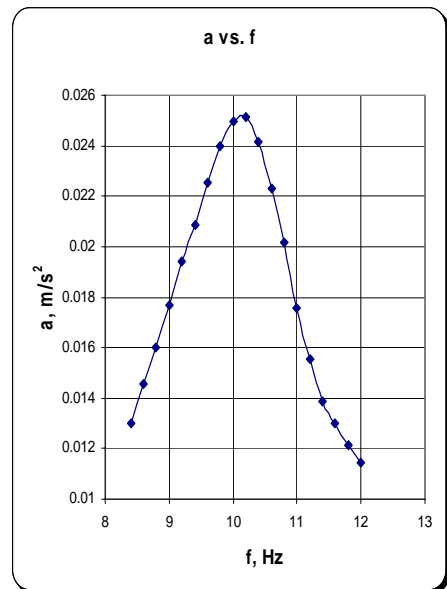
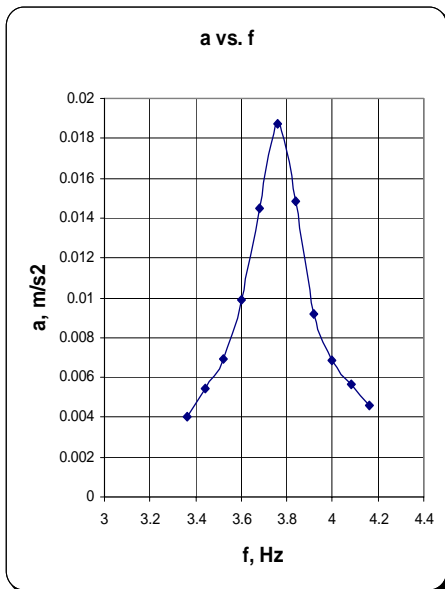


**Figure 46:** Test-3 and Test-4 measurements

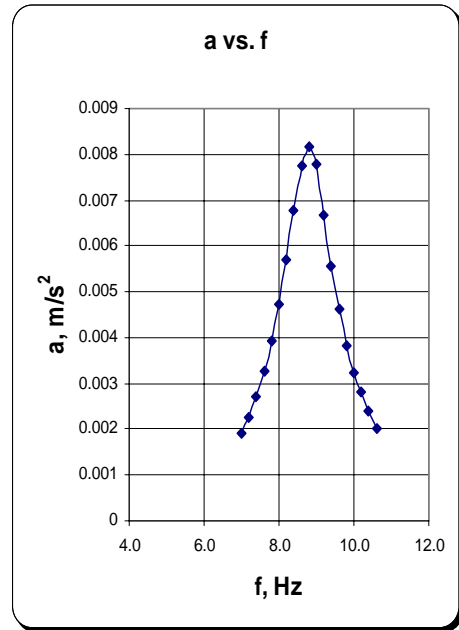
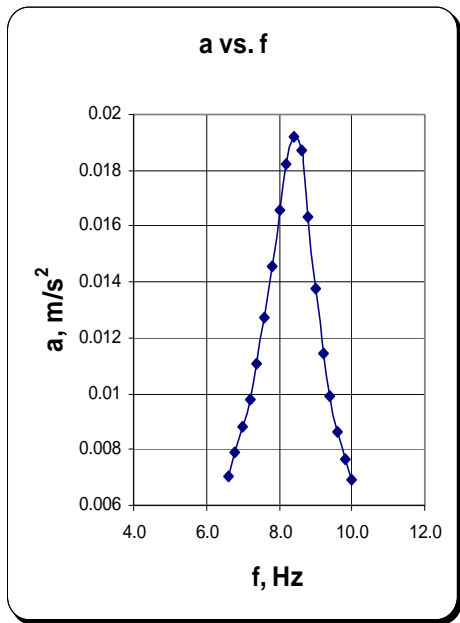


Figure 47: Test-5 and Test-6 measurements

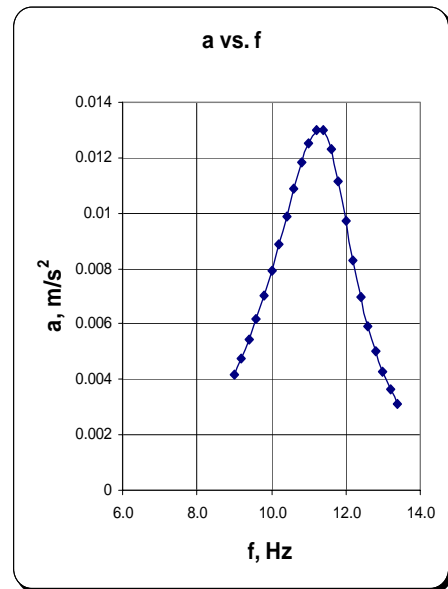
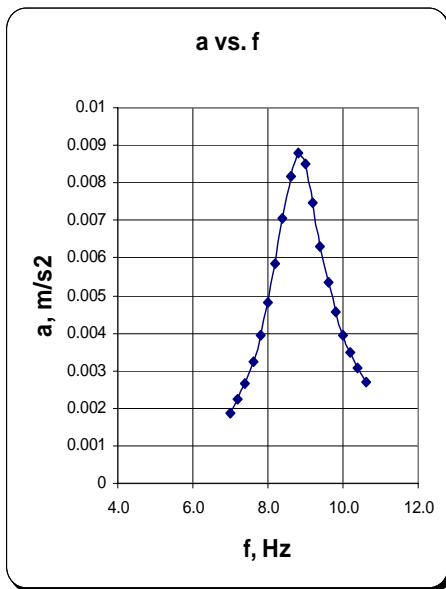
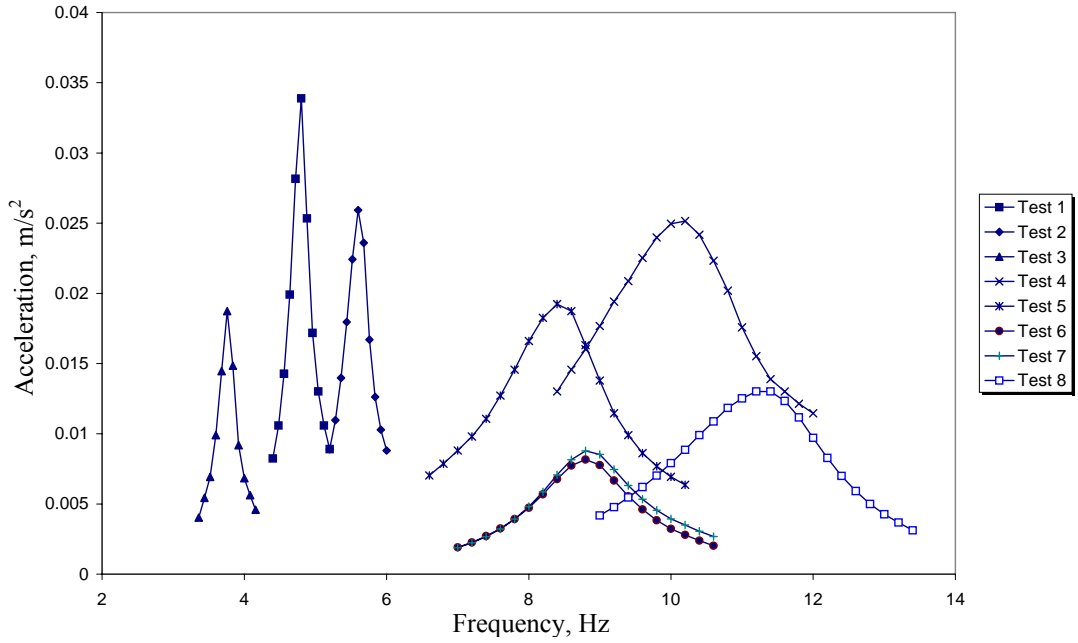


Figure 48: Test-7 and Test-8 measurements



**Figure 49:** Dynamic experiment -1 measurements

**Table 5:** Experiment results,  $f$ ,  $\zeta$  and  $C$  values

Trial	Number of Pads	Number of Beams	Mass $m$ (tons)	Frequency $f$ (Hz)	Damping Ratios, $\zeta$ (%)	Damping, $C$ (kg/s)
Test 1-SREI	2	1	1.1	4.80	2.2	729.85
Test 2-SREI	3	1	1.1	5.60	2.7	696.68
Test 3-SREI	3	2	2.2	3.68	2.7	915.64
Test 4-STP	2	1	1.1	10.10	9.6	6701.39
Test 5-STP	2	2	2.2	8.45	7.9	9227.55
Test 6-STP	2	2	2.2	8.80	6.5	7906.76
Test 7-STP	2	2	2.2	8.70	6.8	8177.69
Test 8-STP	2	1	1.1	11.30	8.4	6560.40

#### 4.6.1.4 Discussion of Results

The resonant frequencies obtained from conducted tests are naturally separated into two groups in Figure 49. The steeper peaks obtained at lower frequencies correspond to the SREI samples whereas shallow and wider curves located at higher frequency range correspond to STP samples which have higher stiffness and higher damping ratios.

The Test-1 against Test-2 comparison in Table 5 shows a frequency increment of 17% due to usage of three SREI specimens. Although the mass is doubled in Test 3, the damping ratios remained fairly constant although it should have been reduced down to about 1.9%. Nevertheless, the damping ratios and damping coefficients are relatively low compared to STP results.

Tests 4 to 8 were conducted using scrap tire pads (STPs). The average damping ratio obtained for STPs is about four times the average damping ratio of elastomer bearings. In addition, the damping values ( $c$ ) obtained for STPs are about 10 times the damping value ( $c$ ) of SREI samples.

The natural vibration frequency of Test 4 is more than two times the frequency obtained from Test 1. This difference in frequencies of specimens implies that horizontal stiffness of scrap tire pads used in this experiment is approximately four times the horizontal stiffness of elastomer pads since the mass is constant.

The difference in damping between Test 4 and Test 5 shows the effect of mass in damping of scrap tire pads. The frequency of the system was decreased 20% with increasing weight; similar to the relationship between Test 2 and 3. Increase in mass also decreased the damping ratio of the system which is not similar to elastomer pad behavior: damping of scrap tire pads may be related with the friction between tire layers. The increase in weight increases the frictional force between layers preventing layers from sliding on each other and causing smaller amount of energy dissipation which results in lowered damping.

Test 6 is similar to Test 5, except that the 2-beam weight of 2200 kg is kept on STPs for 24 hours. The result showed that, keeping weight on pads decreases the damping ratio of scrap tire pads by about 20 % which shows indications of rubber tire pads sticking on each other by time. Test 7 is conducted on the same setup as Test 6; however, the impact point is the upper beam for this test. Similar damping ratio and natural frequency are obtained. Test 8 is carried out after the pads are rotated 90° to have their longitudinal (strong) axis in the direction of testing (impact). The frequency is increased due to higher lateral STP stiffness in longitudinal direction. The increase in damping ratio relative to Test 7 indicates reduction in mass and axial force on STP similar to difference between Tests 4 and 5.

#### **4.6.2 Free Vibration Experiment on Known Brand STPs**

The objective of this experiment was to find damping ratios and dynamic stiffness values of STP specimens which are prepared by using scrap tires of four well-known tire brands. Specimens used in this experiment are the same STP specimens used in compression and static shear experiments. Measurement devices and experiment setup used in this experiment are the same as Dynamic Experiment 1.

##### **4.6.2.1 Measurements**

Damping ratios of specimens has been calculated using Half Power Bandwidth Method. The results are given in the table below. The low-strain stiffness values of STPs are calculated using the below equation.

$$f = \frac{1}{2\pi} \sqrt{\frac{K}{M}} \quad (43)$$

**Table 6:** Dynamic experiment -2 results

Tire *	Dimensions (mm)	Number of Layers	Direction of STP	Frequency, f (Hz)	Damping Ratio, $\zeta$ (%)	K, kN/m	Damping C (kg/s)
G-STP	180 x 200 x 46	4	Transverse	7.7	10.4	1287	5534.73
G-STP	180 x 200 x 46	4	Longitudinal	8.6	11.7	1606	6954.36
M-STP	190 x 200 x 46	4	Transverse	14.1	12.4	4317	12084.07
M-STP	190 x 200 x 46	4	Longitudinal	12.6	14.2	3447	12366.06
P-STP	175 x 200 x 40	4	Transverse	10.6	9.3	2440	6813.36
P-STP	175 x 200 x 40	4	Longitudinal	11.4	9.0	2822	7091.20
L-STP	180 x 200 x 50	4	Transverse	10.2	8.2	2259	5780.78
L-STP	180 x 200 x 50	4	Longitudinal	10.8	7.5	2533	5598.32
G-STP	180 x 200 x 69	6	Transverse	6.7	10.6	975	4908.55
G-STP	180 x 200 x 69	6	Longitudinal	7.4	7.7	1189	3938.17
G-STP	180 x 200 x 92	8	Transverse	5.75	12.0	718	4768.94
G-STP	180 x 200 x 92	8	Longitudinal	5.75	7.7	718	3060.07

\* All tests are conducted using single beam mass of 1100 kg.

#### 4.6.2.2 Discussion of Results

Damping ratios of STP samples presented in table above have a range between the limits of 7.5% to 14.2% but it is recommended to be taken as 7% in order to be on the safe side on the design displacement calculation. The damping value (C) of a scrap tire bearing can be approximately estimated to be about 6500 kg/sec.

For instance, the damping ratio of an isolated mass of 80 tons using 4 STPs can be calculated as 1.5%; whereas, the same system with 4 SREI would yield about 0.3% damping ratio.

The specimens used in this experiment were same that are were used in inclined compression test presented in previous pages. Horizontal stiffness values obtained at the end of Dynamic Experiment-2 do not coincide with the results of inclined compression test. Stiffness values obtained from the low deformation dynamic test

result are about 2 times larger than the large deformation static test results. The difference between the two experiments is devoted to the strain level differences. At vibration tests, the amount of strain is very low, whereas strain levels at static shear test are high (40% to 70% shear strain).

Horizontal stiffness values for four-layer STP specimens obtained from small strain dynamic tests change between the limits of 1287 kN/m and 4317 kN/m. The results show a scattered pattern of stiffness for STP specimens. The smallest value of stiffness belongs to G-STP, whereas the highest value belongs to M-STP. The uncertainty in brand dependent stiffness values brings difficulties for design purposes.

Almost all of the STPs in low-strain shear tests show higher stiffness in longitudinal direction likewise the inclined compression test results.

#### **4.6.3 Free Vibration Experiment using Slab Mass**

The objective of this experiment was to investigate the effect of tire layer numbers on horizontal stiffness of STPs while improving the low-strain test setup using a slab mass of 4500 kg, which would allow simultaneous testing of pads in two orthogonal directions. Slab's rotational degree of freedom (dof) also allowed measurement of angular stiffness of STP, in a direction different than transverse or longitudinal directions.

##### **4.6.3.1 Test Specimens and Experiment Setup**

Specimens tested in this experiment are G-STP type with different numbers of layers (4 to 12 layers) and tested in longitudinal, transverse, and angular directions.

Instead of the R/C beam used in the previous dynamic tests, a 4500 kg, 295cm x 150cm x 40cm R/C slab was used as mass of the setup shown in Figure 50. Four STPs are placed at four corners of the slab mass. The STP layer numbers were

changed from 4 to 12 as the free vibration tests are repeated for each increment of single tire layer.

The two principle direction vibrations are measured using two force-balance and two piezoelectric accelerometers in both directions. The measurements from force-balance accelerometers are manually post-processed to obtain damping ratios and natural vibration frequencies, whereas piezoelectric accelerometer measurements are automatically processed by the HP3582A spectrum analyzer to verify other set of measurements.

The acceleration excitations were performed in the directions of arrows presented in Figure 50. The mid-span impacts were applied to excite the slab mass in principle directions of STPs. The impacts that were applied at the corners caused the slab to be excited in torsional degree of freedom (dof), which allows the measurement of angular stiffness of STPs. The equations of motion for angular dof are given in Equation 44 to Equation 47.

The rotational stiffness of bearings exist, however the contribution to the rotational stiffness ( $K_{\theta}$ ) is small and negligible to the angular stiffness of the pad. The rotational stiffness and rotational frequency of the slab mass is then dominated by the angular stiffness ( $K_{angular}$ ) of each STP in the form of:

$$K_{\theta} = 4 \cdot K_{angular} \cdot d^2 \quad (44)$$

$$m \cdot \ddot{\theta} - \omega^2 \cdot \theta = 0 \quad (45)$$

$$\omega = \sqrt{\frac{K_{\theta}}{M_{\theta}}} = \sqrt{\frac{4 \cdot K_{angular} \cdot d^2}{(a^2 + b^2) \cdot m}} \quad (46)$$

$$K_{angular} = (2 \cdot \pi \cdot \omega) \cdot \frac{(a^2 + b^2)}{12} \cdot m \cdot \frac{1}{4 \cdot d^2} \quad (47)$$

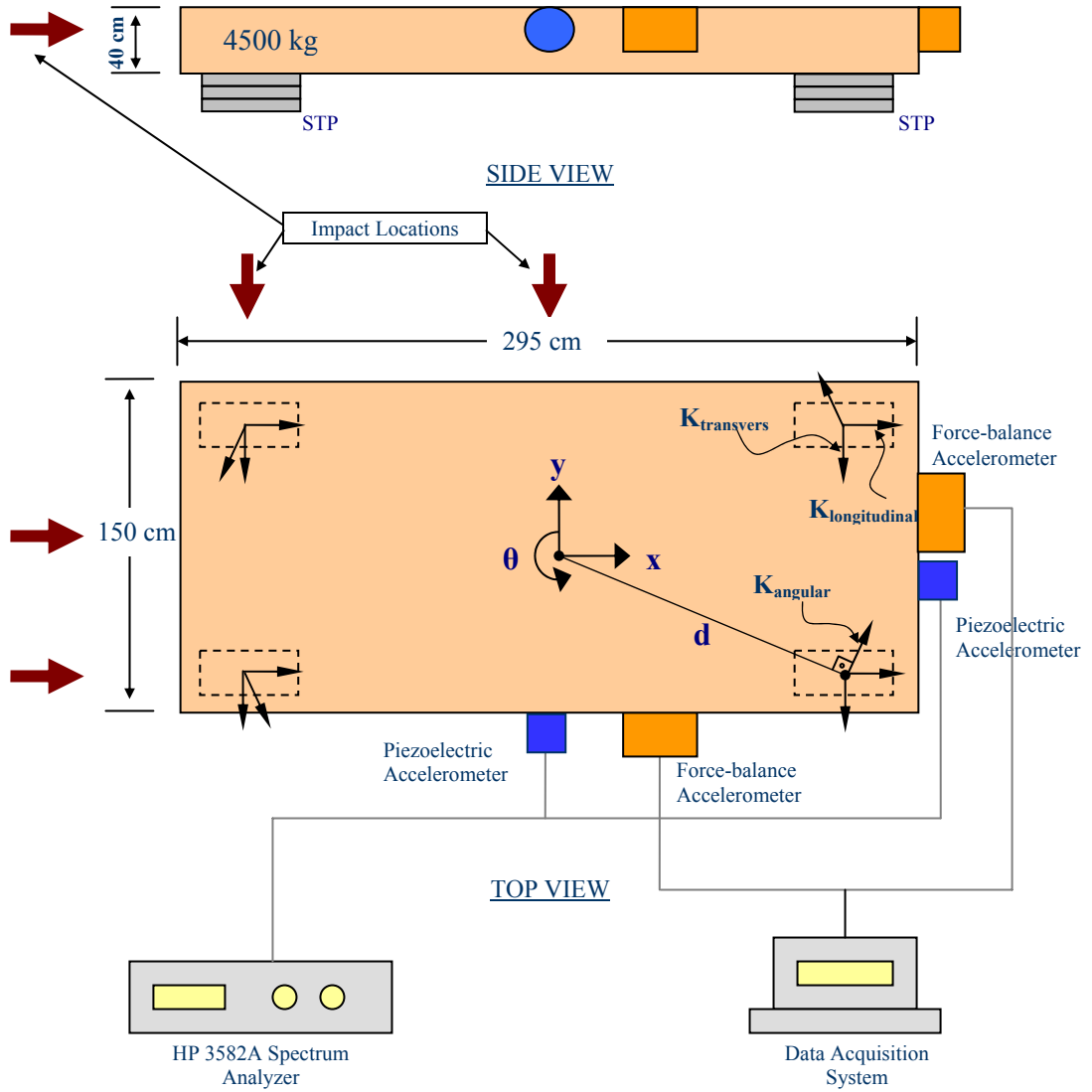


**Figure 50:** Dynamic experiment-3 setup

#### **4.6.3.2 Measurements**

The frequency response functions obtained from free vibration tests are used to extract the shear stiffness and damping ratios of the STPs in transverse, longitudinal, and angular directions, which are summarized in Table 7.

**Table 7:** Dynamic experiment-3 measurements

Number of Layers	Height (mm)	Frequency (Hz)		Stiffness (kN/m)		Damping (%)	
		Longitudinal	Transverse	Longitudinal	Transverse	Longitudinal	Transverse
4	46	5.84	5.52	1515	1353	6.4	7.1
5	57.5	5.44	5.04	1314	1128	6.9	7.3
6	69	5.12	4.64	1164	956	6.5	7.2
7	80.5	4.72	4.32	989	829	6.3	7.4
8	92	4.32	3.84	829	655	6.6	7.2
9	103.5	4.24	3.68	798	601	6.2	6.9
10	115	3.76	3.12	628	432	6.5	7.9
11	126.5	4.00	3.76	711	628	6.3	7.2
12	138	3.44	2.80	526	348	6.2	N.A.

### 4.6.3.3 Discussion of Results

The results of 4500 kg mass free vibration dynamic tests are presented in Figure 51 below. Horizontal stiffness values of STPs linearly decrease as the number of STP tire layer number increase.

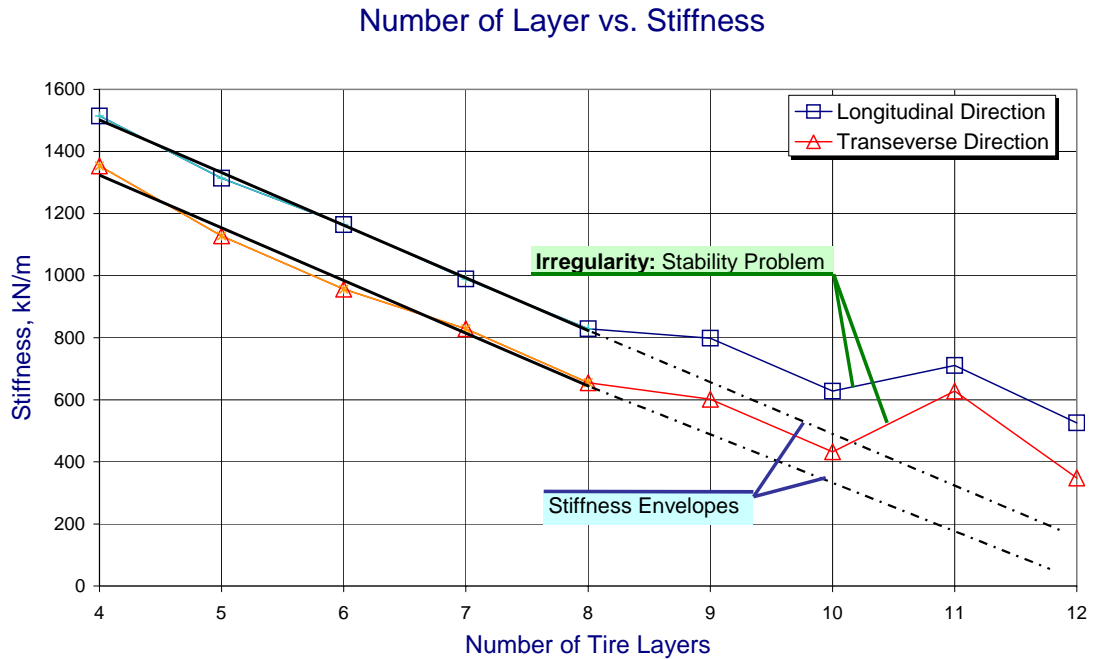


**Figure 51:** Dynamic experiment-3 results

The decrease of stiffness with increasing number of layers is similar to the behavior of common elastomer isolators. Since horizontal stiffness is inversely proportional to height, stiffness decreases with increasing height (Eq. 3).

Irregularities in Figure 51 are observed for high numbers of tire layers. The linear decrease in horizontal stiffness until 9 layers show that, the stiffness of STPs can easily be adjusted based on number of tire layers provided that the stability is maintained.

The stiffness results obtained for 4, 6 and 8 G-STP layers given in are consistent with results presented in Table 6 although different scrap tires of same tire brand were used to obtain G-STPs.

The damping ratios presented in in longitudinal direction changes between 6.2% and 6.9% and the damping ratio in transverse direction is between 6.9% and 7.9%. The damping in transverse direction is slightly larger than damping in longitudinal direction.

The damping ratios in Table 7 are less than G-STP damping ratios for 4, 6 and 8 layers in Table 6. The slab mass per bearing (1125 kg/pad) used in this experiment is larger than the beam mass per bearing (550 kg/pad) in previous experiment. The reason for the difference is believed that increasing axial load on STPs increases the frictional bond between tire layers and consequently decreases the damping of the system by eliminating the friction between tire layers.

The transverse and longitudinal direction test results given in Figure 51 show a linear decline and a parallel relationship between two principal directions as the number of tire layers is increased. The 200 kN/m difference between lateral stiffness terms in the two principal directions is interestingly constant. Since a single reference point in determining the bidirectional stiffness difference of rectangular elastomeric pads is not enough to reach at a generalized conclusion, four additional rectangular isolator pad test results are taken from Kelly and Takhirov [30] and used in the database. Relationship shown in Equation 41 is obtained by normalizing stiffness difference in principal directions by  $G \cdot \sqrt{A}$ . Variable  $K_{\Delta}$  in Equation 48 determines constant difference between two principal directions and is independent from the thickness of the pad. Variables ‘a’ and ‘b’ refer to the base dimensions of elastomeric pad, ‘a’ dimension being the smaller of the two. The correlation between experimental results and analytical predictions are listed in Table 8 and correlations are given in Figure 52.

$$K_{\Delta} = 2 \cdot \left(1 - \frac{a}{b}\right)^{0.6} \cdot G_{ave} \cdot \sqrt{a \cdot b} \quad (48)$$

**Table 8:** Principal direction stiffness differences (N/mm)

Type	Thickness (mm)	Width (mm)	Length (mm)	$K_L$	$K_T$	$K_D$	$G_L$ (MPa)	$G_T$ (MPa)	$G_{ave}$ (MPa)	$K_D$ calculated
<b>P-STP</b>	40	175	200	2822	2440	382	3.225	2.789	3.007	323
<b>G-STP</b>	57.5	180	200	1314	1128	186	2.099	1.802	1.950	186
<b>L-STP</b>	50	180	200	2533	2259	274	3.518	3.138	3.328	317
<b>DRB1</b>	105	183	735	1354	839	515	1.057	0.655	0.856	529
<b>DRB1a</b>	105	183	735	1408	856	552	1.099	0.668	0.884	546
<b>DRB2</b>	105	190	750	1180	764	416	0.869	0.563	0.716	454
<b>DRB3</b>	105	190	740	1137	651	486	0.849	0.486	0.668	419

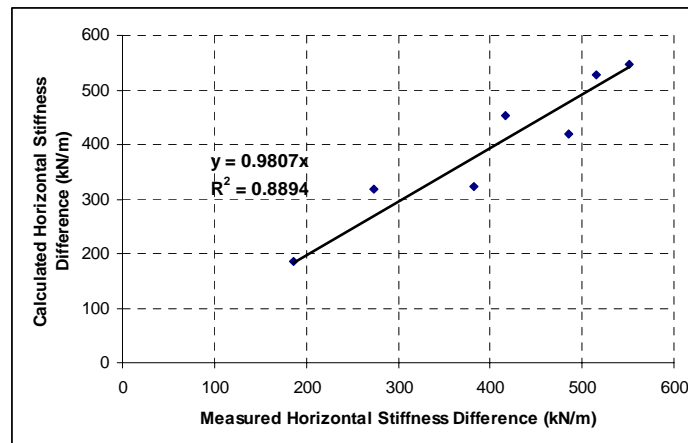
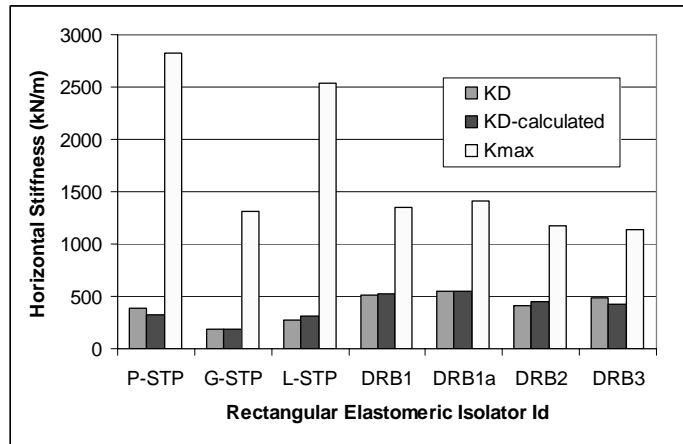


**Figure 52:** Horizontal stiffness differences, predicted versus calculated

#### 4.7 Shaking Table Experiment

The experiments presented in previous sections were conducted to obtain the dynamic and mechanical properties of scrap tire bearings. The aim to obtain these properties was to make the design of STPs available. At the end of the previous experiments it was seen that the rubber used in tires has large strain shear modulus values between 1.0 to 1.85MPa. As it is shown in Equation 18, the isolated structure's period is inversely related with the square root of horizontal stiffness; therefore, STP based isolation might be more suitable for isolation of relatively larger masses. However, the low vertical strength of STP may create problems. In spite of these two constraints, it has been shown that there are possible applications of STP based isolation (see section 4.8).

STPs tested on previous experiments were composed of tire layer piles of 4 to 12 sheets of tread portions of tires. These tire layers were not glued to each other. If the axial load was large enough, the friction between tire layers were able to provide the stability of STP specimens under up to 75% strains in static shear experiments. High strain static shear test results have shown that the friction coefficient between tire layers can be conservatively accepted as 25%. This value is large enough for many base isolation cases since lateral force acting on the isolated mass would normally not reach at  $0.25 \times m \times g$ .

Hitherto, the idea of using scrap tire bearings in seismic base isolation is tested in numerous static and dynamic experiment setups. However, testing the STP applications using a shaking table for real earthquake motions would be beneficiary. The shaking table available in Structural Mechanics Laboratory is 120cm x 220cm in plan. Hence, a scaled version of a shaking table test was planned in accordance with the limitations of the available testing table.

A  $\frac{1}{4}$  scaled masonry house was constructed with using small rectangular shaped hewn stones. A thin layer of plaster of Paris was used as mortar between the hewn stones. Two R/C plates of 100cm x 80cm having a thickness of 3.5 cm were poured

in order to construct the floor and the roof of the model. Some extra weights were also attached on the roof of the model. The total weight of the scaled masonry house was measured to be 550 kg.

The STP samples should be scaled also. Since the rubber used in car tires has large shear modulus than the value required to isolate scaled masonry model, the STP models were produced from softer rubber layers.

First, STP models designed in accordance with the flowchart prepared for the design of steel reinforced elastomer isolators. Then, rubber layers of the designed SREI were produced separately. STP models are then formed by just putting these thin rubber layers on each other as shown in Figure 53. Moreover, 1mm thick steel sheets were used between these rubber sheets to simulate the steel mesh inside the tire layers. No any adhesive was used to keep these steel and rubber layers together as it is similar to the STPs used in previous experiments.



**Figure 53:** STP models

The experiments were conducted using shaking table available on the Structural Mechanics Laboratory of Department of Civil Engineering at METU. The isolated masonry model was exposed to four different earthquake accelerations, which are 1999 Bolu, 1992 Erzincan, 1995 Kobe and 1994 Northridge respectively. The accelerations of shaking table and isolated model were recorded with using two different accelerometers.

The response of a fixed base masonry house during an earthquake would be close to the motion itself because of the high lateral rigidity of the building. Hence, the isolated case accelerations are compared with the accelerations of the shaking table.

The masonry model has a scale factor of  $N=4$ , so the time data of the events are scaled down by  $\sqrt{N} = 2$ . Since the time-scaled displacement data of the ground motions are behind the limits of the shaking table available in laboratory, the motions are re-scaled in displacements of 10%, 20%, 30% and 40% also in order to make the motion data applicable.

#### 4.7.1 Test Specimens

Through the design of STP scaled models, the common design procedure which is valid for SREIs in IBC 2000 was followed [5] [21].

First the weight of the building is measured to be 0.55 tons. The target period of the isolated case does not have to be between 2~3 seconds anymore since the time data of the motions are scaled down by 2.  $T = 0.6$  sec was selected to be the target period  $T_D$  of the isolated structure. The damping of the rubber was assumed to be 10% for calculation purpose. In accordance with UBC-97, the design displacement  $D_D$  was calculated to be 40 mm taking  $C_{VD} = 0.32$ ,  $T_D = 0.6$ ,  $B_D = 1.20$ .

$$D_D = \frac{g \cdot C_{VD} \cdot T_D}{4 \cdot \pi^2 \cdot B_D} \quad (49)$$

Assuming the horizontal strain  $\gamma = 0.8$ , total rubber thickness was calculated to be 50 mm. Then, total horizontal stiffness of the isolation system  $K_H$  was calculated to be 59.2N/mm according to Equation 50. The masonry would be located on four isolators that horizontal stiffness of an individual isolator was calculated to be 14.8 N/mm.

$$K_H = 4 \cdot \pi^2 \cdot \frac{M}{T^2} \quad (50)$$

$$K_H = G \cdot \frac{A}{t_r} \quad (51)$$

Since the model was a lightweight structure, very soft rubber was needed to be evaluated. Manufacturers can produce soft rubbers in shore hardness of at least 30 Shore level. Using the graph given in Figure 54, the value of 30 shore gave out  $E_0=0.90$  MPa and  $G=0.30$  MPa.

Then, the required area was computed to be  $2467\text{mm}^2$ . The isolators were decided to be in square shape. One side of the isolator was calculated as 45 mm. Using the design values  $t_r = 50\text{mm}$  and  $a = 4$  mm, horizontal stiffness of one non-vulcanized elastomeric isolator was re-computed to be 12.15kN/m. The isolated period was then to be 0.66 sec that is slightly greater than the target period. Taking the single layer thickness as  $t = 5$  mm, which is the minimum thickness that can be produced by the manufacturer,  $S = 2.25$  and the vertical frequency is to be 12.3 Hz that is large enough to prevent the masonry model from rocking motion during test.

### Young's Modulus vs. Shore Hardness

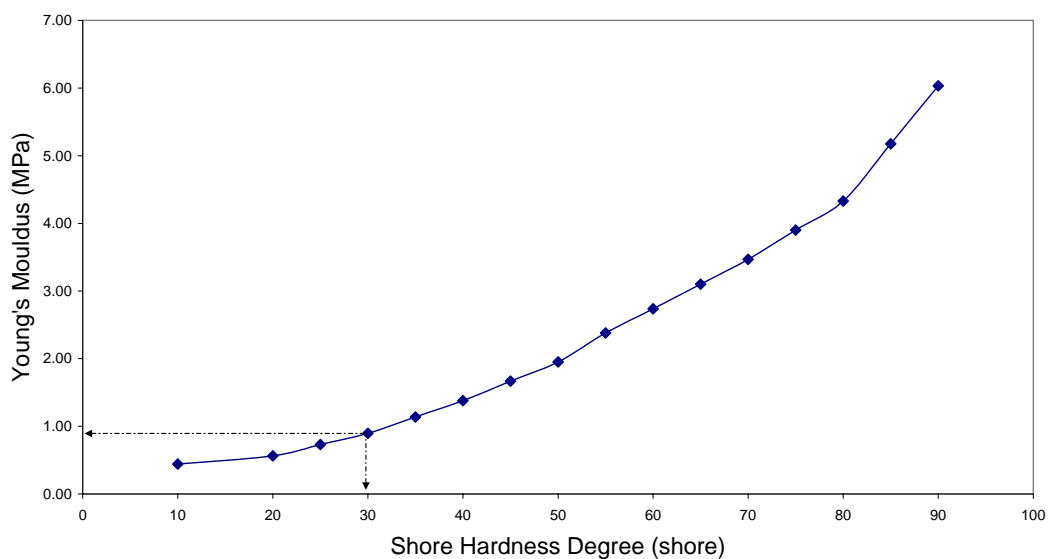


**Figure 54:** Young's modulus vs. shore hardness degree

However, the vertical load on an elastomeric isolator has an attenuator effect on the effective horizontal stiffness. The effective horizontal stiffness is found by considering the vertical load and critical load of the isolator. The critical buckling load of a square elastomeric isolator is calculated in accordance with Equation 52 [5]. The effective horizontal stiffness was then computed to be  $K_{eff} = 10\text{kN/m}$  using Equation 53. The corresponding period was calculated as 0.73sec.

$$P_{crit} = \frac{\sqrt{2} \cdot \pi \cdot G \cdot A \cdot S \cdot r}{t_r} \quad (52)$$

$$K_{eff} = K_H \cdot \left[ 1 - \left( \frac{P}{P_{crit}} \right)^2 \right] \quad (53)$$

Isolators used in this experiment are composed of non-vulcanized rubber layers and steel plates produced separately. The rubber layers have dimensions of 45mm x

45mm and a thickness of 5mm. The steel plates are in same dimensions and their thickness is 1 mm. The isolator models were constructed just by putting rubber layers and steel plates on one by one on each other as shown in Figure 55 and Figure 56 below.

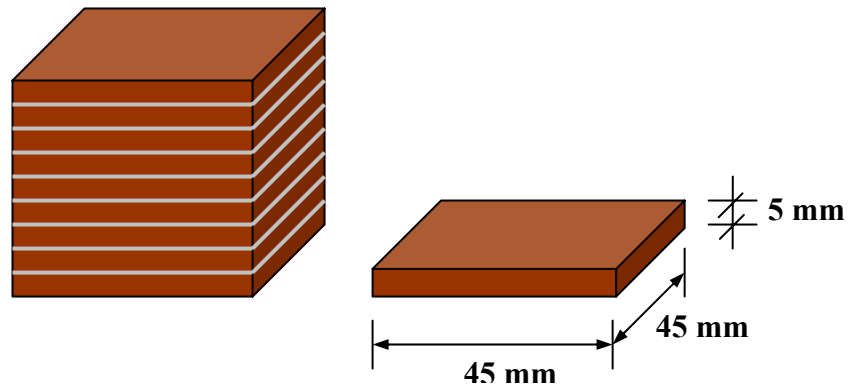


**Figure 55:** Test specimen dimensions



**Figure 56:** Test specimens used in shaking table test

#### 4.7.2 Experiment Setup

The experiment setup is presented in Figure 57 below. The  $\frac{1}{4}$  scaled masonry building is put on four STP model specimens. The details of the specimens are given in previous part of the manuscript. Two force-balanced accelerometers were used in the experiment setup. An accelerometer is attached on the superstructure to measure the response of the masonry model on the isolators. The other accelerometer is used for recording the accelerations of the shaking table.

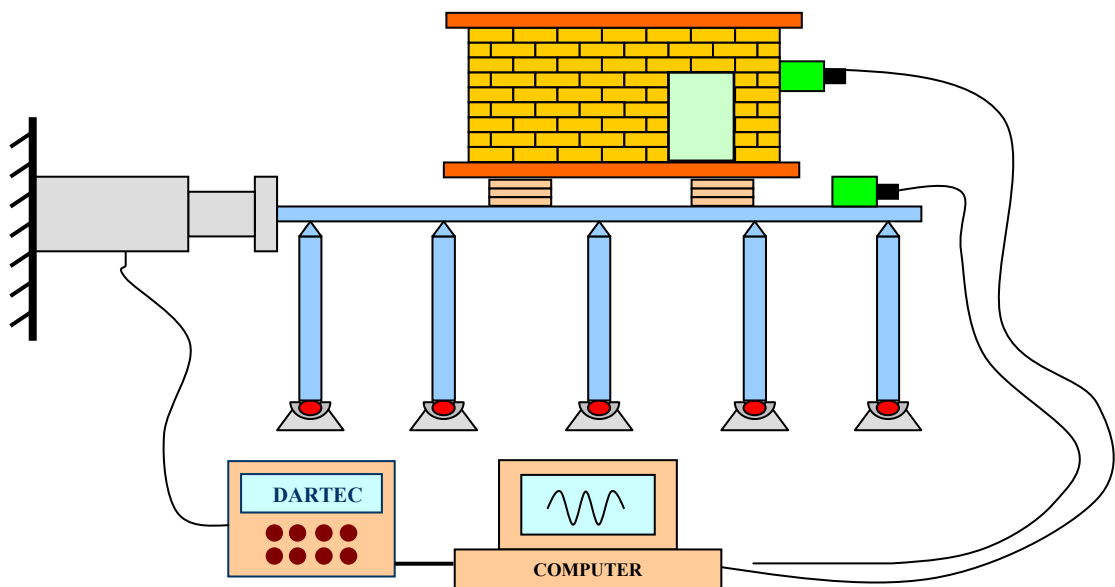


**Figure 57:** Shaking table experiment setup

#### 4.7.3 Measurements

The acceleration data obtained from shaking table and building is given in Figure 58 to Figure 61. The curves show that the isolated case accelerations are less than the table's accelerations.

The maximum accelerations of the table and building for every ground motion applied are provided in Table 9. Isolation ratios are calculated by dividing the maximum table acceleration to the isolated building acceleration and provided in Table 10.

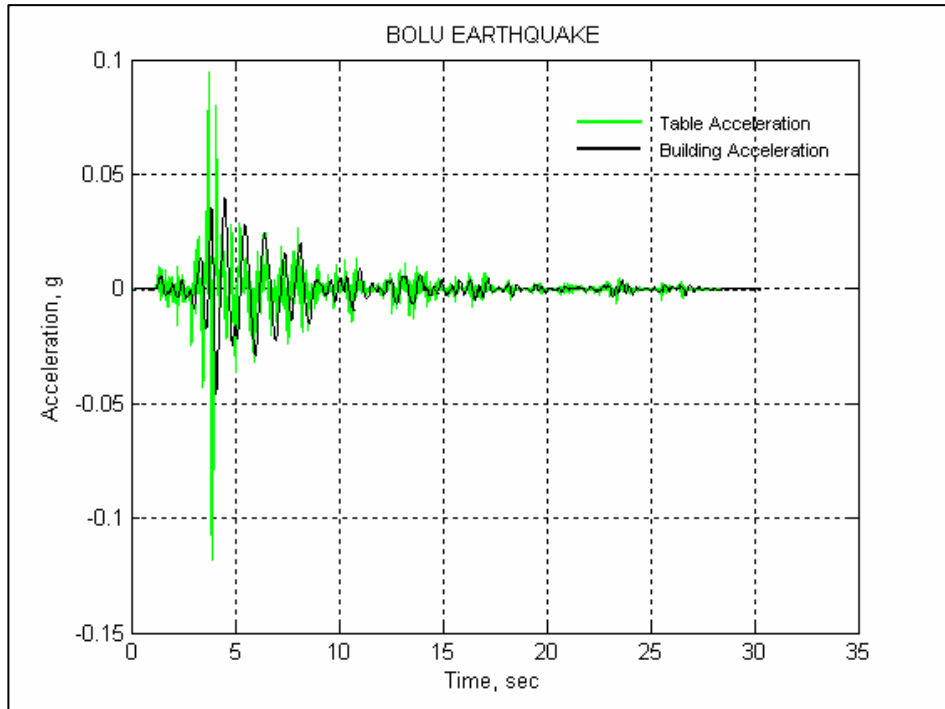


**Figure 58: 1999 Bolu Earthquake, 20%**

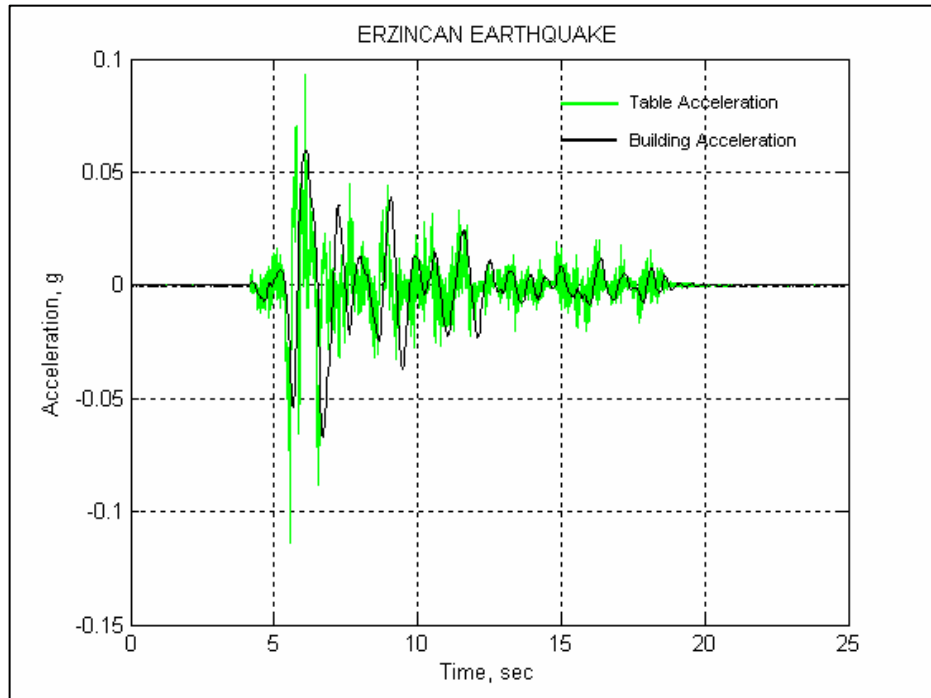


**Figure 59: 1995 Erzincan Earthquake, 20%**

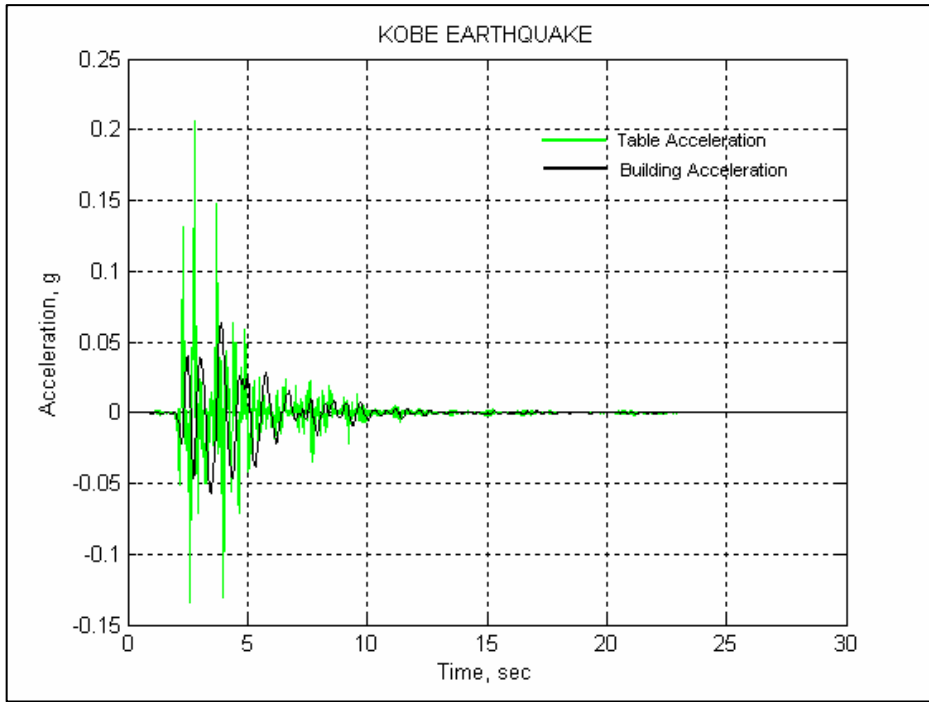


**Figure 60:** 1995 Kobe Earthquake, 20%

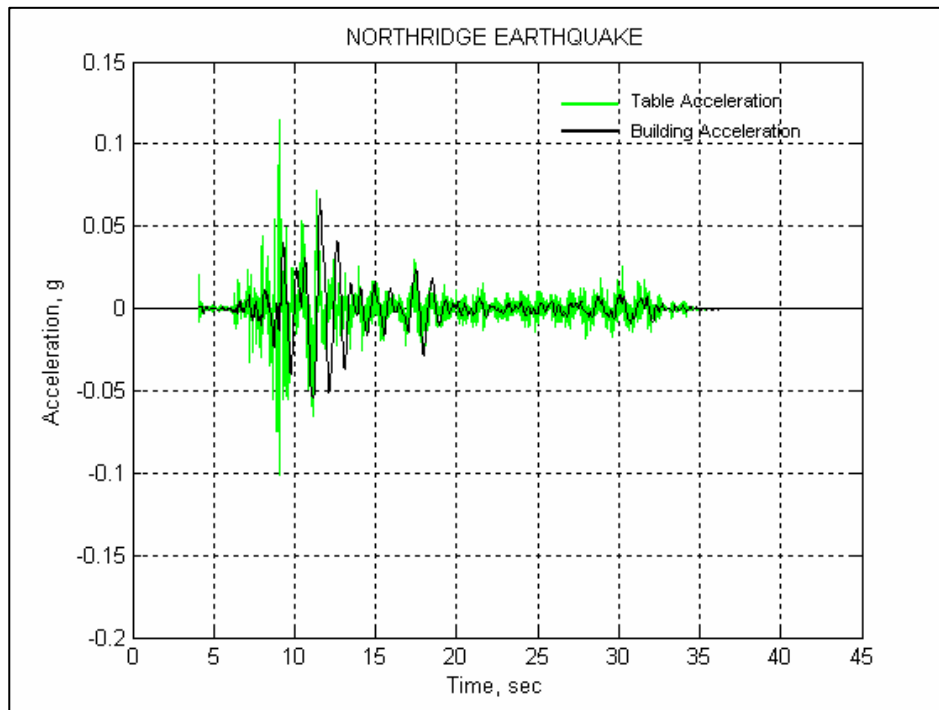


**Figure 61:** 1992 Northridge Earthquake, 40%

**Table 9:** Maximum accelerations in g (9.81m/s<sup>2</sup>)

Earthquake	10 %		20 %		30 %		40 %	
	Table	Building	Table	Building	Table	Building	Table	Building
<b>Bolu</b>	0.052	0.026	0.120	0.046	-	-	-	-
<b>Erzincan</b>	0.082	0.056	0.114	0.067	-	-	-	-
<b>Kobe</b>	0.090	0.037	0.207	0.065	-	-	-	-
<b>Northridge</b>	0.033	0.018	0.062	0.041	0.092	0.058	0.115	0.067

**Table 10:** Isolation Ratios (max table acc / max building acc)

Earthquake	10 %	20 %	30 %	40 %
<b>Bolu</b>	2.00	2.61	-	-
<b>Erzincan</b>	1.46	1.70	-	-
<b>Kobe</b>	2.43	3.19	-	-
<b>Northridge</b>	1.83	1.51	1.59	1.72

#### 4.7.4 Discussion of Results

The natural period of a masonry house is so close to zero that during an earthquake motion the response of the building is almost the ground motion itself. Hence, in Figure 58 to Figure 61, the accelerations of the isolated masonry house are compared with the accelerations obtained from shaking table. The figures show that, isolated building accelerations are much smaller than table accelerations.

The isolation ratios presented in Table 10 shows that the difference between table acceleration and isolated building response is most significant in case of Kobe Earthquake. The maximum acceleration of the building during Kobe event is almost one third of the acceleration of the table during 20% motion.

The response spectrum graphs of the events are plotted by processing the acceleration data obtained from shaking table and presented in Figure 64 to Figure

67. The spectral accelerations corresponding to the isolated case period are marked on the figures. The graphs show how the accelerations are reduced after base isolation applied on masonry model.

The figures below also show the comparison of the accelerations of the isolated building and the shaking table that were measured simultaneously. The isolation ratios can be seen graphically below.

**Acceleration (g)**

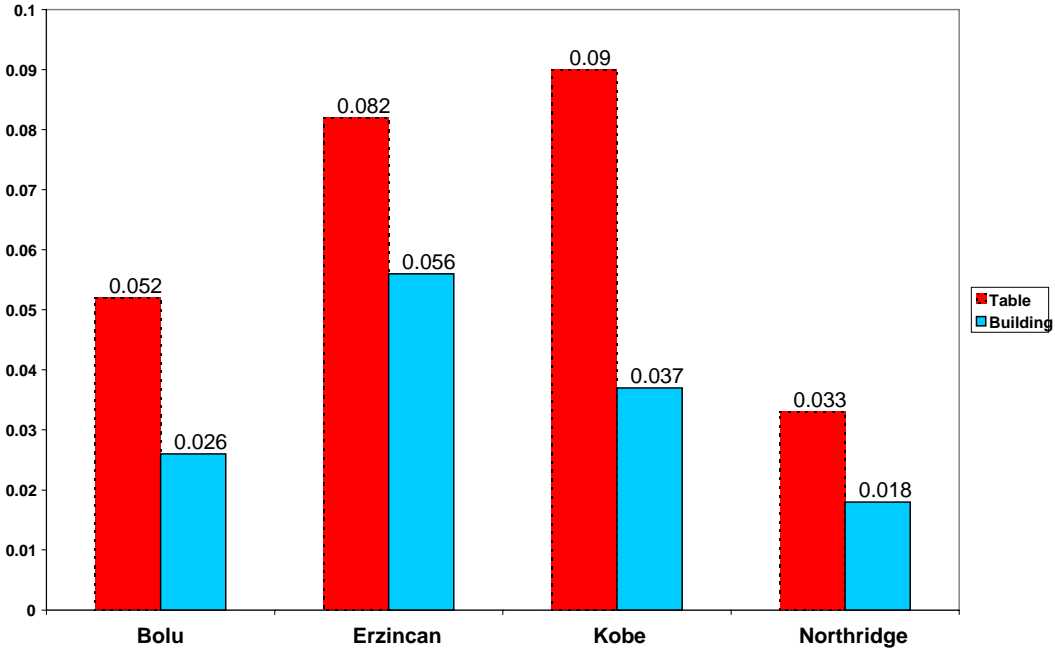


**Figure 62:** Comparison of accelerations during 10% of events

**Acceleration (g)**

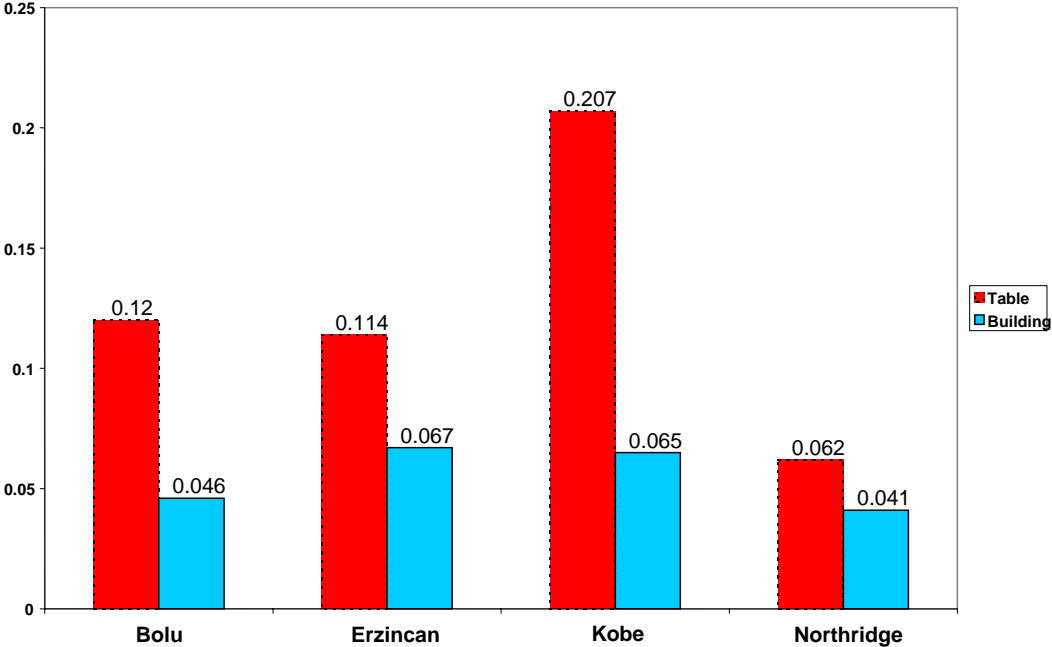


**Figure 63:** Comparison of accelerations during 20% of events

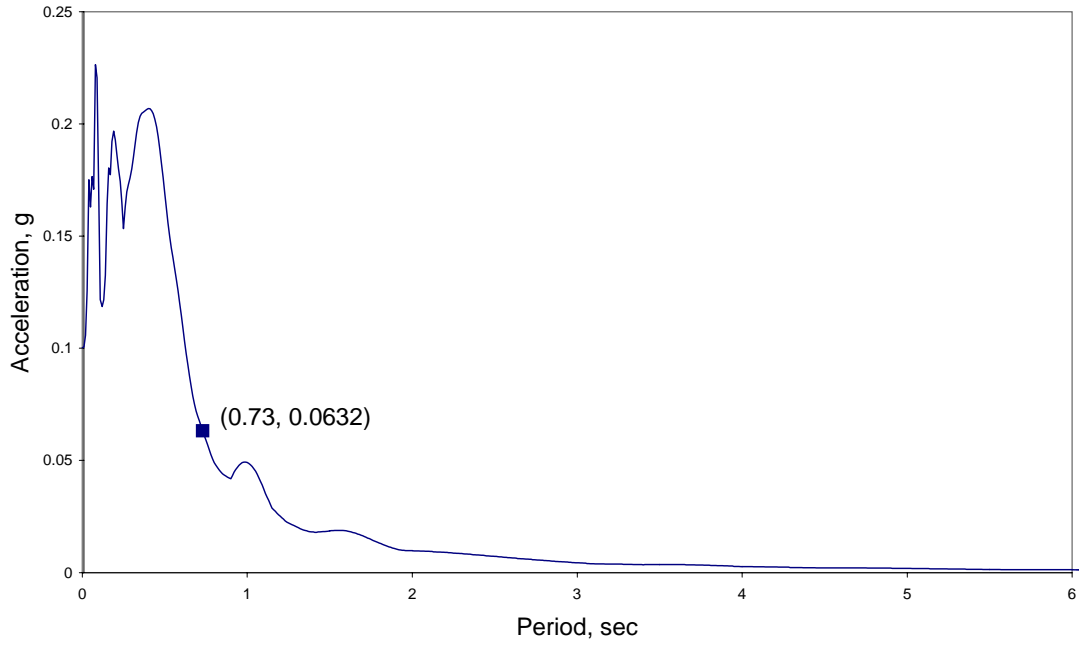


**Figure 64:** Bolu Earthquake Response Spectrum

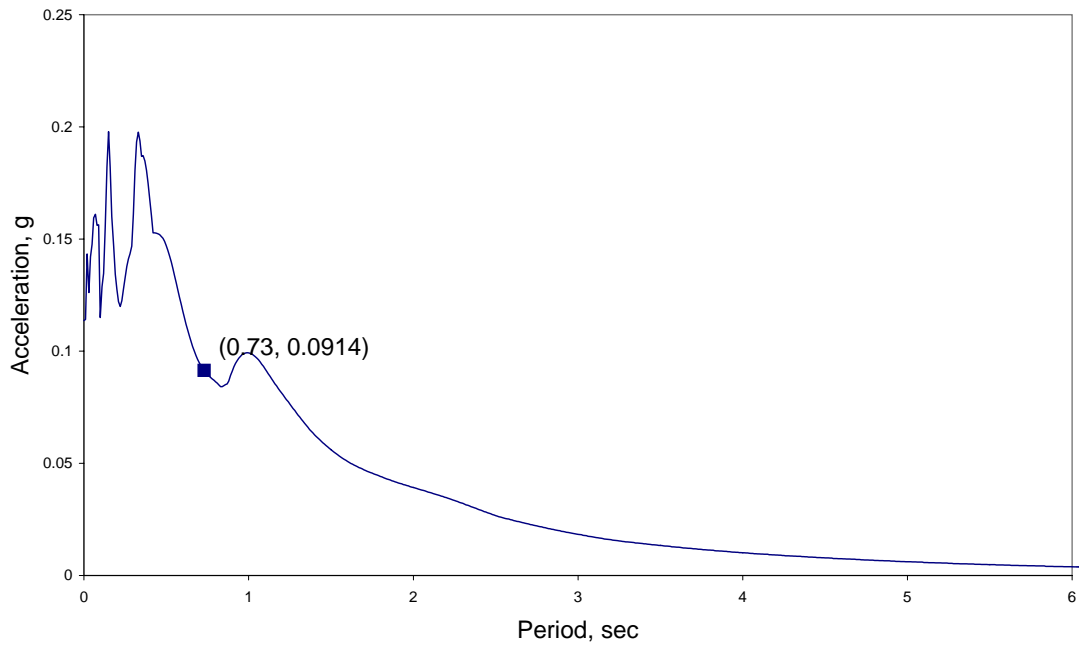


**Figure 65:** Erzinan Earthquake Response Spectrum

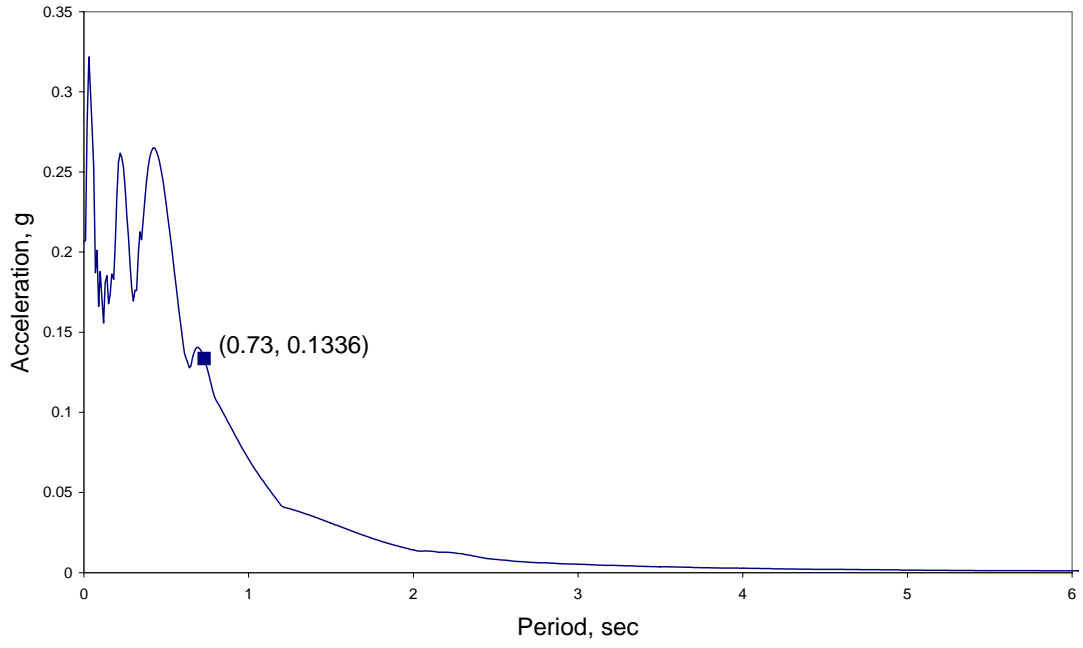


**Figure 66:** Kobe Earthquake Response Spectrum

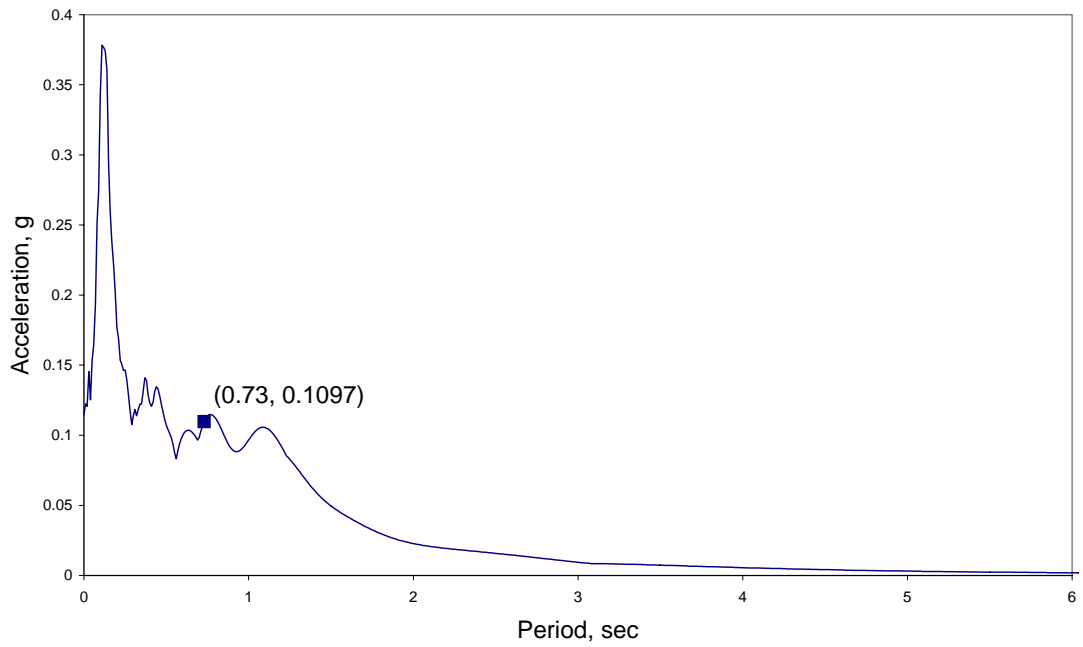


**Figure 67:** Northridge Earthquake Response Spectrum

#### 4.8 Hypothetical Studies

Throughout the experimental study up to here, the mechanical and dynamic properties of STP specimens were tried obtained using several experiment setups. The shear modulus values, compression modulus values, damping values of STP specimens in approximately 180mm x 200mm x 50mm dimensions, were obtained for different tire brands. The experimental results obtained for STPs are now used to design the hypothetical cases below using IBC 2003 provisions.

At the beginning of the study, an STP isolator having similar dimensions that was tested throughout the experiment program thought to isolate 20tons mass for preliminary study. The target period was chosen to be 2 seconds for this case. The shear modulus value is taken as 1.0MPa which is the average value of the test results. Damping ratio is accepted as 7% as the minimum value obtained at the end of dynamic tests. Then the required minimum displacement that the STP should satisfy is calculated as 145mm which is much higher than our STP specimens tested in the previous experiments. The maximum strain level that was applied through shear tests was 70%. Therefore, the dimensions of the STP specimens were to be revised to satisfy the required minimum displacement value. At the end of this preliminary design case study, it is understood that the STP specimens used in the experiments are not able to isolate any mass because it can not satisfy the minimum displacement limits. Hence, in the following hypothetical case studies, different sizes of STP's will be tried to be used.

Case #1 is considered for a single storey masonry house of 150m<sup>2</sup> area. The house is assumed to be located on a 10m x 15m plan with about a total of 75 m long masonry wall. The wall thickness is assumed to be 70cm and the roof is taken as 50cm thick earth (assumed soil density = 2000 kg/m<sup>3</sup>) similar to traditional Turkish rural houses. A 50cm thick R/C slab is considered to support the house on 9 STP isolators which are evenly distributed on a 3 x 3 layout. The total mass of the house is calculated to be 650 tons. Shear modulus ( $G$ ), strain level, damping ratio, and  $C_{vd}$  values are taken as 1.0 MPa, 40%, 7%, and 0.32, respectively.

The STP thickness, width, and length are calculated as 450mm, 600mm, and 600mm, respectively for a target period of 2.0 seconds. The width of a tread section is about 180mm and two sections can be placed side by side in altered directions at each layer. About 40 layers is necessary to reach a height of 450 mm.

The second case is solved for a larger amount of total mass by doubling the area and considering a two storey 2600 tons mass, masonry building. The remaining parameters are kept constant as in the first case study. 15 STPs are placed under the slab in a 3 x 5 pattern. The thickness of each pad is calculated to be 460mm for a square shape of 700 mm x 700 mm. The target period is calculated to be 2.5 seconds. This time three strips can be placed side by side, altering the direction at each one of the 40 layers.

The design acceleration spectrum coefficients,  $S(T)$ , are calculated in accordance with Turkish Seismic Code [4] and listed in the table below.

**Table 11:** Effect of soil type on  $S(T)$  for STP base isolation

Soil Type	$T_B$ (sec)	$S(T)$ Case #1	$S(T)$ Case #2
Z1	0.3	0.48	0.47
Z2	0.4	0.61	0.59
Z3	0.6	0.84	0.81
Z4	0.9	1.16	1.12

The acceleration spectrum coefficients can be taken as 1.0 for the fixed base cases of masonry house due to their high horizontal rigidity. The Z1 through Z4 soil types refer to firm through soft soil, respectively. The low  $S(T)$  values obtained in Table 11 show that the isolators perform much better on firm soil such as rock whereas the efficiency of base isolation drastically decreases for soft soil applications.

In the third case, STP usage is considered as rural bridge supports. Rural bridges generally have low daily traffic volumes, can have multiple spans, and are usually simply supported beam type. Assuming two-lane-bridge with five beams of dimensions 50cm by 80cm which supports a 25cm thick slab would yield 9 ton per mass. Considering an average bridge length of 10m and worst loading of HS20-44 truck and lane loads would yield 250kN vertical load per pad which is within the limits of a 180mm x 200mm STP specimen used in compression tests.

The thermal expansion demand of the bridge can be obtained by considering thermal expansion coefficient of  $11 \times 10^{-6} \mu\epsilon/C^\circ$ . A temperature shift of  $80^\circ C$  from  $-20^\circ C$  to  $+60^\circ C$  would yield a maximum length change of 8.8mm over 10 meters which is about 8% lateral strain of a 55mm thick pad and is within acceptable limits. Therefore STPs can be a low-cost alternative for elastomeric bridge support bearings.

## CHAPTER 5

### CONCLUSIONS

In the thesis study, the experiments have been carried out to investigate the development of low-cost seismic base isolation pads using scrap automobile tires. Within the scope of the work, axial compression, inclined and horizontal static shear, free vibration, and shaking table experiments were conducted.

Compression tests reveal that the axial load capacities of STPs are around 8 MPa level. However, available vertical strength is still enough for design purposes as illustrated in hypothetical examples in Chapter 4. An allowable vertical stress of about 4 MPa is recommended for STP design. The compression modulus values of STPs are found to be 1.2 to 2.0 times the value of SREI sample. The low vertical strength is associated with small amount of steel wire mesh available in scrap tires and additional steel plates may be used between tire layers to significantly improve the axial load capacity of STPs (which would also increase the compression modulus). The STP reinforced with steel plate layers under compression is expected to lose steel wire mesh at a certain load capacity, but steel plates would still continue to function generating a bilinear load-deflection curve.

Reverse cyclic tests and inclined compression tests are conducted in order to obtain the horizontal behavior of STP specimens under large shear deformations. The experiments revealed that shear modulus of STP specimens change between 0.70MPa and 1.85MPa.

Damping ratios of STP specimens are measured to be around 7% to 10% for small displacement dynamic tests ( $C \cong 6500$  kg/s) whereas 16% and 22% for large displacement static tests. STP damping ratio is relatively better than the measured 2% SREI damping ratio. Considering the scatter in STP properties, usage of damping value of about 6500 kg/s is recommended for design purposes since the damping percentage is dependant on mass and stiffness of the isolated system.

Although STP layers have no physical bond in between them and only rely on frictional forces, the inclined plate high-strain static shear tests have shown that the layers do not slip even at high shear strains up to 70%. In inclined shear tests, the axial loads on the STP specimens increase as a function of the vertical load. The lateral load to the vertical load ratio is 1/10 and the friction is always 10 % of the vertical load. Since the friction coefficient between the tire layers is larger than 0.1 no slippage was observed.

In 4500kg lumped mass free vibration dynamic tests, the 180mm x 200mm size G-STP specimens started to loose stability after 8 layers, which corresponds to a height of 90mm. The loss of stability is dominantly attributed to the lack of continuity between tire layers.

The transverse and longitudinal stiffness values linearly decrease as the number of tire layers is increased. The stiffness slope changes are the same for both principal directions indicating that the stiffness change by addition of a tire layer is same in both directions. The horizontal stiffness values of STPs are found to be dependent on pad orientation. The transverse direction stiffness is measured to be smaller than the longitudinal direction stiffness values. Equation 48 is derived to determine the horizontal stiffness difference between two principal directions of rectangular elastomeric pads using the base dimensions and average shear modulus values.

Shaking table tests were carried out for the seismic isolation of a  $\frac{1}{4}$  scaled masonry building. In order to be able to isolate this light structure, the STP models were to be manufactured specially for this experiment. The rubber and steel sheets were not

glued to each other but only relied on the friction between the rubber and steel layers. The test results showed that the STP models were able to reduce the super structure acceleration response and isolate the masonry model from shaking table.

In the hypothetical case study, the STP specimens used in the experiments were tried to be used in different hypothetical base isolation cases. Firstly, it was tried to use STP specimens having similar dimensions to STP specimens tested before. However, it is concluded that the STP specimens used in the experiments are not able to isolate any mass since, the specimens does not satisfy the minimum required displacement limits. In order to satisfy the requirements, STP specimens with different dimensions were used in the hypothetical cases. Two of the cases were about base isolation of masonry houses in two different dimensions and the latter was about the usage of STPs as rural bridge bearings.

It is also noted that a peripheral beam with concrete slab would minimally be needed for masonry house seismic base isolation and cost associated with such construction would be more than the pad savings. However, foundation-basement type structural requirements are not specific to STPs but a general problem for all seismic isolators to be used in economy class housings. This study concentrates on development and testing of alternative free-of-charge isolators and pads made from scrap tires. On the other hand, the STPs would not require additional preparation for small bridges. The idea and investigation of using scrap tires and tinplates instead of conventional elastomeric pads is to have no-cost seismic isolation. Weight reduction, ease of handling, simple shear stiffness adjustment by changing the layer numbers, and positive environmental impact are complementary advantages. The study concentrates on the characteristics of STP itself and the potential implementation problems during usage remains to be an issue which are common to all isolator applications for masonry.

## REFERENCES

1. Kelly T.E. Base Isolation of Structures. Holmes Consulting Group Ltd., July 2001
2. Yaming Wan. 1997. Modeling, Analysis and Comparative Study of Several Seismic Passive Protective Systems for Structures. Master of Science, Rice University, Houston, Texas.
3. Kulkarni JA, Jangid R.S., 2002. Rigid Body Response of Base-Isolated Structures. *Journal of Structural Control*; 9: 171-188
4. Turkish Ministry of Public Works, 1997. Turkish Seismic Code
5. Naeim F, Kelly J.M., 1999. Design of Seismic Isolated Structures. John Wiley & Sons.
6. Lissa Wipplinger, A Design Methodology for the Application of Kansas State University's Stiffness Decoupler to Masonry Structures
7. Moon B.Y, Kang G.J., Kang B.S., Kelly J.M. 2002. Design and Manufacturing of Fiber Reinforced Elastomeric Isolator for Seismic Isolation, *Journal of Materials Processing Technology* 130-131, 145-150
8. Kang B.S., Kang G.J., Moon B.Y., 2003. Hole and Lead Plug Effect on Fiber Reinforced Elastomeric Isolator for Seismic Isolation, *Journal of Materials Processing Technology* 140, 592-597
9. Tsai HC, Kelly JM. Stiffness Analysis of Fiber-Reinforced Elastomeric Isolators. PEER Report 2001/5
10. Tsai Hsiang-Chuan, 2004. Compression Stiffness of Infinite-Strip Bearings of Laminated Elastic Material Interleaving with Flexible Reinforcements. *International Journal of Solids and Structures* 41 (2004) 6647-6660
11. Kelly J.M., 1996. Analysis of Fiber-Reinforced Elastomer Isolators, *Journal of Seismic Engineering*, 2(1): 19-34
12. Kelly J.M., M.EERI. Seismic Isolation Systems for Developing Countries, Pacific Earthquake Engineering Research Center, University of California, Berkeley 94720

13. Zayas V, Low SS, Mahin SA. 1987. The FPS Earthquake Resisting System: Experimental Report. Report No UCB/EERC-87/01, Earthquake Engineering Research Center, University of California, Berkeley, CA.
14. Mostaghel N, Khodaverdian M. 1987. Dynamic of Resilient-Friction Base Isolator (R-FBI). Earthquake Engineering and Structural Dynamics. Vol.15, 379-390 (1987)
15. Narasimhan S. 2002. Analytical Study of Base Isolated Buildings with Smart Devices: STFT Controller. Master of Science, Rice University, Houston, Texas.
16. OHIO Department of Natural Resources, "The Nature of Rubber", <http://www.dnr.state.oh.us>, fast accessed, January (2005)
17. OHIO Department of Natural Resources, "Charles Goodyear", <http://www.dnr.state.oh.us>, fast accessed, January (2005)
18. Discount Tire Direct, "Tire Term", <http://www.discounttiredirect.com>, fast accessed, January (2006)
19. Tire School, "Manufacturing Flowchart", <http://www.maxxis.com>, fast accessed, January (2006)
20. Bruce Tire, "How to Read a Tire", <http://www.brucestire.com>, fast accessed, January (2006)
21. International Building Code 2000, IBC 2000
22. Gent AN, Lindley PB. 1959. The compression of Bonded Rubber Blocks. Proceedings Institution of Mechanical Engineers. 173-324
23. Nagarajaiah S., Ferrell K., 1999. Stability of Elastomeric Seismic Isolation Bearings. Journal of Structural Engineering, Vol.125, No.9, September 1999.
24. Buckle I.G., Kelly J.M., 1986. Properties of Slender Elastomeric Isolation Bearings during Shaking Table Studies of a Large-Scale Model Bridge Deck. Joint Sealing and Bearing Systems for Concrete Structures, Vol.1, American Concrete Institute, Detroit, Mich., 247-269
25. Havinga J.S., S de Meij, 1999. Engineering with Natural Rubber. Natuurrubber 13, Newsletter of the Rubber Foundation Information Center, February 1999
26. Butterworth J., Lee J.H., Davidson B., 2004. Experimental Determination of Modal Damping from Full Scale Testing. 13<sup>th</sup> World Conference on Earthquake Engineering. Vancouver, B.C., Canada. August 1-6, 2004. Paper No.310

27. Topkaya C., Yura J.A., 2002. Test Method for Determining the Shear Modulus of Elastomer Bearings. ASCE Journal of Structural Engineering 128 (6), 797-805
28. Topkaya C., 2004. Analysis of Specimen Size Effects in Inclined Compression Test on Laminated Elastomeric Bearings. Engineering Structures 26, 1071-1080
29. Kelly JM, Takhirov SM. Analytical and Experimental Study of Fiber-Reinforced Strip Isolators. PEER Report 2002/11
30. Kelly JM, Takhirov SM. Analytical and Experimental Study of Fiber-Reinforced Elastomer Isolators. PEER Report 2001/11
31. Chopra A., 2002. Dynamics of Structures. John Wiley & Sons
32. International Conference of Buildings Officials, 1997. Earthquake Regulations for Seismic-Isolated Structures. Uniform Building Code, Appendix Chapter 16, Whittier, CA.